School of Chemical and Petroleum Engineering

Fuels and Energy Technology Institute

Evolution of Char Structure and Reactivity during Gasification

Shuai Wang

This thesis is presented for the Degree of
Doctor of Philosophy
of
Curtin University

July 2016

Declaration

To the best of my knowledge and belief this thesis contains no material previously published by any other person except where due acknowledgment has been made.

This thesis contains no material which has been accepted for the award of any other degree or diploma in any university.

Signature: ……..……

Date: ……..

Abstract

Biomass gasification is an effective thermochemical conversion process to produce syngas that can be further used to generate electricity or synthesise liquid fuels and chemicals. The gasification of the solid char with gasifying agents is the rate-limiting step of the overall gasification. The physico-chemical structure of char is an important factor that can directly determines the gasification reactivity. Understanding the effect of char structure on its gasification behaviour is significantly important for the development of gasification technology.

The purpose of this study was to investigate the changes in char structure and its reactivity during the gasification of an Australia mallee wood in different gasifying atmospheres. The gasification experiments were carried out in a fluidised-bed quartz reactor. The thermogravimetric analyser, FT-IR/Raman and X-ray photoelectron spectroscopies were applied to characterise the gasification reactivity and the chemical structural feature of char.

The results of this study showed that the second-order Raman spectroscopy can also be used to characterise the char structures during gasification. Intra-particle diffusion of the gasifying agent was not a rate-limited step and biomass particle size had minimal effect on char structures during the gasification in steam and CO_2 atmospheres under present experimental conditions. The amount of aromatic C-O structure left in char during the gasification under reducing atmosphere was lower than that under oxidising atmosphere, while the consumption of aromatic C=O structure was related to the progress of gasification regardless of the atmosphere. The additional formation of aromatic C-O structures was most likely to be responsible for enhancing the gasification rate of char in the oxidising atmospheres. The char prepared from 600 and 900 ˚C followed different reaction pathway during the low-temperature gasification in air. The oxidation of char was much fierce at the initially stage of the low-temperature gasification in air, and different types of O-containing structures would form during char oxygenation according to their different behaviour in the total Raman and IR intensity.

Acknowledgements

I would like to express my deepest gratitude to my supervisor, Professor Chun-Zhu Li, who provided me the precious opportunity for this research and gave me his expertise, understanding and patience to my study. His professional attitude towards research has been an inspiration for me throughout my Ph.D candidature. This Ph.D would not have been possible without his invaluable comments and guidance.

I would also like to express my appreciation to all the members in our institute. My research has gone smoothly with their cooperation, valuable discussion and warm advice.

I also thank Curtin University for awarding me a Curtin International Postgraduate Research Scholarship. The financial supports of this study from Australian Government through ARENA's Emerging Renewables Program, the Australian Research Council (DP110105514) and the Commonwealth of Australia under the Australia-China Science and Research Fund are greatly acknowledged.

Finally, appreciation and thanks go to my parents, my wife Liping Wu and my young daughter Anni Wang for all of their love, support and encouragement.

Table of Contents

List of Tables

List of Figures

Chapter 1

Introduction

1.1 Importance of bio-energy

1.1.1 Biomass as an energy source

The discovery and utilisation of fossil fuels such as crude oil and coal accelerated the industrialised process of the word as well as improved the quality of people's life. However, in recent years, the depletion of fossil fuel resources and the rising environmental problems have made it imperative to seek a renewable resource to meet the world's continuously growing energy demand [1]. On that basis, biomass is currently among the top choices, not only because it is the sustainable source of organic carbon, but also due to its abundance around the world [2-5]. Lots of inexpensive biomass can be chosen as the feedstock for producing bio-fuels, including energy crops, forest products, waste materials and even aquatic biomass [1,6-8]. In addition, the production process of bio-fuels can have significantly less environmental impact than the fossil fuels and can be near zero CO_2 emission if advanced biomass processing technology is developed [1,9-12]. The International Energy Agency estimated that the worldwide raw biomass energy potential should be between 150 and 450 EJ/year in 2050 [13]. Therefore, biomass resource is poised to make great contribution to the world energy market.

Edible biomass is not suggested to be the feedstock because it will directly lead to the rise of food price [6]. Therefore, more attention should be paid on the non-food biomass as the bio-energy feedstock. In Australia, mallee, as a non-food biomass, is the top choice as the renewable energy sources due to many reasons. Firstly, mallee can be planted in the dry land agriculture systems for various environmental benefits such as erosion control and salinity mitigation [14,15]. Secondly, mallee can be planted in form of long narrow belts, which means the planting of mallee does not need to occupy too much farmland. In addition, the effective use of the rainfalls and groundwater means no supplemental water supply is required for the growth of mallee [14,15]. Thirdly, mallee can be harvested on a very short cycle, usually 3 to 5 years after the first harvest [15]. Fourthly, mallee production can achieve an energy ratio of 40 (unit of energy for every unit of energy input) and an energy productivity

of over 200 GJ ha^{-1} $year^{-1}$, which are significantly higher than other annual energy crops [16].

1.1.2 Thermo-chemical conversion of biomass

Gasification is an effective technology to convert biomass into product gas that mainly contains H_2, CO, CH_4 and CO_2 in various proportions [1,17-20]. Such product gas is usually combusted to generate electricity or used to synthesise liquid fuels and chemicals [21-23], as is shown in Figure 1-1.

Biomass gasification is a complex combination of reactions mainly involving two consecutive steps [21]. The first step is the thermal decomposition of biomass to produce volatiles and solid char, usually termed as pyrolysis or devolatilisation. The second step is the gasification of solid char and the reforming of volatiles by reacting with the gasifying agents. The first step occurs much more quickly than the second step [21]. The reaction temperature as well as heating rate will determine the relative yields of volatiles and char [24-26]. The volatiles and solid char produced from the first step will then react with the gasifying agents (e.g. steam) to produce H_2, CO and CO_2. The gasification of solid char is relatively slow and is the rate-limiting step for the overall gasification process [21]. Meanwhile, other two important reactions will also take place during gasification. One is the water-gas-shift reaction converting CO and H_2O to CO_2 and H_2. The other is methanation converting H_2 and CO to H_2O and CH_4 [1,21].

The required heat to drive the endothermic reactions such as char-H_2O, char-CO_2, methanation and water-gas-shift reaction during gasification can be provided by two ways: heat is generated outside and then transferred into the gasifier, or heat is generated by partial combustion reactions inside the gasifier. Usually, for a practical gasifier, the required energy for the endothermic process is afforded by the energy produced from the combustion of char and/or volatiles without any external supply of thermal energy into the gasifier [27-29].

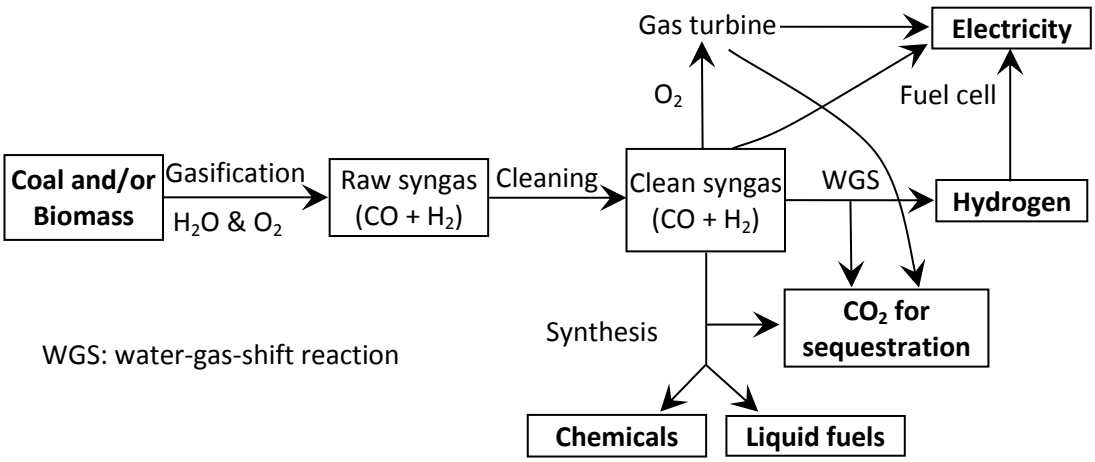

Figure 1-1. Gasification as the core of many versatile near-zero emission energy technologies. Reprinted from Ref. 21, Copyright (2013), with permission from Elsevier.

Biomass is particularly suitable for gasification due to its high volatile yield and low content of aromatic moieties [21]. Biomass gasification can take place at lower temperature than coal gasification because of the relatively high reactivity of bio-char compared with coal-char [21]. In addition, the volatiles produced from biomass gasification contain high concentrations of oxygen and aliphatic moieties, which indicate that these volatiles matters are very reactive and can be easily reformed by the gasifying agents [21].

1.2 Importance of char structure to its gasification reactivity

The physico-chemical structure of char could directly determine the preferential sites for the gasification reaction to take place. Therefore, a lot of research has been aimed at the evolution of char structure and reactivity during gasification.

1.2.1 Characterisation of char structure

There are many analytical techniques that can be used to characterise the structure of carbonaceous materials. However, many of them are only suitable for the analysis of

highly ordered carbon materials such as graphite and carbon nanotubes. Compared with the well-ordered carbon materials, char produced from the thermo-chemical conversion of biomass or coal is highly disordered. The characterisation method for such amorphous carbon material is very limited. For example, X-ray diffraction (XRD) that has been widely used in providing useful quantitative information for graphite and carbon nanotubes can not be successfully applied to char characterisation because no clear peak can be observed in the XRD spectrum [30]. The scanning electron microscopy (SEM) or transmission electron microscopy (TEM) can be applied to observe the surface profile of char and the carbon structure, while detailed quantitative information about char structure can not be easily provided [20].

Raman spectroscopy is a powerful method to characterise various carbon-based materials because of its outstanding ability to detect the symmetric vibration of less or non-polar bonds [31-36]. Obviously, the Raman spectra of char differ significantly from those of well-ordered materials. A clear-resolved strong peak of G (1600 cm^{-1}) and a peak of D (1300 cm^{-1}) were shown in the spectra of graphite-liked carbon materials, while the spectra of char exhibit a broad band in the region of 800-1800 cm^{-1}. Therefore, quantitative information about char structures needs to be obtained through spectral deconvolution. Based on our previous study [37], the first-order Raman spectra in the range of 800-1800 cm^{-1} were curve-fitted with 10 Gaussian bands. In addition, considering the significant structural difference between char and graphite-liked materials, a simple adoption of the band assignment for well-ordered materials would be very inapplicable for the analysis of char structure. The positions and assignments of these 10 bands are summarised in Table 1-1. Briefly, the D band here mainly represents aromatics with not less than 6 fused benzene rings rather than ‘‘defects’’, and the G_R (1540 cm^{-1}), V_L (1465 cm^{-1}) and V_R (1380 cm^{-1}) bands located at the overlap region between G and D bands mainly represent aromatics with 3-5 rings.

Table 1-1. Summary of peak/band assignment. Reprinted from Ref. 37, Copyright (2006), with permission from Elsevier.

Band name	Position, cm^{-1}	Description	Bond type
G_L	1700	Carbonyl group C=O	sp^2
G	1590	Graphite E_{2g}^2; aromatic ring quadrant breathing; alkene C=C	sp^2
G_R	1540	Aromatics with 3~5 rings; amorphous carbon structures	sp^2
V_L	1465	Methylene or methyl; semi-circle breathing of aromatic rings; amorphous carbon structures	sp^2; sp^3
V_R	1380	Methyl group; semi-circle breathing of aromatic rings; amorphous carbon structures	sp^2; sp^3
D	1300	D band on highly ordered carbonaceous materials; C-C between aromatic rings and aromatics with not less than 6 rings	sp^2
S_L	1230	Aryl-alkyl ether; para-aromatics	sp^2; sp^3
S	1185	$C_{aromatic}$-C_{alkyl}; aromatic (aliphatic) ethers; C-C on hydroaromatic rings; hexagonal diamond carbon sp^3; C-H on aromatic rings	sp^2; sp^3
S_R	1060	C-H on aromatic rings; benzene (ortho-di-substituted) ring	sp^2
R	960-800	C-C on alkanes and cyclic alkanes; C-H on aromatic rings	sp^2; sp^3

1.2.2 Evolution of char structure during gasification

Gasification temperature would have a great influence on the evolution of char structures. The previous studies [38-40] have demonstrated that, based on the FT-Raman spectroscopy, the $I_D/I_{Gr+Vl+Vr}$ ratio of char increased very significantly with increasing gasification temperature. When the temperature was lower than 800 ˚C where the pyrolysis was the dominant reaction, this increase was mainly because of the enhanced thermal cracking reactions, converting some small aromatic rings into large ones with increasing temperature. When the temperature was higher than 800 ˚C where the gasification reaction became much fierce, the thermal cracking reactions combined with the selective consumption of small aromatic ring systems by the gasifying agents were mainly responsible for the increase of that ratio with increasing temperature.

Gasifying agent is another important factor that can affect the evolution of char structure during gasification. Based on previous studies [37], the total Raman intensity of char can be used to indicate the presence of oxygen species which have a resonance effect with the aromatic ring it is connected to. Tay and co-workers [41] reported that the total Raman intensity of char decreased with the progress of gasification in the reducing atmosphere, indicating the loss of such kinks of oxygen species during gasification. On the other hand, the observed Raman intensity tended to increase during the gasification in oxidising atmosphere [42-45]. In addition, Li and co-workers [45] reported that the content of oxygen species connected with the aromatic ring systems during the gasification in steam was higher than that during the gasification in CO_2. The previous studies [41,45] also indicated that the presence of H radicals in the H_2O or H_2 atmosphere could induce the ring condensation reactions, resulting in a higher $I_D/I_{Gr+Vl+Vr}$ ratio of char compared with that in other gasification atmospheres at the same char conversion levels.

The volatile-char interactions could also have an effect on the evolution of char structure during gasification [21,46-51]. Volatiles released from biomass thermal cracking would inevitably contact and interact with the nascent char during

gasification. Zhang and co-workers [52] reported that the volatile-char interactions could inhibit char conversion during gasification, which is mainly because the additional radicals, especially H radicals, released from biomass thermal cracking are able to penetrate deep into the char matrix and intensify or initiate ring condensation reactions to convert small aromatic ring systems into large ones.

1.3 Purpose of this study

It is clear that investigating the evolution of char structure and reactivity during gasification are quite essential for a better understanding of the gasification mechanisms. Therefore, a suitable and powerful characterisation method is imperative. Raman spectroscopy has been extensively used in characterising the char structure. However, lots of efforts were paid on the study of the first-order Raman spectra to obtain the structural information of char through deconvolution and analysis of various bands in the first-order region, the second-order Raman spectra has not been further investigated. Detailed information about the char structure can also be provided through the investigation of the second-order Raman spectra if a proper deconvolution method has been established. Therefore, establishing a new spectral deconvolution method for the second-order Raman spectra of chars from the gasification of low rank fuels is one aim of this study.

The size range of the feedstock is one of the practical problems that biomass gasification must overcome before its commercial implementation. It is impractical to use fine biomass particle as the feedstock for a commercial gasifier because the size reduction will be very labour-intensive and time-consuming, making it commercially unattractive. Therefore, the feedstock for a commercial gasifier necessarily consists of particles with a wide range of sizes. However, gasification rate is a main consideration in the design and operation of a commercial gasifier because it would determine the overall efficiency of the gasifer, and biomass particle size would play an important role in the ultimate char yield during gasification. Therefore, understanding the gasification behaviour of different biomass particle size is one objective of this study.

The O-containing functional groups of char will also determine the gasification behaviour to some extent, especially for the low temperature gasification of the low-rank fuels. Although the total Raman intensity can be used as an indirect indication of the relative amounts of the O-containing functional groups in char, it is only limited to the oxygen species that have a resonance effect with the aromatic ring structures they are connected to. Obviously, not all oxygen species in char could have the resonance effect with the aromatic ring. X-ray photoelectron spectroscopy can be applied to characterise carbon and oxygen species of chars produced from gasification. Therefore, investigating the evolution of O-containing structures of char during gasification by XPS spectroscopy is also one aim of this study.

Char-O_2 reaction is also a very important gasification reaction. For a practical gasifier, the required energy for the endothermic process is afforded by the energy produced from the combustion of bio-char itself without any external supply of thermal energy into the gasifier. It is well known that gasifying agents such as CO_2, H_2O and H_2 will be continuously released in a practical gasifier, and the devolatilised chars could have the chance to be partially gasified by such agents before it reacts with O_2. Therefore, one purpose of this study is to understand the structural changes in the partially gasified char during low-temperature gasification in air.

Biomass is rich in oxygen and various O-containing structures were left in char after devolatilisation. The evolution of O-containing structures is also an important factor that can influence the char gasification behaviour. Gasification temperature would have a great influence on the evolution of the O-containing structures of char because the thermal cracking would tend to reduce the oxygen content of char. In addition, different kinds of O-containing functional groups would form in char with the progress of gasification in oxidising atmosphere. Therefore, investigation on the changes in the O-containing structures of char during gasification as revealed with FT-IR/Raman and X-ray photoelectron spectroscopies is also one objective of this study.

1.4 Scope of thesis

Chapter 2 describes the establishment of a new spectral deconvolution method for the second-order Raman spectra. The information about char structure from the second-order region was compared with that from the first-order region and complementary or additional information about the structural features of char was found through that analysis of the second-order Raman spectra.

Chapter 3 presents the evolution of char structure during the gasification of mallee biomass with different particle size ranges in two atmospheres (15% H_2O-Ar, pure CO_2) in a fluidised-bed reactor. The mass transfer resistance, intra-particle gas diffusion and char structure during gasification are discussed.

Chapter 4 presents the evolution of O-containing structures of char during gasification of mallee wood in a fluidised-bed reactor at 600-900 ˚C in oxidising (pure CO_2, 15% H_2O-Ar) and reducing atmosphere (15% H_2-Ar) respectively. The XPS analysis results of char are discussed.

Chapter 5 presents the structural changes in bio-char produced under different gasification conditions (gasification in 15% H_2O-Ar at 600 ˚C, gasification in pure CO_2 at 900 ˚C, gasification in 15% H_2O-Ar at 900 ˚C and gasification in 15% H_2-Ar at 900 ˚C) during gasification in air in TGA at 375 ˚C. FT-IR/Raman spectroscopy was applied to characterise the structural features of char.

Chapter 6 presents the changes in O-containing structures during biomass gasification in steam at different temperatures ranging from 600 to 900 ˚C, and bio-chars (produced from gasification in steam at 600 and 900 ˚C) gasification in air in TGA at 375 ˚C. The XPS, Raman and IR results of char during gasification are discussed.

Chapter 7 summarises all the conclusions of this study and make recommendations for future work.

1.5 References

[1] G.W. Huber, S. Iborra, A. Corma, Synthesis of transportation fuels from biomass: chemistry, catalysts and engineering, Chemical Reviews, 106 (2006) 4044-4098.

[2] D.L. Klass, Biomass for renewable energy, fuels and chemicals, Academic Press, San Diego, 1998.

[3] P. McKendry, Energy production from biomass (part 1): overview of biomass, Bioresource Technology, 83 (2002) 37-46.

[4] D.L. Klass, Biomass for renewable energy and fuels, Encyclopedia of Energy, 1 (2004) 193-212.

[5] L.R. Lynd, C.E. Wyman, T.U. Gerngross, Biocommodity engineering, Biotechnology Progress, 15 (1999) 777-793.

[6] S.N. Naik, V.V. Goud, P.K. Rout, A.K. Dalai, Production of first and second generation biofuels: A comprehensive reviews, Renewable and Sustainable Energy Reviews, 14 (2010) 578-597.

[7] R.E.H. Sims, W. Mabee, J.N. Saddler, M. Taylor, An overview of second generation biofuel technologies, Bioresource Technology, 101 (2010) 1570-1580.

[8] G.P. Towler, A.R. Oroskar, S.E. Smith, Development of a sustainable liquid fuels infrastructure based on biomass, Environmental Progress, 23 (2004) 334-341.

[9] C.E. Wyman, Alternative fuels from biomass and their impact on carbon dioxide accumulation, Applied Biochemistry and Biotechnology, 45 (1994) 897-915.

[10] K.G. Roberts, B.A. Gloy, S. Joseph, N.R. Scott, J. Lehmann, Life cycle assessment of biochar systems: estimating the energetic, economic and climate change potential, Environmental Science & Technology, 44 (2009) 827-833.

[11] D. Woolf, J.E. Amonette, F.A. Street-Perrott, J. Lehmann, S. Joseph, Sustainable biochar to mitigate global climate change, Nature Communications, 1 (2010) 56.

[12] R. Ibarrola, S. Shackley, J. Hammond, Pyrolysis biochar systems for recovering biodegradable materials: A life cycle carbon assessment, Waste Management, 32 (2012) 859-868.

[13] IEA, Biofuels for transport: an international perspective, International Energy Agency, Paris, France, 2004.

[14] D. Cooper, G. Olsen, J. Bartle, Capture of agricultural surplus water determines the productivity and scale of new low-rainfall woody crop industries, Australia Journal of Experimental Agriculture, 45 (2005) 1369-1388.

[15] J. Bartle, G. Olsen, D. Cooper, T. Hobbs, Scale of biomass production from new woody crops for salinity control in dryland agriculture in Australia, International Journal of Global Energy Issues, 27 (2007) 115-137.

[16] H. Wu, Q. Fu, R. Giles, J. Bartle, Production of mallee biomass in Western Australia: energy balance analysis, Energy & Fuels, 22 (2007) 190-198.

[17] H. Lasa, E. Salaices, J. Mazumder, R. Lucky, Catalytic steam gasification of biomass: catalysts, thermodynamics and kinetics, Chemical Reviews, 111 (2011) 5404-5433.

[18] R.M. Navarro, M.A. Pena, J.L.G. Fierro, Hydrogen production reactions from carbon feedstocks: fossil fuels and biomass, Chemical Reviews, 107 (2007) 3952-3991.

[19] C.-Z. Li, Special issue-gasification: A route to clean energy, Process Safety and Environmental Protection, 84 (2006) 407-408.

[20] C.-Z. Li, Some recent advances in the understanding of the pyrolysis and gasification behaviour of Victorian brown coal, Fuel, 86 (2007) 1664-1683.

[21] C.-Z. Li, Importance of volatile-char interactions during the pyrolysis and gasification of low-rank fuels – A review, Fuel, 112 (2013) 609-623.

[22] A.V. Bridgwater, The technical and economic feasibility of biomass gasification for power generation, Fuel, 74 (1995) 631-653.

[23] A.V. Bridgwater, Renewable fuels and chemicals by thermal processing of biomass, Chemical Engineering Journal, 91 (2003) 87-102.

[24] D. Mohan, C.U. Pittman, P.H. Steele, Pyrolysis of wood/biomass for bio-oil: a critical review, Energy & Fuels, 20 (2006) 848-889.

[25] A.R. Fraga, A.F. Gaines, R. Kandiyoti, Characterization of biomass pyrolysis tars produced in the relative absence of extraparticle secondary reactions, Fuel, 70 (1991) 803-809.

[26] T. Ogada, J. Werther, Combustion characteristics of wet sludge in a fluidized bed: release and combustion of the volatiles, Fuel, 75 (1996) 617-626.

[27] Y. Sakurai, S. Yamamoto, S. Kudo, K. Norinaga, J.-I. Hayashi, Conversion characteristics of aromatic hydrocarbons in simulated gaseous atmospheres in reducing section of two-stage entrained-flow coal gasifier in air-and O_2/CO_2-blown modes, Energy & Fuels, 27 (2013) 1974-1981.

[28] L. Wang, C.L. Weller, D.D. Jones, M.A. Hanna, Contemporary issues in thermal gasification of biomass and its application to electricity and fuel production, Biomass and Bioenergy, 32 (2008) 573-581.

[29] P.M. Lv, Z.H. Xiong, J. Chang, C.Z. Wu, Y. Chen, J.X. Zhu, An experimental study on biomass air–steam gasification in a fluidized bed, Bioresource Technology, 95 (2004) 95-101.

[30] X. Guo, H.-L. Tay, S. Zhang, C.-Z. Li, Changes in char structure during the gasification of a Victorian brown coal in steam and oxygen at 800 ˚C, Energy & Fuels, 22 (2008) 4034-4038.

[31] C. Sheng, Char structure characterised by Raman spectroscopy and its correlations with combustion reactivity, Fuel, 86 (2007) 2316-2324.

[32] A. Guedes, B. Valentim, A.C. Prieto, F. Noronha, Raman spectroscopy of coal macerals and fluidized bed char morphotypes, Fuel, 97 (2012) 443-449.

[33] V.P. Chabalala, N. Wagner, S. Potgieter-Vermaak, Investigation into the evolution of char structure using Raman spectroscopy in conjunction with coal petrography; Part 1, Fuel Processing Technology, 92 (2011) 750-756.

[34] C.A. Johnson, J.W. Patrick, K.M. Thomas, Characterization of coal chars by Raman spectroscopy, X-ray diffraction and reflectance measurements, Fuel, 65 (1986) 1284-1290.

[35] S. Dong, P. Alvarez, N. Paterson, D.R. Dugwell, R. Kandiyoti, Study on the effect of heat treatment and gasification on the carbon structure of coal chars and metallurgical cokes using Fourier Transform Raman Spectroscopy, Energy & Fuels, 23 (2009) 1651-1661.

[36] A. Sadezky, H. Muckenhuber, H. Grothe, R. Niessner, U. Poschl, Raman microspectroscopy of soot and related carbonaceous materials: Spectral analysis and structural information, Carbon, 43 (2005) 1731-1742.

[37] X. Li, J.-I. Hayashi, C.-Z. Li, FT-Raman spectroscopic study of the evolution of char structure during the pyrolysis of a Victorian brown coal, Fuel, 85 (2006) 1700-1707.

[38] M. Asadullah, S. Zhang, Z. Min, P. Yimsiri, C.-Z, Li Importance of biomass particle size in structural evolution and reactivity of char in steam gasification, Industrial & Engineering Chemistry Research, 48 (2009) 9858-9863.

[39] S. Zhang, Z. Min, H.-L. Tay, Y. Wang, L. Dong, C.-Z. Li, Changes in char structure during the gasification of mallee wood: Effect of particle size and steam supply, Energy & Fuels, 26 (2012) 193-198.

[40] D.M. Keown, J.-I. Hayashi, C.-Z. Li, Drastic changes in biomass char structure and reactivity upon contact with steam, Fuel, 87 (2008) 1127-1132.

[41] H.-L. Tay, S. Kajitani, S. Wang, C.-Z. Li, A preliminary Raman spectroscopic perspective for the roles of catalysts during char gasification, Fuel, 121 (2014) 165-172.

[42] X. Li, J.-I. Hayashi, C.-Z. Li, Volatilisation and catalytic effects of alkali and alkaline earth metallic species during the pyrolysis and gasification of Victoria brown coal. Part VII. Raman spectroscopic study on the changes in char structure during the catalytic gasification in air, Fuel, 85 (2004) 1509-1517.

[43] D.M. Keown, X. Li, J.-I. Hayashi, C.-Z. Li, Evolution of biomass char structure during oxidation in O_2 as revealed with FT-Raman spectroscopy, Fuel Processing Technology, 89 (2008) 1429-1435.

[44] H.-L. Tay, C.-Z. Li, Changes in char reactivity and structure during the gasification of a Victorian brown coal: comparison between gasification in O_2 and CO_2, Fuel Processing Technology, 91 (2010) 800-804.

[45] T. Li, L. Zhang, L. Dong, C.-Z. Li, Effects of gasification atmosphere and temperature on char structural evolution during the gasification of Collie sub-bituminous coal, Fuel, 117 (2014) 1190-1195.

[46] S. Krerkkaiwan, C. Fushimi, H. Yamamoto, A. Tsutsumi, P. Kuchonthara, Influences of heating rate during coal char preparation and AAEMs on volatile–char interaction with different sources of biomass volatile, Fuel Processing Technology, 119 (2014) 10-18.

[47] S. Xu, Z. Zhou, J. Xiong, G. Yu, F. Wang, Effects of alkaline metal on coal gasification at pyrolysis and gasification phases, Fuel, 90 (2011) 1723-1730.

[48] X. Li, H. Wu, J.-i. Hayashi, C.-Z. Li, Volatilisation and catalytic effects of alkali and alkaline earth metallic species during the pyrolysis and gasification of Victorian brown coal. Part VI. Further investigation into the effects of volatile-char interactions, Fuel, 83 (2004) 1273-1279.

[49] C. Fushimi, T. Wada, A. Tsutsumi, Inhibition of steam gasification of biomass char by hydrogen and tar, Biomass and Bioenergy, 35 (2011) 179-185.

[50] L.J. McKenzie, F.-J. Tian, C.-Z. Li, Effects of volatile–char interaction on the formation of HCN and NH_3 during the gasification of Victorian brown coal in O_2 at 500 ˚C, Fuel, 85 (2006) 2148-2154.

[51] S. Zhang, J.-i. Hayashi, C.-Z. Li, Volatilisation and catalytic effects of alkali and alkaline earth metallic species during the pyrolysis and gasification of Victorian brown coal. Part IX. Effects of volatile-char interactions on char-H_2O and char-O_2 reactivities, Fuel, 90 (2011) 1655-1661.

[52] S. Zhang, Z. Min, H.-L. Tay, M. Asadullah, C.-Z. Li, Effects of volatile–char interactions on the evolution of char structure during the gasification of Victorian brown coal in steam, Fuel, (2011) 1529-1535.

Every reasonable effort has been made to acknowledge the owners of copyright material. I would be pleased to hear from any copyright owner who has been omitted or incorrectly acknowledged.

Chapter 2

Second-order Raman spectroscopy of char during gasification

2.1 Introduction

Gasification is an effective method to convert a solid fuel into a high value gaseous fuel [1]. An important aspect of gasification is the reaction between char and gasifying agents to produce syngas [2]. This is a heterogeneous gas-solid reaction and is very complicated as a result of changes in the char structure during gasification [2,3]. Therefore, understanding the transformation of structural feature of char during gasification and the effects of char structure on its gasification reactivity is critically important for a better understanding of the gasification mechanisms [4-7].

Raman spectroscopy has been widely used as a powerful tool to characterise various carbonaceous materials due to its ability to response to symmetric vibration of less or non-polar bonds [8,9]. A Raman spectrum represents the scattering due to many types of distinctly different bonds in the char. There are two Raman spectral regions, in the ranges of ~ 800 to 1800 cm^{-1} (first order) and ~ 2000 to 3300 cm^{-1} (second order), that are of interests in understanding the structural features of a carbonaceous material. Much has been done to investigate the char structure through deconvolution and analysis of various bands in the first-order Raman spectra [10-15]. Like a first-order Raman spectrum, a second-order Raman spectrum is also the summation of scattering from many bonds. If deconvoluted properly, a second-order spectrum can also provide additional detailed information about the skeletal structure of a carbon-based material. However, second-order Raman spectroscopy has been mainly used for the characterisation of highly ordered carbon materials such as graphite [9,16,17]. Little study has been carried out on the highly disordered carbon materials such as chars from the pyrolysis and gasification of coal and biomass. Even for some research that analysed the second-order Raman spectrum of some highly disordered carbon materials [18-25], most samples have undergone a high temperature treatment (higher than 1000 ˚C) [18,19,24,25], resulting in the samples have become crystallisation and graphitization. Therefore, the second-order Raman spectra of such samples were simply deconvoluted into three or four bands and the interpretation of these bands follow the bands assignment of highly ordered carbon materials [19-25].

Obviously, the second-order spectra of chars from the pyrolysis and gasification process (<1000 ˚C) differ considerably from that of highly ordered materials or highly graphitized materials. A simple adoption of the concept of bands in the second-order spectra for highly ordered carbon materials would be very inappropriate for the analysis of char structure. Unlike the second-order spectra of graphite-like materials that exhibit a clearly-resolved strong peak of 2D (overtone of D band) and a peak of D+G (combination of D band and G band) [9,16,17], the second-order spectrum of a char could show a very broad band. The overlaps between the 2D and D+G bands as well as the shoulders at the two sides of the 2D and D+G broad bands in the second-order Raman spectrum of a char could contain much information about the structural feature of the char. Therefore, instead of just considering the 2D and G+D bands, the second-order Raman spectrum could be deconvoluted into more bands in order to acquire detailed information about the chemical structure of the char. In addition, because of the differences in crystal structure between graphite and amorphous carbon, simple applications of the interpretation of the second-order Raman spectra of highly ordered materials to chars would result in some misleading information and miss some important information about the skeletal carbon structures.

In our previous study [26], a WA Collie sub-bituminous coal was gasified at different temperatures (800, 850 and 900 ˚C) in atmospheres containing steam and CO_2. The Raman spectra of char samples collected after varying extents of gasification were acquired by using a laser with a wavelength of 1,064 nm [11,26]. In this study, the same spectra in the second-order region have been analysed. Compared with our previous work [4,6,7,11-15,26] which mainly focused on the analysis of the first-order Raman spectra, a new spectral deconvolution method for the Raman spectra in the second-order region was established in order to acquire detailed information about the changes in char structure during gasification. The information about char structure from the second-order region is compared with that of the first-order region and complementary or additional information was found through analysis of the second-order Raman spectra.

2.2 Experimental

2.2.1 Gasification of coal

The details of the gasification experiments have been presented previously [26]. Briefly, Collie sub-bituminous coal, supplied by the Muja Power Station in Western Australia, was used. It has an ultimate composition of 75.7% C, 4.5% H, 1.4% N, 0.5% S and 17.9% O [26]. The gasification experiments were carried out in a fluidised-bed/fixed-bed reactor [26,27] with coal particles being heated up rapidly.

2.2.2 Char characterisation

The acquisition of Raman spectra of chars were detailed before [26]. The same spectra were used in this study. Briefly, a Perkin-Elmer Spectrum GX FT-IR/Raman spectrometer with an excitation laser of 1064 nm was used to acquire the Raman spectra of chars [11,26]. A char sample was firstly ground into powder and then diluted and ground with spectroscopic grade KBr [11,26]. The char concentration of 0.25 wt% in KBr-char mixture exhibited the plateau total Raman intensity in the first-order Raman region [26]. The total Raman peak area in the second-order Raman region had also reached the plateau with this char concentration as shown in Figure 2-1. An InGaAs detector was used to collect Raman scattering using a back scattering configuration [11,26]. Each spectrum represents the average of 200 scans and the spectral resolution was 4 cm^{-1} [11,26]. Baseline correction was carried out on each spectrum using the software provided by Perkin-Elmer with the spectrometer [11,26]. The first-order and second-order regions had different baselines.

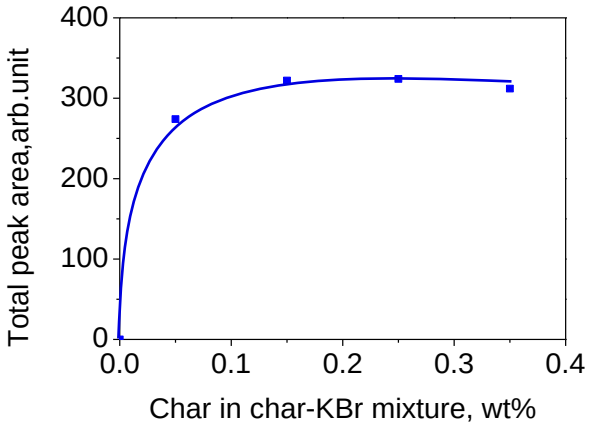

Figure 2-1. Effects of char concentration in char-KBr mixture on the total second-order Raman area (2000-3300 cm^{-1}). Char was prepared from the gasification of the Collie sub-bituminous coal in 15% H_2O balanced with Ar at 900 ˚C.

2.3 Deconvolution and band assignment of the second-order Raman spectra

The second-order Raman spectra of chars in the range between 2000 and 3300 cm^{-1} were curve-fitted with 7 mixed Gaussian and Lorentz bands using the GRAM/32 software. The position and assignment of these 7 bands are briefly summarized in Table 2-1, which we believe represent the typical structural features of chars from the pyrolysis and gasification of coal and biomass.

In the second-order spectra of sp^2 carbon materials, there is a strong Raman feature appearing in the range of 2500-2700 cm^{-1}, and it is called the 2D band to mean that it is the overtone of D band in the first-order region [9,16,17]. In the study of the second-order Raman spectra of highly ordered carbonaceous materials, the 2D band was considered to originate from a double resonance, involving two iTO phonons near the *K* point of the unit cell [9]. The intensity of the 2D band was believed to be related to the number of grapheme layers and the stacking order [9,16,17]. Unlike the defect-induced D band in the first-order region, the 2D band does not indicate any kinds of disorder or defect for the graphite-like material [9,16,17,28,29]. However, the "crystal" structure of char is quite different from the graphite-like carbon materials. Chars from the pyrolysis and gasification of coal and biomass are highly

disordered carbonaceous materials with a wide variety of O-containing groups and sp^2-sp^3 or sp^3-sp^3 cross-linking structures [11]. According to the bands assignment for the highly dis-ordered materials [11], the D band mainly represents aromatics with not less than 6 rings. For graphitic materials, the D band and 2D band come from two different physical scattering processes so there is no direct relationship in band intensity between these two bands [9,16,17,28,29]. However, a char from the gasification of coal or biomass does not have similar lattice structure and therefore its D and 2D bands do not necessarily originate from two scattering processes. Based on the vibrational theory of the overtone process for chemical structures [8,30], it is believed that the D band and the 2D band come from the same vibration mode for the amorphous carbon materials. Therefore, the interpretation of the 2D band in the second-order spectra of char should be the same as the D band in the first-order [11], i.e. representing the large aromatic ring systems (no less than 6 fused rings). It is also expected to have close relationship with the D band in term of the band intensity in the second-order Raman spectra.

Another main band in the second-order spectra of carbonaceous materials is the D+G band located in the range of 2800-2950 cm^{-1} with an exciting laser in the visible range [16,17,24,25]. In the study of the highly ordered carbon materials, this band is considered as a disorder-induced band and would disappear with increasing crystallinity [16,24]. Amorphous carbon materials such as char from gasification would not have a band of the same nature in their second-order spectra. Instead, in this study, the D+G band is assigned to the aromatic ring structures of amorphous carbon materials.

Table 2-1. Summary of peak/band assignment**.**

Band Name	Position, cm^{-1}	Description	Bond type	References
2G	3180	Overtone of G band; aromatic rings	sp^2	11,17, this work
$(D+G)_L$	3060	Aryl CH stretch vibration	sp^2	23
D+G	2860	Combination of D band and G band; aromatic rings	sp^2	11,17,24, this work
$2V_R$	2750	Overtone of the aryl CH_3 in-phase bend vibration; amorphous carbon structures	sp^2; sp^3	23
$(2D)_L$	2650	Small aromatic rings system; amorphous carbon structures	sp^2; sp^3	This work
2D	2560	Overtone of D band; C-C between aromatic rings; large aromatic rings system	sp^2	11,17,24, this work
2S	2350	Overtone of S band; $C_{aromatic}$-C_{alkyl}; C-C on hydroaromatic rings;	sp^2; sp^3	11,17, this work

Different from the graphite-like materials, vast amounts of spectral residue would be left if only 2D and D+G bands were considered to deconvolute the second-order Raman spectra of chars. Based on the spectra of some model aromatic compounds [30] and considering the structure of char from coal/biomass gasification process [11-15], two bands have been assigned in the region between the 2D band and D+G band. One is the overtone of the fundamental vibrations of aryl methyl functional groups at around 2750 cm^{-1} [30] and named as $2V_R$ (in order to correspond with the band name V_R in the first-order [11]). The other is the $(2D)_L$ band (standing for 2D left) at around 2650 cm^{-1}. These two bands are mainly found in amorphous carbon materials [24,25,30]. In this case, $2V_R$+$(2D)_L$ can represent the small aromatic ring systems, and it is believed to decrease with the condensation of aromatic ring

systems according to some Raman spectra of amorphous carbon materials that have been heat-treated at high temperature [24,25].

In addition, there is a weak peak [16,25,31,32] in the range of 2350-2500 cm^{-1} that can be found in the second-order Raman spectra of some highly ordered carbon materials by an exciting laser in the visible range, showing no dispersive behaviour with different laser excitation energy [31,32]. Some believe that this band is related to 2LO phonons second-order scattering [31], while others explain that this band originates from the combination of the D band and the modulation around 1100 cm^{-1} [32]. Based on the band assignment in the first-order Raman spectra [11], in the second-order Raman spectra of chars by an exciting laser at 1064 nm, the frequency of this band is almost twice of that of the S band. Therefore, in this study, this band is assigned to the overtone of S band, named as 2S band, indicating the sp^3-rich structures, sp^2-sp^3 carbonaceous structures and other cross-linking structures in char.

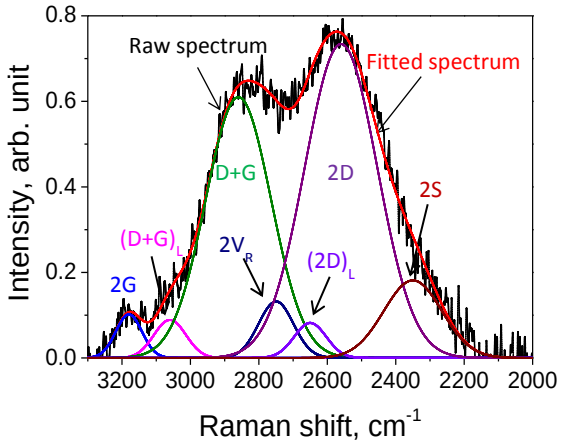

Figure 2-2. Spectral deconvolution of a Raman spectrum (second-order region) of the char from the gasification of the Collie sub-bituminous coal in 15% H_2O balanced with Ar at 900 ˚C.

In addition to the five bands assigned above, other two bands, a $(D+G)_L$ band (standing for D+G band left) at 3060 cm^{-1} [28] and a 2G band (overtone of G band) at 3180 cm^{-1} [16,25], were assigned to the aryl CH vibration and aromatic ring structures respectively.

During spectral deconvolution, band positions were fixed whilst different maximum limits were applied to restrain the bandwidths. A typical example of the spectral deconvolution/curve-fitting of a second-order Raman spectrum of char using the 7 bands is shown in Figure 2-2. Similar degrees of successful curve-fitting can be found for all other char samples investigated in this study.

Although the second-order Raman spectra of chars were curve-fitted with 7 bands, the discussion of Raman spectroscopic data will be mainly focused on three bands, 2D, $2V_R+(2D)_L$ and 2S, which represent the main chemical structure in char and are much sensitive to the structural changes. D+G band and two other minor bands, 2G and $(D+G)_L$, actually represent the typical aromatic structures in carbon-based materials and are less sensitive to the structural changes. Thus, they will not be discussed further here.

2.4 Results and discussion

2.4.1 Total peak areas of the second-order Raman spectra of chars from the gasification of WA Collie sub-bituminous coal

The observed Raman intensity would be affected by both Raman light scattering ability and the light absorption ability of char. In the first-order region, the electron-rich structures such as the O-containing groups in char tend to have high Raman scattering ability mainly due to the resonance effect between O and O-connected aromatic ring [11]. Therefore, their presence tends to increase the total first-order Raman intensity [11]. On the other hand, the increasing condensation of the aromatic ring systems in char would increase the light absorptivity and thus tends to decrease the observed Raman intensity [11].

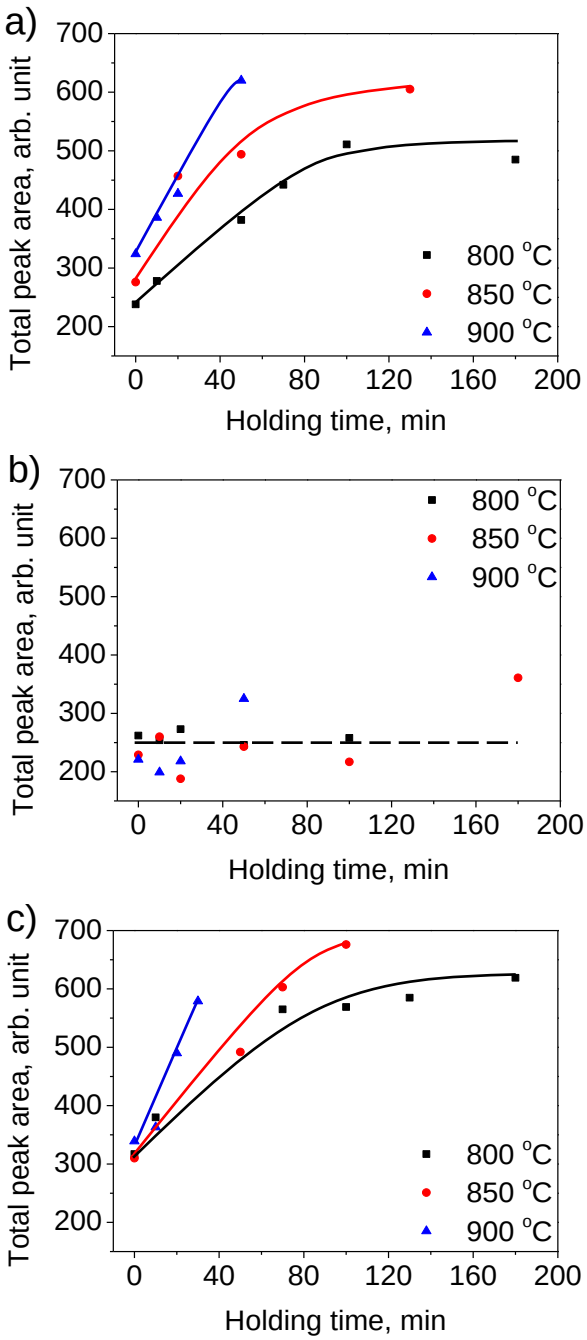

Figure 2-3. Total second-order Raman area as a function of holding time for the chars from the gasification of Collie sub-bituminous coal at 800, 850 and 900 ˚C in (a) 15% H_2O balanced with Ar; (b) pure CO_2; (c) 15% H_2O balanced with CO_2.

The presence of O-containing structures and the condensation of aromatic ring systems are expected to have effects on the observed second-order Raman intensity similar to those in the first order region. Figure 2-3 exhibits the total peak areas of the second-order Raman spectra in the region of 2000-3300 cm^{-1}, considered as the total second-order Raman intensity, of chars as a function of the gasification holding time. For the chars produced from the gasification in steam-containing atmospheres (15% H_2O-Ar and 15% H_2O-CO_2), the total second-order Raman intensity increased with increasing gasification temperature and holding time. However, the second-order total Raman intensity is almost constant (with large scatters) for the chars produced from the gasification in pure CO_2. These results are consistent with the first-order Raman data [26]. These two different behaviours in terms of the total Raman intensity indicate that the gasification reaction mechanisms of char in H_2O and CO_2 atmospheres are different [26]. The results suggest that the oxygen-containing species derived from steam increased the O-containing groups in char [26]. With increasing holding time and gasification temperature, more and more O-containing groups have formed, hence increasing the total Raman peak areas of chars obtained from the gasification in steam-containing atmospheres. While for CO_2 gasification, the concentration of such structure is almost constant (with large scatters). In addition, the generally lower total Raman peak areas of chars from gasification in CO_2 indicate that the concentration of O-containing groups in char must be lower for gasification in CO_2 than that in steam.

2.4.2 Ratios of some major bands to the total Raman intensity in the second-order spectra

2.4.2.1 The ratio of the 2D band to the total second-order Raman peak area

As are exhibited in Figure 2-4, for the chars produced from the gasification in steam-containing atmospheres, a higher temperature resulted in a higher I_{2D}/I_{Total} ratio, indicating the growth in the relative concentrations of large aromatic ring systems in char. In addition, with increasing gasification holding time, the I_{2D}/I_{Total} ratio increased initially before it reached a plateau. The same results can also be found in

the first-order Raman in term of the I_D/I_{Total} ratio [26]. However, the change of such intensity ratio is not obvious for the chars from CO_2 gasification in the second-order

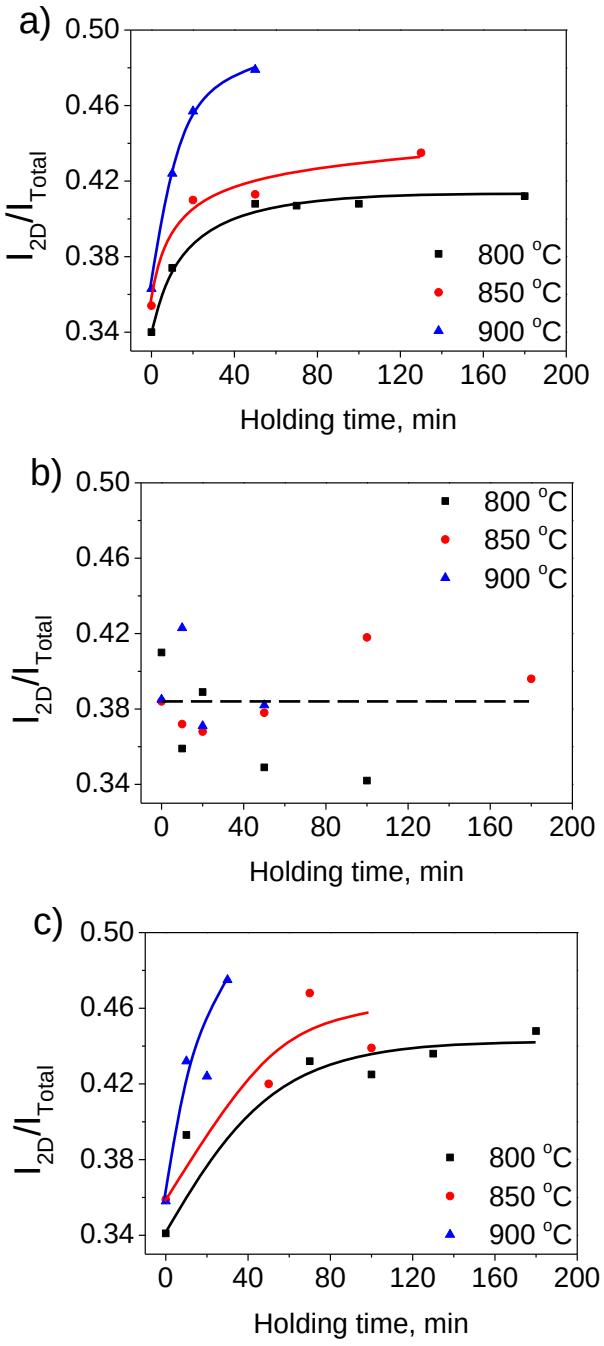

Figure 2-4. Raman band area ratios 2D/Total as a function of holding time for the chars from the gasification of Collie sub-bituminous coal at 800, 850 and 900 ˚C in (a) 15% H_2O balanced with Ar; (b) pure CO_2; (c) 15% H_2O balanced with CO_2.

Raman, possibly because of the low total Raman intensity, and thus the low signal-to-noise ratios for the chars from the gasification in CO_2. Actually, in the first-order Raman, the I_D/I_{Total} ratio increased with increasing gasification temperature and holding time for the chars from CO_2 gasification [26].

2.4.2.2 The ratio of the $2V_R+(2D)_L$ band to the total Raman intensity

The overlap between the 2D band and the D+G band has been deconvoluted into $2V_R$ band and $(2D)_L$ band, the intensity of these two bands can be taken as a brief reflection of the concentrations of smaller aromatic ring systems in char.

As is shown in Figure 2-5, the decreases in the band ratio $I_{2VR+(2D)L}/I_{Total}$ for chars from the gasification in steam-containing atmospheres indicate that the relative concentrations of small aromatic ring systems decreased with increasing gasification temperature and holding time. These results are consistent with the first-order Raman data [26] and suggest that the smaller aromatic ring systems were either preferentially consumed by gasification or converted into large ones during gasification [13-15,26]. On the other hand, for the chars from CO_2 gasification, there is no obvious trend except a possible decrease in the band ratio $I_{2VR+(2D)L}/I_{Total}$ with increasing gasification temperature from 800 to 900 ˚C. However, the relative band ratio $I_{(Gr+Vl+Vr)}/I_{Total}$ in the first-order Raman decreased with increasing gasification temperature and holding time [26]. This difference is also possibly because of the low signal-to-noise ratios in the second-order Raman for the chars from the gasification in CO_2, which made it difficult to resolve weak trends in band area ratios. In addition, the relative concentrations of small aromatic rings in the chars from gasification in CO_2 were higher than those in the chars from gasification in steam-containing atmospheres, also demonstrating that the presence of H radicals from H_2O dissociation can enhance the transition from the relatively small to large aromatic ring systems in char as we revealed in the previous studies [14,15,26].

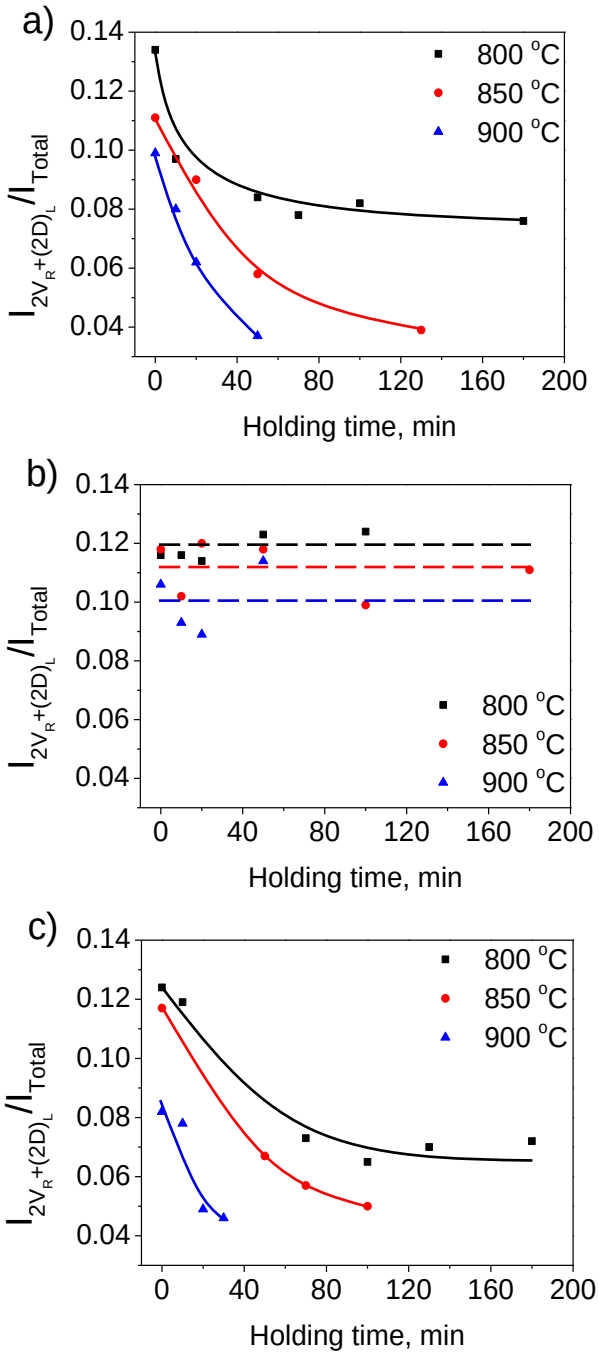

Figure 2-5. Raman band area ratios $2V_R+(2D)_L$/Total as a function of holding time for the chars from the gasification of Collie sub-bituminous coal at 800, 850 and 900 ˚C in (a) 15% H_2O balanced with Ar; (b) pure CO_2; (c) 15% H_2O balanced with CO_2.

2.4.2.3 The ratio of the 2D band to the $2V_R+(2D)_L$ band

The Raman band area ratio $I_{2D}/I_{2VR+(2D)L}$ can be used as a more direct indication of the transition of small to large aromatic ring systems in char samples. As shown in Figure 2-6, for the chars produced from the gasification in steam-containing atmospheres, this band area ratio increased with increasing gasification temperature and holding time, which indicate that small aromatics are gradually consumed and/or converted into large ones in char structure. The same trends can also be found in the related ratio $I_D/I_{(Gr+Vl+Vr)}$ in the first-order Raman spectral data [26]. Moreover, the intensity ratio $I_{2D}/I_{2VR+(2D)L}$ of the char from the gasification in pure CO_2 was lower than the char from the gasification in the steam-containing atmospheres. This can also be explained by considering that the H radicals generated by H_2O could penetrate into char matrix and induce the condensation of the aromatic rings [14,15,26], thereby increasing the relative concentrations of large aromatic ring systems in char structure.

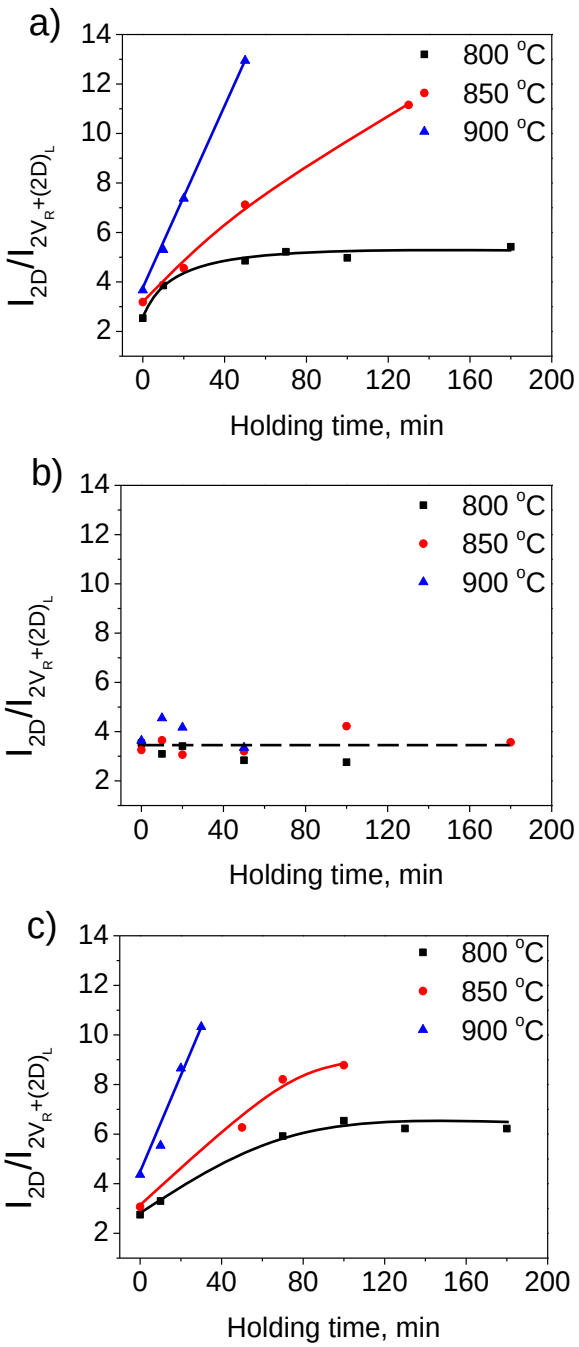

Figure 2-6. Raman band area ratios $2D/2V_R+(2D)_L$ as a function of holding time for the chars from the gasification of Collie sub-bituminous coal at 800, 850 and 900 ˚C in (a) 15% H_2O balanced with Ar; (b) pure CO_2; (c) 15% H_2O balanced with CO_2.

2.4.2.4 The ratio of the 2S band to the total Raman intensity

The intensity of 2S band can be used as indication of the sp^3-rich structures such as alkyl-aryl C-C structures, the crossing-linking density as well as the substitutional groups (other than O-containing ones) in char. However, unlike the S band that increased with the increasing crossing-linking density of char, lots of studies indicate that the bandwidth as well as the intensity of 2S band decreased with the increasing crystallinity of the carbon-based materials [19,22,31].

From Figure 2-7, it can be seen that, for the gasification in steam-containing atmosphere, the intensity ratio I_{2S}/I_{Total} decreased from 800 to 900 ˚C, and also showed a decrease with increasing holding time and then achieved a plateau value. These results suggested that high temperature and long reaction time tend to enhance the structural compactness of char. There were much less changes in the intensity ratio I_{2S}/I_{Total} if the holding time is long enough, indicating that the amount of such crossing-linking structure in char reached a dynamic balance between their generation and consumption. For the chars from CO_2 gasification, there is no clear trend for the ratio I_{2S}/I_{Total}, and the data show obvious fluctuations. This is also because that the total Raman intensity of the second-order as well as the 2S band is very weak for the chars from CO_2 gasification, giving rise to high noise-to-signal ratios and causing some inaccuracy during curve-fitting.

An important difference between the first-order and second-order Raman spectra of chars from gasification in steam-containing atmospheres is that the ratio I_S/I_{Total} in the first-order Raman did not change clearly with gasification temperature and holdings time while the ratio I_{2S}/I_{Total} in the second-order Raman showed a decrease with increasing gasification temperature and holding time. It should be noted that there is less interference from the neighbouring bands in the analysis of the intensity of 2S band than that with the S band. Not all peaks in the region of the first-order region have their corresponding peaks in the second-order region, which has facilitated the spectral deconvolution of some bands such as 2S band. Therefore, the

second-order Raman spectra can provide additional details about the changes in char structure.

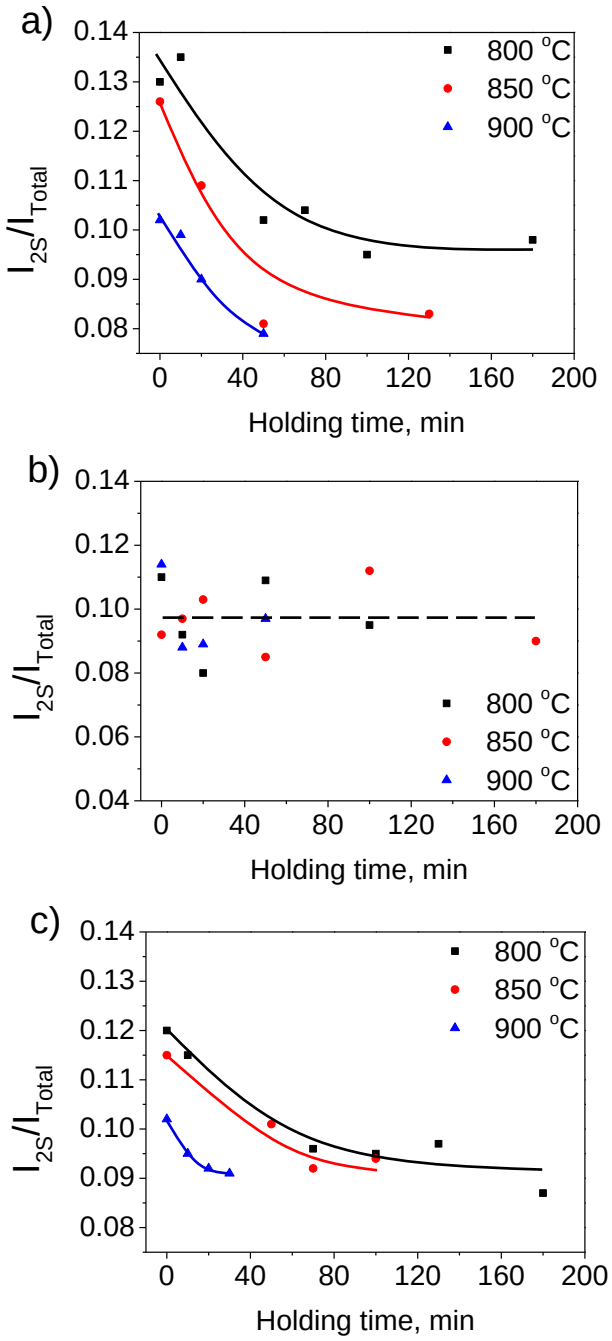

Figure 2-7. Raman band area ratios 2S/Total as a function of holding time for the chars from the gasification of Collie sub-bituminous coal at 800, 850 and 900 ˚C in (a) 15% H_2O balanced with Ar; (b) pure CO_2; (c) 15% H_2O balanced with CO_2.

2.5 Conclusions

This study has demonstrated that the second-order Raman spectroscopy can be used as a powerful technique to analyse the skeletal structure of highly disorder carbon-based materials such as the chars from the gasification of Collie sub-bituminous coal. A novel deconvolution method has been established and the second-order Raman spectra of chars were curved-fitted with 7 bands representing the typical chemical structures in the char.

During the gasification in steam-containing atmospheres, the relative contents of O-containing groups and large aromatic ring systems in char increased, while the relative contents of small aromatic ring systems decreased as gasification proceeded. These results are consistent with the findings in the first-order Raman analysis. However, the second-order spectra of chars from gasification in CO_2 showed high noise-to-signal ratio than the first-order Raman spectra, making the spectral deconvolution of the second-order spectra less reliable than that of the first-order spectra.

Compared with the first-order Raman results, additional information is found in the second-order Raman spectra of chars from the gasification in steam-containing atmospheres. The area ratio I_S/I_{Total} of char did not change clearly with gasification temperature in the first-order Raman spectroscopy. However, there is a significant change with gasification temperature and holding time in the ratio of the overtone of S band (I_{2S}) in the second-order Raman spectroscopy, indicating that the structural compactness of char increased as gasification proceeded.

The second-order Raman spectroscopy of chars from the gasification in CO_2 and H_2O atmospheres indicates that the gasification mechanisms of char in these two atmospheres are different, confirming our earlier conclusions.

2.6 References

[1] C.-Z. Li, Special issue-gasification: A route to clean energy, Process Safety and Environmental Protection, 84 (2006) 407-408.

[2] C.-Z. Li, Importance of volatile-char interactions during the pyrolysis and gasification of low-rank fuels – A review, Fuel, 112 (2013) 609-623.

[3] C.-Z. Li, Some recent advances in the understanding of the pyrolysis and gasification behaviour of Victorian brown coal, Fuel, 86 (2007) 1664-1683.

[4] D.M. Keown, J.-I. Hayashi, C.-Z. Li, Drastic changes in biomass char structure and reactivity upon contact with steam, Fuel, 87 (2008) 1127-1132.

[5] X. Li, H. Wu, J.-I. Hayashi, C.-Z. Li, Volatilisation and catalytic effects of alkali and alkaline earth metallic species during the pyrolysis and gasification of Victoria brown coal. Part VI. Further investigation into the effects of volatile-char interactions, Fuel, 83 (2004) 1273-1279.

[6] X. Li, J.-I. Hayashi, C.-Z. Li, Volatilisation and catalytic effects of alkali and alkaline earth metallic species during the pyrolysis and gasification of Victoria brown coal. Part VII. Raman spectroscopic study on the changes in char structure during the catalytic gasification in air, Fuel, 85 (2004) 1509-1517.

[7] X. Li, C.-Z. Li, Volatilisation and catalytic effects of alkali and alkaline earth metallic species during the pyrolysis and gasification of Victoria brown coal. Part VIII. Catalysis and changes in char structure during gasification in steam, Fuel, 85 (2006) 1518-1525.

[8] F. Tuinstra, J.L. Koeing, Raman spectrum of graphite, Journey of Chemical Physics, 53 (1970) 1126-1130.

[9] L.M. Malard, M.A. Pimenta, G. Dresselhaus, M.S. Dresselhaus, Raman spectroscopy in grapheme, Physics Reports, 473 (2009) 51-87.

[10] C.A. Johnson, J.W. Patrick, K.M. Thomas, Characterization of coal chars by Raman spectroscopy, X-ray diffraction and reflectance measurements, Fuel, 65 (1986) 1284-1290.

[11] X. Li, J.-I. Hayashi, C.-Z. Li, FT-Raman spectroscopic study of the evolution of char structure during the pyrolysis of a Victorian brown coal, Fuel, 85 (2006) 1700-1707.

[12] H.-L. Tay, C.-Z. Li, Changes in char reactivity and structure during the gasification of a Victorian brown coal: Comparison between gasification in O_2 and CO_2, Fuel Processing Technology, 91 (2010) 800-804.

[13] H.-L. Tay, S. Kajitani, S. Zhang, C.-Z. Li, Effects of gasifying agent on the evolution of char structure during the gasification of Victoria brown coal, Fuel, 103 (2013) 22-28.

[14] D.M. Keown, X. Li, J.-I. Hayashi, C.-Z. Li, Evolution of biomass char structure during oxidation in O_2 as revealed with FT-Raman spectroscopy, Fuel Processing Technology, 89 (2008) 1429-1435.

[15] X. Guo, H.-L. Tay, S. Zhang, C.-Z. Li, Changes in char structure during the gasification of a Victoria brown coal in steam and oxygen at 800 ˚C, Energy & Fuels, 22 (2008) 4034-4038.

[16] S. Vollebregt, R. Ishihara, F.D. Tichelaar, Y. Hou, C.I.M. Beenakker, Influence of the growth temperature on the first and second-order Raman band ratios and widths of carbon nanotubes and fibers, Carbon, 50 (2012) 3542-3554.

[17] M.S. Dresselhaus, A. Jorio, M. Hofmann, G. Dresselhaus, R. Saito, Perspectives on carbon nanotubes and graphene Raman spectroscopy, Nano Letters, 10 (2010) 751-758.

[18] S. Dong, P. Alvarez, N. Paterson, D.R. Dugwell, R. Kandiyoti, Study on the effect of heat treatment and gasification on the carbon structure of coal chars and metallurgical cokes using Fourier Transform Raman Spectroscopy, Energy & Fuels, 23 (2009) 1651-1661.

[19] A. Zaida, E. Bar-Ziv, L.R. Radovic, Y.-J. Lee, Further development of Raman microprobe spectroscopy for characterization of char reactivity, Proceeding of the Combustion Institute, 31 (2007) 1881-1887.

[20] J. Jehlicka, C. Beny, First and second order Raman spectra of natural highly carbonified organic compounds from metamorphic rocks, Journal of Molecular Structure, 480-481 (1999) 541-545.

[21] H.J. Seong, A.L. Boehman, Evaluation of Raman parameters using visible Raman microscopy for soot oxidative reactivity, Energy & Fuels, 27 (2013) 1613-1624.

[22] A. Sadezky, H. Muckenhuber, H. Grothe, R. Niessner, U. Poschl, Raman microspectroscopy of soot and related carbonaceous materials: Spectral analysis and structural information, Carbon, 43 (2005) 1731-1742.

[23] A. Cuesta, P. Dhamelincourt, J. Laureyns, A. Martinez-Alonso, J.M.D. Tascon, Raman microprobe studies on carbon materials, Carbon, 32 (1994) 1523-1532.

[24] Y.-J. Lee, The second order Raman spectroscopy in carbon crystallinity, Journal of Nuclear Materials, 325 (2004) 174-179.

[25] S. Bernard, O. Beyssac, K. Benzerara, N. Findling, G. Tzvetkov, G.E. Brown, XANES, Raman and XRD study of anthracene-based cokes and saccharose-based chars submitted to high-temperature pyrolysis, Carbon, 48 (2010) 2506-2516.

[26] T. Li, L. Zhang, L. Dong, C.-Z. Li, Effects of gasification atmosphere and temperature on char structural evolution during the gasification of Collie sub-bituminous coal, Fuel, 117 (2014) 1190-1195.

[27] D.M. Quyn, H. Wu, J.-I. Hayashi, C.-Z. Li, Volatilisation and catalytic effects of alkali and alkaline earth metallic species during the pyrolysis and gasification of Victoria brown coal. Part IV. Catalytic effects of Nacl and ion-exchangeable Na in coal on char reactivity, Fuel, 2 (2003) 587-593.

[28] M. Ramsteiner, J. Wagner, Resonant Raman scattering of hydrogenated amorphous carbon: Evidence for π-bonded carbon clusters, Applied Physics Letters, 51 (1987) 1355-1357.

[29] M.J. Matthews, M.A. Pimenta, G. Dresselhaus, M.S. Dresselhaus, M. Endo, Origin of dispersive effects of the Raman D band in carbon materials, Physical Review B, 59 (1999) 6585-6588.

[30] P. Larkin, Infrared and Raman spectroscopy: principles and spectral interpretation, Elsevier, Oxford, 2010.

[31] T. Shimada, T. Sugai, C. Fantini, M. Souza, L.G. Cancado, A. Jorio, M.A. Pimenta, R. Saito, A. Grüneis, G. Dresselhaus, M.S. Dresselhaus, Origin of the 2450 cm^{-1} Raman bands in HOPG, single-wall and double-wall carbon nanotubes, Carbon, 43 (2005) 1049-1054.

[32] P. Tan, Y. Deng, Q. Zhao, Temperature-dependent Raman spectra and anomalous Raman phenomenon of highly oriented pyrolytic graphite, Physical Review B, 58 (1998) 5435-5439.

Chapter 3

Effects of particle size and gasification atmosphere on the changes in char structure during the gasification of mallee biomass

3.1 Introduction

With the depletion of fossil fuel resources and the rising concerns about global warming, biomass as a renewable energy source has received a great deal of interests in recent years due to its abundance and low environmental impacts [1-2]. Biomass gasification is an effective technology to convert solid biomass into a gaseous fuel for further use [3-6]. However, biomass gasification must overcome some practical problems before its widespread commercial implementation. One of the problems is the size range of the feedstock [7-11]. It is impossible to obtain a specified narrow biomass particle size range as the feedstock for a practical gasifier/pyroliser because the size reduction of biomass will be very labour-intensive and time-consuming, making it commercially unattractive [12]. Therefore, the feedstock for a commercial gasifier necessarily consists of particles with a wide range of sizes [12].

Gasification rate is a major consideration in the design and operation of a practical gasifier because it would determine the overall efficiency and economic feasibility of the gasifer [12-17]. The evolution of char structure is an important factor that can influence the gasification behaviour [1,2]. Therefore, understanding the influence of biomass particle size on the ultimate char yield and the structural feature of char during gasification is significantly important for the development of gasification technologies.

Conceptually, the gasification process consists of two consecutive steps [2]. The first step is the biomass devolatilisation, leaving behind a carbon-enriched solid char. Because of the high contents of oxygen and aliphatic moieties of biomass, large amounts of volatile precursors would be formed in this step [2,18,19]. This new formed volatile precursors could lead to the deposition reaction in char matrix [20-23]. Because there are differences in the heating transfer resistance as well as the intra-particle mass transfer resistance between small and large particles, the deposition reaction would be more severe for large particles [21-26]. The second step is the bio-char gasification and volatiles reforming through their reactions with gasifying agents. The difference in the intra-particle diffusion of the gasifying agent

between small and large particles might also have an effect on the gasification rate and the overall char structure.

Some studies have been carried out to investigate the effect of biomass particle sizes on the evolution of char structure as revealed by the Raman spectroscopy [20-23]. Mohammad and co-workers reported that biomass particle size would greatly influence the char yield during pyrolysis [20,21], and this could be mainly responsible for the different char yield during gasification of biomass with different particle sizes in steam atmosphere [22]. Shu and co-workers [23] reported that, based on the negligibly small influence of the biomass particle size on the change in char structure during gasification in steam atmosphere, the gasification might take place uniformly throughout the whole particles. However, these researches did not provide the direct evidence that whether the size of bio-char produced from the biomass devolatilisation would affect the ultimate char yield and char structures during the subsequent gasification. In other words, the effect of intra-particle diffusion of the gasifying agent between small and large particles during gasification has not been directly investigated. Char-H_2O gasification and char-CO_2 gasification are both fundamentally important reactions. A better understanding the mechanisms of the char-H_2O reaction and char-CO_2 reaction is necessary for the development of gasification technologies [27]. One question raised is: does biomass particle size affect the evolution of char structure during the gasification in steam atmosphere and CO_2 atmosphere. Therefore, investigation on the gasification behaviour of different biomass particle sizes in steam atmosphere and CO_2 atmosphere can provide another aspect to understand the char-H_2O and char-CO_2 reaction mechanism. In addition, second-order Raman spectroscopy can also be used to characterise the char structure [28]. Complementary or additional information about the structural feature of char can be found through that analysis of the second-order Raman spectra.

The objective of this research is to comprehensively investigate the influence of biomass particle size and gasification atmosphere on the ultimate char yield as well as the evolution of char structure, especially in the aspect of the intra-particle diffusion of the gasifying agent during gasification of bio-char with different particle

sizes. As discussed above, the devolatilisation and the gasification might be both influenced by the biomass particle size. In order to clarify these two possibilities, two series of experiments were carried out in this study. The first series was the gasification of biomass with different particle sizes at the temperatures from 700 to 900 ˚C in two atmospheres: 15 % H_2O balance with Ar and pure CO_2. The other series was the bio-char gasification experiments, which would separate the biomass devolatilisation step and bio-char gasification step during gasification. The collected char samples were analysed with a FT-Raman spectrometer both in the first-order Raman spectra and second-order Raman spectra to obtain information about the chemical structure features of the chars.

3.2 Experimental

3.2.1 Sample preparation

Australia mallee wood was used as the feedstock in this research. It has a proximate analysis of 0.9 wt% ash yield and 81.6 wt% volatiles yield together with an ultimate composition of 48.2 wt% C, 6.1 wt% H, 0.2 wt% N and 45.5 wt% O (dry and ash-free basis) [20-23]. The preparation of the wood sample can be found elsewhere [20-23]. Briefly, the mallee wood was firstly debarked and crushed into chips using a cutting mill and then eight wood samples with different particle sizes were obtained by sieving. The particle sizes of the eight wood samples are as follow: 0.18-0.40, 0.40-0.80, 0.80-1.00, 1.00-2.00, 2.00-3.35, 3.35-4.00, 4.00-4.75, 4.75-5.60 mm. All biomass samples were stored in a freezer to avoid any biological degradation and the samples were dried in oven overnight at 105 ˚C before the experiment.

3.2.2 Gasification

Biomass gasification experiments were carried out in a modified fluidised-bed quartz reactor [20]. The schematic diagram of the modified fluidized-bed reactor is shown in Figure 3-1 and the description of the reactor can be found elsewhere [20]. Briefly, the reactor was heated up to the target temperature (700, 800 or 900 ˚C) with an

external furnace together with the introduction of the gasifying agent (15 % H_2O balance with Ar or pure CO_2) into the reactor. When all the parameters were stabilised, about 2 g biomass (weighed accurately) was fed into the reactor within 4 minutes. The reactor was lifted out of the furnace immediately when the feeding was completed and was cooled down naturally with argon flowing inside the reactor instead of the gasifying agent.

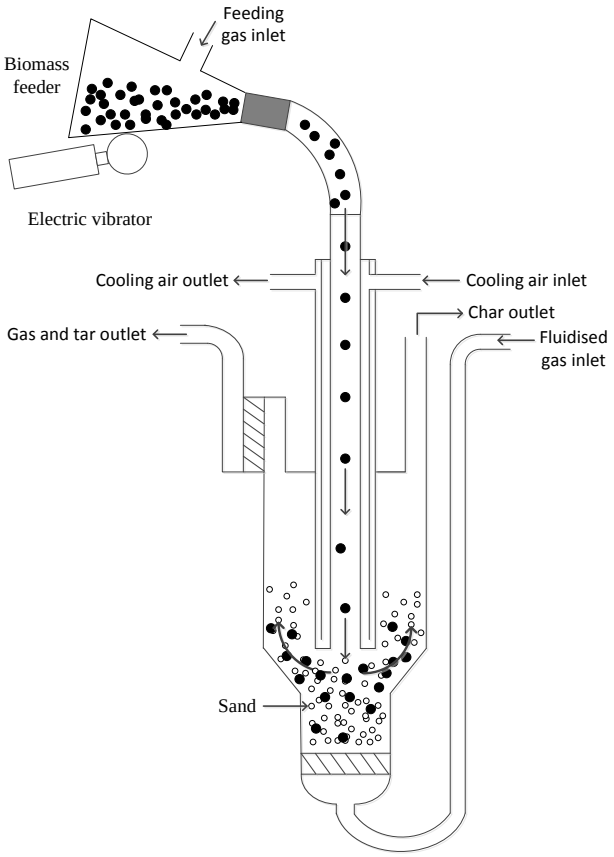

Figure 3-1. A schematic diagram of the fluidized-bed reactor for the gasification of biomass under the fast heating rate conditions. (Redraw based on Ref [20] with some modifications)

Bio-char gasification experiments were carried out in the same reactor, which would separate the pyrolysis process and gasification process during the biomass gasification. The first step was the bio-char preparation. Mallee wood with the particle size between 4.75-5.60 mm was pyrolysed at 900 ˚C under fast heating rates by feeding the biomass into the pre-heated reactor continuously. When the feeding was completed, the reactor was held for 30 minutes at 900 ˚C. The collected bio-char sample was grounded and sieved to the following five particle sizes: 0.18-0.50, 0.50-1.00, 1.00-2.00, 2.00-3.35, 3.35-4.75 mm. The next step was to use these char samples as the feedstock to do the bio-char gasification experiments. About 0.2 g bio-char (weighed accurately) was pre-loaded into the fluidised-bed reactor and the reactor was heated up to 900 ˚C in argon atmosphere. When the desired temperature was reached, the gasifying agent was introduced into the reactor for 10 minutes. The experiment was also terminated by lifting the reactor out of the furnace.

3.2.3 Char characterisation

A Perkin-Elmer GX FT-IR/Raman spectrometer with an excitation laser of 1064 nm was used for the characterisation of char structure. A procedure has been established in our group [29]. Briefly, the char sample was mixed and ground with spectroscopic grade KBr which acted as a heat-dissipating medium to prevent char sample from being heated up by the laser. A concentration of 0.5 wt% char in the char-KBr mixture was selected, which achieved the plateau in total Raman area both for the first-order Raman region (800-1800 cm^{-1}) [20-23] and the second-order Raman region (2000-3300 cm^{-1}). Each of the acquired Raman spectra was further deconvoluted in order to understand the specific chemical structure of the char. The first-order Raman spectra were deconvolution into 10 Gaussian bands and the second-order Raman spectra were deconvolution into 7 Gaussian bands to obtain the detailed structural features of char. The detail assignment of these bands can be found elsewhere [28,29].

3.3 Results and discussion

3.3.1 Char yield

Figure 3-2 shows the char yield as a function of biomass particle size as well as temperature. As expected, high temperature would enhance the devolatilisation and gasification of char [20-23]. Therefore, for a given particles size, the char yield decreased with increasing temperature. In addition, at a specified temperature, the char yield increased with increasing particle size both for the gasification in steam atmosphere and CO_2 atmosphere. Two reasons could be responsible for this trend. One is the differences between small and large particles in transporting the volatile precursors especially the tarry compounds to the out surface of the char during pyrolysis [21]. The mallee wood sample used in this research has a volatiles yield of 81.6 wt% [21-23], and large amounts of volatiles would be released during pyrolysis. The residence time of the volatile precursors would be much longer in a large particle than in a small one. In addition, a high heating rate for a small particle could cause the quick formation of volatile precursors and thus result in a rapid pressure increase in the particle, which could also lead to a short residence time of volatile precursors in char. Therefore, more volatile precursors would recondense or reabsorb on the internal surface of the char from a large particle than that from a small one, resulting in increases in the char yield. The other reason for the increasing char yield with increasing particle size in Figure 3-1 could be the difference in the intra-particle diffusion of the gasifying agent between small and big particles, which could potentially result in different gasification rates for different particle sizes.

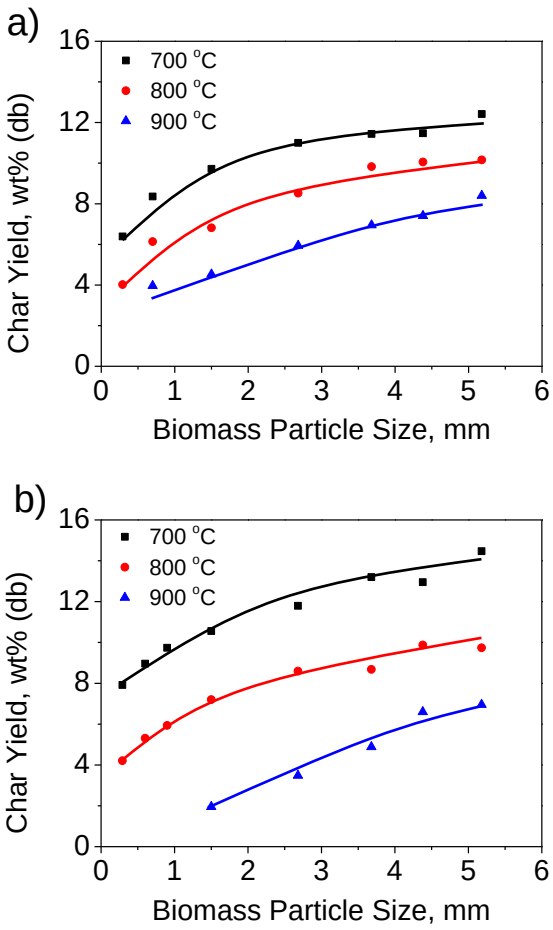

Figure 3-2. Char yields as a function of average biomass particle size during the gasification of mallee wood at 700, 800 and 900 ˚C in (a) 15% H_2O balanced with Ar; (b) pure CO_2.

Further experiments were then carried out on the gasification of bio-char to understand the relative importance of above-mentioned two possible reasons. Figure 3-3 illustrates the effect of bio-char particle size on the conversion of char in steam atmosphere and CO_2 atmosphere. It can be seen that the conversion of char was almost the same regardless of particle size in the cases of gasification in steam atmosphere and in CO_2 atmosphere, which indicated that there was plenty of time for the gasifying agent to penetrate into the char particles before the reaction took place. In other words, the intra-particle gas diffusion was not the rate-limiting step during gasification for the conditions used in this study. Therefore, the changes in the char yield with biomass particle size (Figure 3-2) were mainly due to the difference in the residence time of volatile precursors in small and big particles. A long residence time

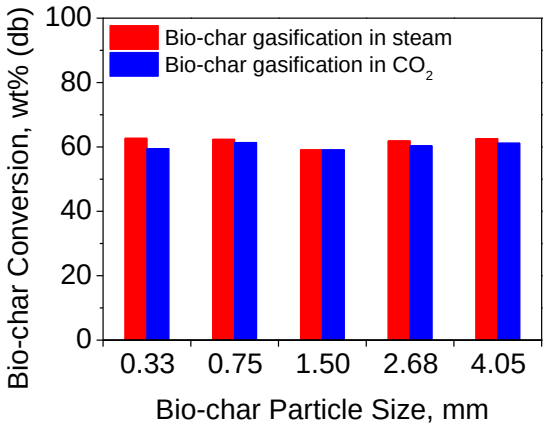

Figure 3-3. Bio-char conversion as a function of the average bio-char particle size during the gasification of bio-char at 900 ˚C in 15% H_2O balanced with Ar and in pure CO_2. Bio-char samples of different particle sizes were prepared by crushing the same large bio-char sample.

would tend to enhance the formation of additional coke from the volatile precursors within a pyrolysing biomass particle.

3.3.2 Char structure

3.3.2.1 Oxygenation of the char

The total peak area of a first-order Raman spectrum was taken as the total intensity in the range between 800 and 1800 cm^{-1}. Both Raman scattering ability and light absorption ability of char could affect the observed Raman intensity [29]. The presence of Raman-active oxygen species in char can exert a resonance effect between oxygen and aromatic ring to which oxygen is connected, which could enhance the total Raman intensity. On the other hands, the light absorptivity of char would be enhanced by the growth of aromatic ring systems, resulting in a decline in the observed total Raman intensity [29]. Figure 3-4 exhibits the influence of biomass particle size on the total band area of the first-order Raman at different gasification temperatures. For the biomass gasification in steam atmosphere and CO_2 atmosphere, the total Raman intensity decreased with increasing gasification temperature,

especially from 700 to 800 ˚C. This decrease implied that the release of O-containing structure through thermal cracking and the growth of the aromatic ring system of char during gasification [20-23,27]. These changes would be intensified when the temperature reached 800 ˚C. In addition, there should be much more recondenced volatile precursors in the char matrix of big particle than that of small particle [21,23]. However, the total intensity of the fist-order Raman was not affected by biomass particle size. Therefore, this result indicated that the recondensed volatile precursors did not change the overall Raman-active oxygen species of char during gasification. This observation was in agreement with our previous study [23].

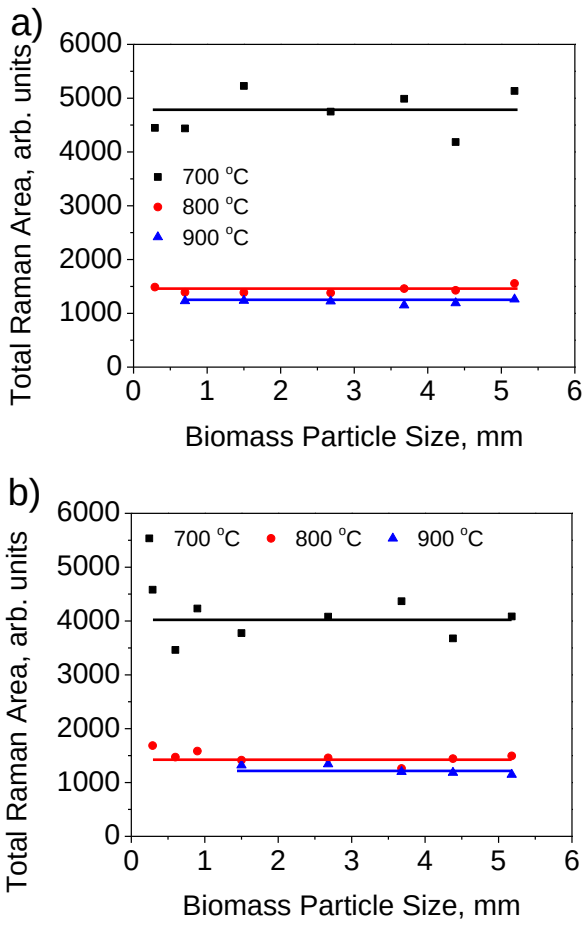

Figure 3-4. Total first-order Raman area as a function of average biomass particle size during the gasification of mallee wood at 700, 800 and 900 ˚C in (a) 15% H_2O balanced with Ar; (b) pure CO_2.

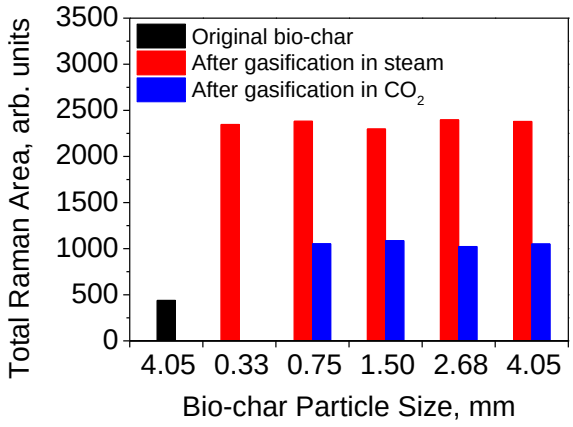

Figure 3-5. Total first-order Raman area as a function of average bio-char particle size during the pyrolysis of mallee wood at 900 ˚C in Ar, pyrolysis and subsequent gasification of bio-char at 900 ˚C in 15% H_2O balanced with Ar, pyrolysis and subsequent gasification of bio-char at 900 ˚C in pure CO_2.

Figure 3-5 illustrates the total intensity of the first-order Raman of char prepared from pyrolysis and then experienced the gasification in steam atmosphere or CO_2 atmosphere with different bio-char particle sizes. The total Raman intensity of char produced from pyrolysis was significantly lower than that after experiencing the gasification, indicating that some oxygen derived from H_2O and CO_2 would possibly form oxygen complexes on char matrix [27,30,31]. In addition, for different bio-char particle sizes, the total Raman intensity of char was almost the same, both for the gasification in steam atmosphere and CO_2 atmosphere. It meant that the gasification may take place uniformly throughout the whole particles [23], regardless the particle size. Furthermore, comparing the total Raman intensity of char from gasification in steam with that in CO_2, the total intensity of char prepared from the gasification in steam was much higher than that in CO_2, indicating that more O-containing species connected with aromatic ring system in steam atmosphere than that in CO_2 atmosphere [27]. Moreover, comparing the total Raman intensity of char produced from the biomass gasification (Figure 3-4) with that from the bio-char gasification (Figure 3-5) under 900 ˚C, it can be seen that for the gasification in steam, the total Raman intensity of char produced from bio-char gasification with 10 minutes holding time was higher than that produced form biomass gasification with 4 minutes feeding

time, which meant the char structures became increasingly oxygenated with the progress of gasification in steam atmosphere. However, for the gasification in CO_2, the total Raman intensity was almost the same, regardless of the reaction time. This result indicated that the oxygen complexes formed on char during the gasification in steam atmosphere and CO_2 atmosphere were different. The oxygen spices formed in steam atmosphere should be more Raman-active than that formed in CO_2 atmosphere. Therefore, the different gasification behaviour in terms of the total Raman intensity between the gasification in steam atmosphere and CO_2 atmosphere indicated that the char-H_2O and char-CO_2 reactions followed different reaction pathway [27].

3.3.2.2 Change in the aromatic ring systems in char

Based on the bands assignment of the first-order Raman spectrum [29], the I_D mainly represents the large aromatic ring systems with no less than 6 fused rings, while the $I_{(Gr+Vl+Vr)}$ mainly represents the small aromatic ring systems with less than 6 fused rings. Therefore, the band area ratio $I_D/I_{(Gr+Vl+Vr)}$ can be used as an indirect indication of the relative ratio of small to large aromatic ring systems in char [29].

As is shown in Figure 3-6, for the gasification in steam atmosphere and CO_2 atmosphere, a higher temperature tended to result in a higher $I_D/I_{(Gr+Vl+Vr)}$ ratio. High temperature meant fierce thermal cracking and gasification reaction which would enhance the selective removal of small aromatic systems and the conversion of small aromatic systems to large ones in char [27,30,31]. Furthermore, for a given temperature, this ratio was constant, regardless of particle sizes, which confirmed that the coke or soot formed from the recondensed volatile precursors had structural features (as observed with FT-Raman spectroscopy) similar to those in char during gasification [23].

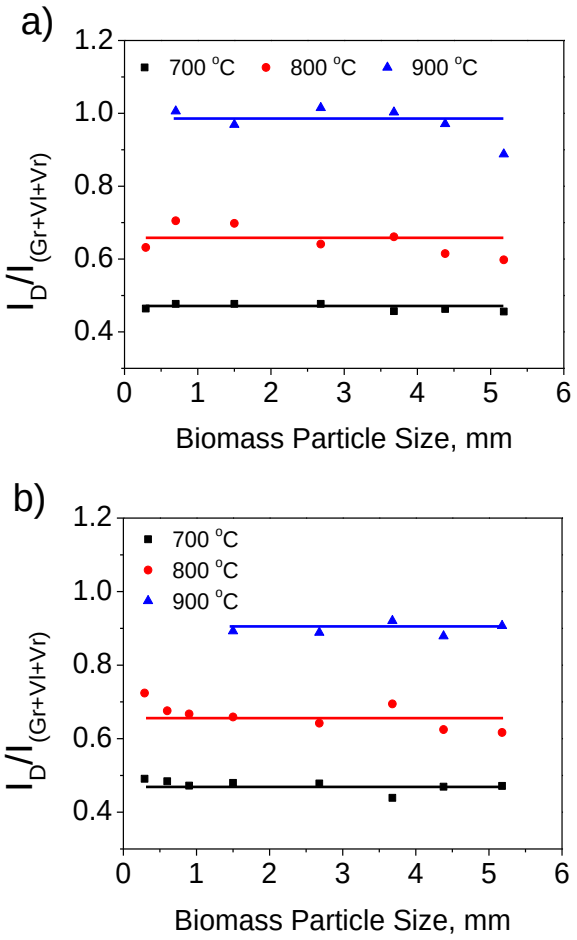

Figure 3-6. Raman band area ratios D/Gr+Vl+Vr as a function of average biomass particle size during the gasification of mallee wood at 700, 800 and 900 ˚C in (a) 15% H_2O balanced with Ar; (b) pure CO_2.

Figure 3-7 illustrates the band area ratios $I_D/I_{(Gr+Vl+Vr)}$ of chars prepared from pyrolysis and chars that also experienced the gasification in steam atmosphere and CO_2 atmosphere. The band ratios $I_D/I_{(Gr+Vl+Vr)}$ of chars produced from pyrolysis was lower than that after gasification, indicating that the gasification process would enhance the selective removal of small aromatic systems and the conversion of small aromatic systems to large ones in char [27,30,31]. In addition, both for the gasification in steam and CO_2, the band ratios $I_D/I_{(Gr+Vl+Vr)}$ of chars were almost constant with the particle size. These results were consistent with the analysis results of the total Raman intensity of chars of different particle sizes during the bio-char gasification experiments, confirming that the gasification took place uniformly throughout the whole particles [23].

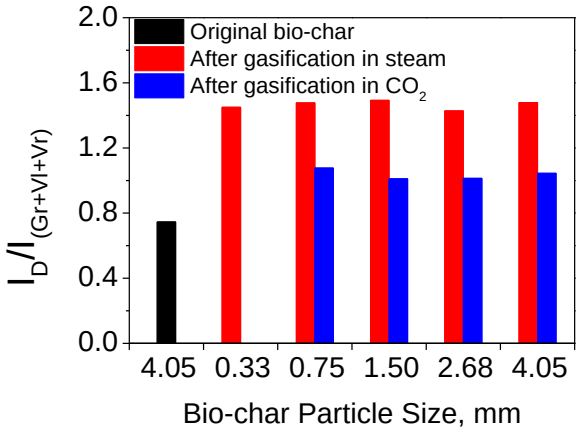

Figure 3-7. Raman band area ratios D/Gr+Vl+Vr as a function of average bio-char particle size during the pyrolysis of mallee wood at 900 ˚C in Ar, pyrolysis and subsequent gasification of bio-char at 900 ˚C in 15% H_2O balanced with Ar, pyrolysis and subsequent gasification of bio-char at 900 ˚C in pure CO_2.

Furthermore, the band ratios $I_D/I_{(Gr+Vl+Vr)}$ of chars produced from gasification in steam were much higher than those produced from gasification in CO_2. This was mainly due to the H radicals generated from H_2O during gasification would penetrate into the char matrix and induce the aromatic ring condensation reactions [27]. Therefore, the conversion of small aromatic systems to large aromatic systems was more pronounced in steam atmosphere than that in CO_2 atmosphere, resulting in the higher band area ratio. Moreover, making the comparison of the band ratios $I_D/I_{(Gr+Vl+Vr)}$ of chars between that from the biomass gasification with 4 minutes feeding time (Figure 3-6) and that from the bio-char gasification with 10 minutes holding time (Figure 3-7) at 900 ˚C, both for the gasification in steam atmosphere and CO_2 atmosphere, the small aromatic rings were more preferred to be consumed by the gasifying agent than the large aromatic rings with the progress of gasification, resulting in increases in the band ratio $I_D/I_{(Gr+Vl+Vr)}$.

3.3.2.3 Change in the structural compactness in char

Amorphous carbon such as chars produced from gasification should contain lots of sp^3-rich structures [28,29]. Based on the band assignment of the Raman spectrum,

the presence of the alkyl-aryl C-C structures, substitutional groups (other than O-containing ones) as well as the crossing-linking density in char can be indicated by the intensity of S band [29]. Meanwhile, the intensity of the 2S band in the second-order can also be used as an indication of the structural compactness of char [28]. However, unlike the S band that increased with the increasing crossing-linking density of char, lots of studies indicated that the bandwidth as well as the intensity of 2S band decreased with the increasing crystallinity of the carbon-based materials [32-34]. The most important additional finding in the analysis of the second-order spectrum was the changes in the intensity of the 2S band during gasification while the intensity of S band in the first-order Raman did not show clear change during gasification.

Figure 3-8 shows the intensity ratios I_{2S}/I_{Total} as a function of the biomass particle size and gasification temperature. Both for the gasification in steam atmosphere and CO_2 atmosphere, the ratios I_{2S}/I_{Total} were almost the same for chars produced at 800 ˚C and 900 ˚C and were significantly lower than that at 700 ˚C. These results indicated the enhancing structural compactness of char with increasing gasification temperature, especially when the temperature was reached 800 ˚C. Also this ratio did not change with the biomass particle size. It can be seen that the data show some fluctuation when the gasification temperature reached 800 ˚C. This was mainly because that the total Raman intensity of the second-order was very weak for the chars produced from gasification in steam atmosphere and CO_2 atmosphere at 800 ˚C and 900 ˚C. Therefore, the deconvolution of the second-order spectrum would suffer from low signal-to-noise ratios, resulting in increased scatters.

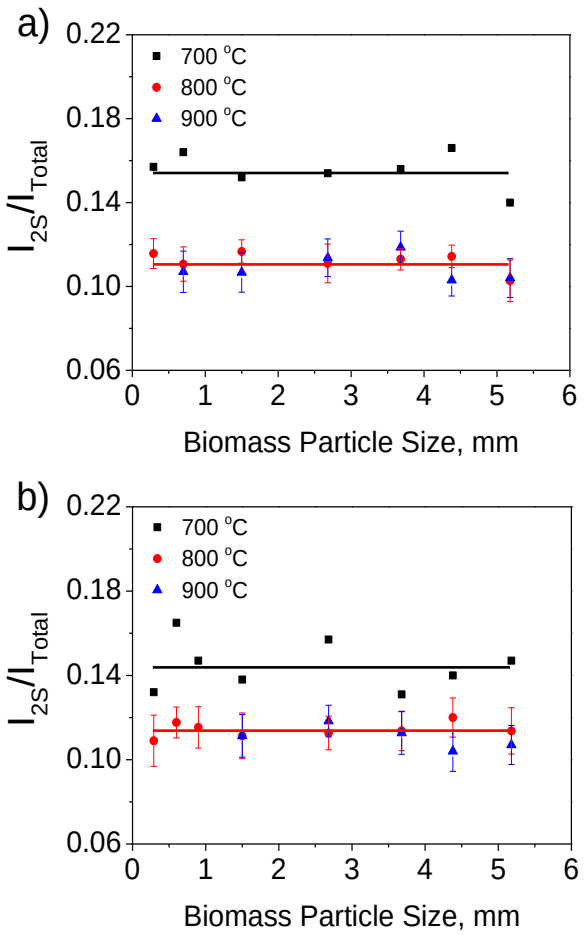

Figure 3-8. Raman band area ratios 2S/Total as a function of average biomass particle size during the gasification of mallee wood at 700, 800 and 900 ˚C in (a) 15% H_2O balanced with Ar; (b) pure CO_2.

Figure 3-9 illustrates the effect of bio-char particle on the change in the band area ratio I_{2S}/I_{Total} during gasification in steam atmosphere and CO_2 atmosphere at 900 ˚C (such ratio of char from pyrolysis at 900 ˚C is not displayed here due to the low intensity of the second-order Raman making it very difficult to get a reliable deconvolution result). It can be seen that the band area ratio I_{2S}/I_{Total} of char from the gasification in steam tended to be lower than that from the gasification in CO_2. This could be also explained by the presence of H radicals during gasification in steam, which would greatly activate the aromatic rings of char for the drastic growth of large aromatic ring systems, resulting in the enhanced structural compactness of char compared with that from gasification in CO_2.

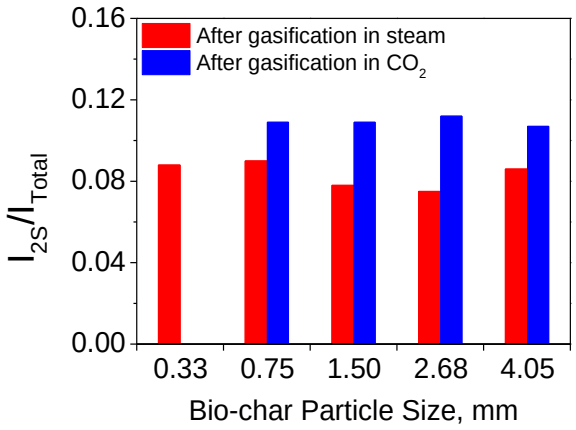

Figure 3-9. Raman band area ratios 2S/Total as a function of average bio-char particle size during the pyrolysis of mallee wood in Ar and subsequent gasification of bio-char in 15% H_2O balanced with Ar at 900 ˚C, pyrolysis of mallee wood in Ar and subsequent gasification of bio-char in pure CO_2 at 900 ˚C.

3.4 Conclusions

The influence of biomass particle size and gasification atmosphere in the char yield and evolution of char structure was investigated. The increased char yield with increasing biomass particle size during the gasification of biomass was mainly due to the increased heat and intra-particle mass transfer resistance in transporting the volatile precursors out of particles during the devolatilistion step. The subsequent gasification was not rate-limited by intra-particle diffusion of the gasifying agent under the present experimental conditions. The structural features of char changed drastically during the subsequent gasification. The biomass particle size had minimal effect on char structure, both for the gasification in steam atmosphere and CO_2 atmosphere, which meant that the recondensed volatile precursors did not result in significant changes in the overall char structure during gasification and the gasification might take place uniformly throughout the char particle, regardless of the particle size under the present experimental conditions. The differences in char structure as revealed by Raman spectroscopy confirmed that the char-H_2O and char-CO_2 reaction follow different reaction pathway.

3.5 References

[1] P. McKendry, Energy production from biomass (part 1): overview of biomass, Bioresource Technology, 83 (2002) 37-46.

[2] C.-Z. Li, Importance of volatile-char interactions during the pyrolysis and gasification of low-rank fuels – A review, Fuel, 112 (2013) 609-623.

[3] C.-Z. Li, Special issue-gasification: A route to clean energy, Process Safety and Environmental Protection, 84 (2006) 407-408.

[4] H. Lasa, E. Salaices, J. Mazumder, R. Lucky, Catalytic steam gasification of biomass: catalysts, thermodynamics and kinetics, Chemical Reviews, 111 (2011) 5404-5433.

[5] G.W. Huber, S. Iborra, A. Corma, Synthesis of transportation fuels from biomass: chemistry, catalysts, and engineering, Chemical Reviews, 106 (2006) 4044-4098.

[6] R.M. Navarro, M.A. Pena, J.L.G. Fierro, Hydrogen production reactions from carbon feedstocks: fossil fuels and biomass, Chemical Reviews, 107 (2007) 3952-3991.

[7] J.J. Hernandez, G. Aranda-Almansa, A. Bula, Gasification of biomass wastes in an entrained flow gasifier: Effect of the particle size and the residence time, Fuel Processing Technology, 91 (2010) 681-692.

[8] R. Yin, R. Liu, J. Wu, X. Wu, C. Sun, C. Wu, Influence of particle size on performance of a pilot-scale fixed-bed gasification system, Bioresource Technology, 119 (2012) 15-21.

[9] K.R. Gaston, M.W. Jarvis, P. Pepiot, K.M. Smith, W.J. Frederick, M.R. Nimlos, Biomass pyrolysis and gasification of varying particle sizes in a fluidized-bed reactor, Energy & Fuels, 25 (2011) 3747-3757.

[10] S. Luo, B. Xiao, X. Guo, Z. Hu, S. Liu, M. He, Hydrogen-rich gas from catalytic steam gasification of biomass in a fixed bed reactor: influence of particle size on gasification performance, International Journal of Hydrogen Energy, 34 (2009) 1260-1264.

[11] P. McKendry, Energy production from biomass (part 3): gasification technologies, Bioresource Technology, 83 (2002) 55-63.

[12] V.M. Tiangco, B.M. Jenkins, J.R. Goss, Optimum specific gasification rate for static bed rice hull gasifiers, Biomass and Bioenergy, 11 (1996) 51-62.

[13] G. Jin, Multiscale coupling framework for modeling of large-size biomass particle gasification in fluidized beds, Industrial & Engineering Chemistry Research, 52 (2013) 11344-11353.

[14] F.V. Tinaut, A. Melgar, J.F. Perez, A. Horrillo, Effect of biomass particle size and air superficial velocity on the gasification process in a downdraft fixed bed gasifier. An experimental and modelling study, Fuel Processing Technology, 89 (2008) 1076-1089.

[15] R. Warnecke, Gasification of biomass: comparison of fixed bed and fluidized bed gasifier, Biomass and Bioenergy, 18 (2000) 489-497.

[16] E. Cetin, B. Moghtaderi, R. Gupta, T.F. Wall, Influence of pyrolysis conditions on the structure and gasification reactivity of biomass chars, Fuel, 83 (2004) 2139-2150.

[17] P.M. Lv, Z.H. Xiong, J. Chang, C.Z. Wu, Y. Chen, J.X. Zhu, An experimental study on biomass air–steam gasification in a fluidized bed, Bioresource Technology, 95 1 (2004) 95-101.

[18] A.R. Fraga, A.F. Gaines, R. Kandiyoti, Characterization of biomass pyrolysis tars produced in the relative absence of extraparticle secondary reactions, Fuel, 70 (1991) 803-809.

[19] Z. Luo, S. Wang, Y. Liao, J. Zhou, Y. Gu, K. Cen, Research on biomass fast pyrolysis for liquid fuel, Biomass and Bioenergy, 26 (2004) 455-462.

[20] M. Asadullah, S. Zhang, Z. Min, P. Yimsiri, C-Z Li, Importance of biomass particle size in structural evolution and reactivity of char in steam gasification, Industrial & Engineering Chemistry Research, 48 (2009) 9858-9863.

[21] M. Asadullah, S. Zhang, C.-Z. Li, Evaluation of structural features of chars from pyrolysis of biomass of different particle sizes, Fuel Processing Technology, 91 (2010) 877-881.

[22] M. Asadullah, S. Zhang, Z. Min, P. Yimsiri, C.-Z. Li, Effects of biomass char structure on its gasification reactivity, Bioresource Technology, 101 (2010) 7935-7943.

[23] S. Zhang, Z. Min, H.-L. Tay, Y. Wang, L. Dong, C.-Z. Li, Changes in char structure during the gasification of mallee wood: Effect of particle size and steam supply, Energy & Fuels, 26 (2012) 193-198.

[24] A. Demirbas, Effects of temperature and particle size on bio-char yield from pyrolysis of agricultural residues, Journal of Analytical and Applied Pyrolysis, 72 (2004) 243-248.

[25] C.A. Koufopanos, N. Papayannakos, G. Maschio, A. Lucchesi, Modelling of the pyrolysis of biomass particles. Studies on kinetics, thermal and heat transfer effects, The Canadian Journal of Chemical Engineering, 69 (1991) 907-915.

[26] H. Lu, E. Ip, J. Scott, P. Foster, M. Vickers, L.L. Baxter, Effects of particle shape and size on devolatilization of biomass particle, Fuel, 89 (2010) 1156-1168.

[27] T. Li, L. Zhang, L. Dong, C.-Z. Li, Effects of gasification atmosphere and temperature on char structural evolution during the gasification of Collie sub-bituminous coal, Fuel, 117 (2014) 1190-1195.

[28] S. Wang, T. Li, L. Wu, L. Zhang, L. Dong, X. Hu, C.-Z. Li, Second-order Raman spectroscopy of char during gasification, Fuel Processing Technology, 135 (2015) 105-111.

[29] X. Li, J.-I. Hayashi, C.-Z. Li, FT-Raman spectroscopic study of the evolution of char structure during the pyrolysis of a Victorian brown coal, Fuel, 85 (2006) 1700-1707.

[30] H.-L. Tay, C.-Z. Li, Changes in char reactivity and structure during the gasification of a Victorian brown coal: Comparison between gasification in O_2 and CO_2, Fuel Processing Technology, 91 (2010) 800-804.

[31] H.-L. Tay, S. Kajitani, S. Zhang, C.-Z. Li, Effects of gasifying agent on the evolution of char structure during the gasification of Victoria brown coal, Fuel, 103 (2013) 22-28.

[32] A. Sadezky, H. Muckenhuber, H. Grothe, R. Niessner, U. Poschl, Raman microspectroscopy of soot and related carbonaceous materials: Spectral analysis and structural information, Carbon, 43 (2005) 1731-1742.

[33] T. Shimada, T. Sugai, C. Fantini, M. Souza, L.G. Cancado, A. Jorio, et al, Origin of the 2450 cm^{-1} Raman bands in HOPG, single-wall and double-wall carbon nanotubes, Carbon, 43 (2005) 1049-1054.

[34] A. Zaida, E. Bar-Ziv, L.R. Radovic, Y.-J. Lee, Further development of Raman microprobe spectroscopy for characterization of char reactivity, Proceeding of the Combustion Institute, 31 (2007) 1881-1887.

Chapter 4

An X-ray photoelectron spectroscopic perspective for the evolution of O-containing structures in char during gasification

4.1 Introduction

Char gasification is the rate-limiting step for the overall solid fuel gasification process [1,2]. There are a few important factors influencing the char gasification rate [3]. Firstly, the inherent alkali and alkaline earth metallic (AAEM) species in char can act as excellent catalysts for char gasification [3]. The presence of highly dispersed AAEM species can not only significantly speed up the gasification reaction, affect the properties of pyrolysis products, but also in turn have a great impact on the evolution of char structure [4-6]. Secondly, the transformation of aromatic ring systems in char will greatly influence char reactivity during gasification. It has become clear that the small ring systems (equivalent to 3-5 fused benzene rings) are preferentially consumed while the large ones (more than 6 fused rings) are left and/or formed during gasification, making the residual char more condensed and hard to be gasified [7-9]. Thirdly, the O-containing functional groups in char will also greatly influence the gasification rate to some extent, especially for the gasification of the low-rank fuels at low temperature. It is believed that some kinds of O-containing structures in char are responsible for enhancing the char gasification rate [4,7]. For a better understanding of the gasification mechanisms, the changes in char structure, especially the evolution of O-containing structures, must be quantified during gasification.

FT-Raman spectroscopy has been demonstrated to be a powerful analytical method to characterise the evolution of aromatic ring systems in char during gasification due to its outstanding ability to respond to the non-polar bond vibration [10-14]. However, only limited information can be obtained from the Raman spectrum about the changes of O-containing structures in char, especially the changes in the chemical bonding between oxygen and carbon during gasification. Although the total Raman intensity can be used as an indication of the relative amount of the O-containing functional groups in char, it only restricts to the oxygen species which has a resonance effect with the aromatic ring structure to which it is connected [10]. Not all oxygen species in char could have the resonance effect with the aromatic ring. Therefore, other techniques must be applied to study all O-containing functional

groups in char and provide useful information on the evolution of O-containing structures in char during gasification. X-ray photoelectron spectroscopy has been proved to be one of the most powerful tools in detecting the surface structure of carbonaceous materials [15-18]. Although the validity of XPS analysis is limited to determine the surface structure of material, its high sensitivity to the chemical nature of atomic species has make it extensively developed as an useful technique for identifying the structural features of different types of carbon materials [19,20]. In addition, the ability to identify elemental bonding states has make it widely used in determining the organic functional group composition of char through a detailed analysis of the high-resolution band of each elements [21,22].

The purpose of this study is to investigate the effects of gasification temperature and gasification atmosphere on the evolution of O-containing structures in char. X-ray photoelectron spectroscopy was applied to characterise carbon and oxygen species in chars produced from the gasification of mallee wood at 600-900 ˚C in three different atmospheres (pure CO_2, 15% H_2O-Ar, 15% H_2-Ar). The high-resolution O 1s peak of the XPS spectra were further analysed in order to gain insights into the nature of oxygen bonding with carbon in addition to the determining of the contents of carbon and oxygen in char. Our data provided further insight into the char gasification mechanisms.

4.2 Experimental

4.2.1 Biomass sample

Mallee wood in the size range of 4.75-5.60 mm from Western Australia was used as the feedstock in this research. The preparation of the wood sample can be found elsewhere [23]. The proximate analysis of the sample gave a 0.9% ash yield and 81.6% volatiles yield, and the elemental analysis of the sample gave a 48.2% C, 6.1% H, 0.2% N and 45.5% O (wt%, dry and ash-free basis) [23]. Before each experiment, the samples were taken out from the freezer and dried in oven overnight at 105 ˚C to remove the moisture.

4.2.2 Biomass Gasification

A fluidised-bed quartz reactor was used to carry out the biomass gasification experiments. About 2 g biomass (weighed accurately) was pre-loaded into the feeder. Before feeding, the reactor was heated to the target temperature with the flow of Ar through the reactor. The feeding of biomass into the reactor was started with the help of an electrical vibrator. When the feeding was finished, the reactor was held for 20 minute to make sure that all volatiles have been released. The reaction gas was switched from Ar to the gasifying agent. For gasification in steam atmosphere, it was 15% steam balanced with Ar. For gasification in H_2 atmosphere, it was 15% H_2 balanced with Ar. For gasification CO_2 atmosphere, pure CO_2 was used. After 4 minutes of holding in the gasification atmosphere, the reactor was lifted out of the furnace immediately and cooled down naturally with Ar flowing into the reactor instead of the gasifying agents. After each experiment, the collected char sample was put in sealed vials and stored in a freezer to avoid further oxidation by the ambient oxygen.

4.2.3 Char characterisation

X-ray photoelectron spectroscopy (XPS) was performed on a Kratos AXIS Ultra DLD Thermo Escalab 250 with monochromated Al Kα X-rays (photon energy 1486.7 eV). XPS measurements were carried out under ultra-high vacuum conditions ($< 2.0\times10^{-10}$ mbar) at room temperature. The survey scans were taken across the sample with binding energy from 1400 to 0 eV to determine all elements present in char. A pass energy of 40 eV was used for the collection of high-resolution spectrum of each of the selected elements.

Elemental analysis was carried out on a FLASH 200 Elemental Analyser. Char sample was firstly ground to powder and then about 2.5 mg (weighed accurately) sample was loaded into a 157 µL tin capsule. The tin capsule was fold sealing and put into the autosampler. When the analysis started, the sealed tin capsule would drop into a quartz reactor placed in a furnace at the temperature of 900 ˚C. All

organic compound of the sample were combusted into gases and passed through the thermal conductivity detector TCD for quantitative analysis.

4.3 Deconvolution and band assignment of the XPS spectra

Datum processing of the acquired XPS spectra of chars was performed using the CasaXPS Peak fitting software. The binding energy of original XPS spectra was calibrated with respect to the adventitious carbon component of the C 1s peak at 284.5 eV. The spectra were curve-fitted after linear pre-edge and Shirley background subtraction, using mixed Gaussian and Lorentzian bands. The position and assignment of the bands in the O 1s spectra are briefly summarised in Table 4-1.

The curve-fitting of the high-resolution O 1s spectra was taken in the range between 528.0 and 539.0 eV. The broadening of the O 1s spectra meant large varieties of O-containing structures presented in char. Based on the XPS spectra of some model compounds [9,24,25], one band at around 531.3 eV was assigned to the O=C (aromatic) functional groups such as benzoquinone type structure in char. Another band at around 531.6 eV was attributed to the R-(C=O)-C (aromatic) functional groups such as aromatic ketone or carbonyl structure in char [21,25,26]. It is clear that these two kinds of O-containing functional groups have very close binding energies and they can not be reliably distinguished through the curve-fitting procedure. Therefore, in this study, the band in the range of 531.0-531.8 eV was assigned to all aromatic C=O structures in char. On the high binding energy side, one band at the position around 533.2 eV was attributed to oxygen inside the carbon ring such as epoxide or furan type structure in char [21,25,27]. Another band around 533.3 eV was assigned to the O-C (aromatic) structure such as phenol or diphenyl ether [17,25,26]. Moreover, the band located at around 533.6 eV was assigned to the O*-(C=O)-C (aromatic) functional group such as carboxyl structure in char [25]. Similarly, because of the close binding energies among these three oxygen-carbon structures and the complexity of O-contaning functional groups in char, the band in the range between 533.0 and 533.8 eV was assigned to all aromatic C-O structures in char. In addition to the two main bands assigned above, another weak peak appearing

Table 4-1. Summary of peak/band assignment.

Spectra	Band position, eV	Description	References
	531.4	Aromatic C=O structure	9,21,24-26
O 1s	533.4	Aromatic C-O structure	17,21,25-27
	536.0	Absorbed O_2	9,17

from 535.6 to 536.4 eV was identified as the absorbed O_2 existing on char surface [9,17].

A typical example of the spectral deconvolution/curve-fitting of the high-resolution O 1s peak of char using three bands is shown in Figure 4-1. Similar success of curve-fitting can also be achieved for all other char samples investigated in this study.

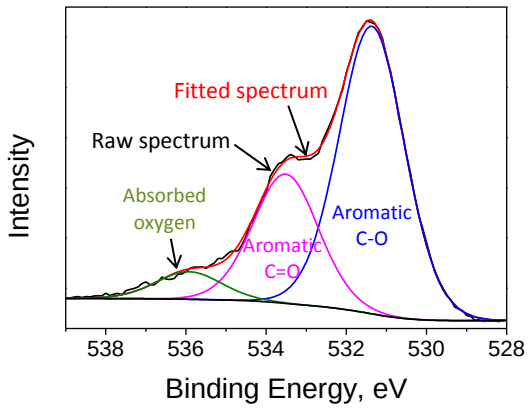

Figure 4-1. Spectral deconvolution of a XPS O 1s peak of char from the gasification of mallee wood at 700 ˚C in 15% H_2O balanced with Ar.

4.4 Results and discussion

4.4.1 Char yield

The gasification of mallee woody biomass was carried out at different temperatures ranging from 600 to 900 ˚C in three gasifying agents (pure CO_2, 15% H_2O-Ar, 15% H_2-Ar). Figure 4-2 shows the char yields as a function of gasification temperature in three gasifying atmospheres. As expected, the char yield decreased with increasing temperature because of the enhanced thermal cracking and gasification reaction. In addition, for different gasification atmospheres, when the temperature was below 700 ˚C, there was not much difference in the char yield, indicating that the main reaction was pyrolysis at this stage. However, when the temperature was higher than 700 ˚C, the gasification reaction became fierce and the gasification in CO_2 proceeded the fastest among the three atmospheres. As expected, the conversion of char proceeded the slowest during the gasification in H_2 atmosphere, confirming that the char-H_2 reaction was much slower than the char-H_2O and char-CO_2 reaction [4,12].

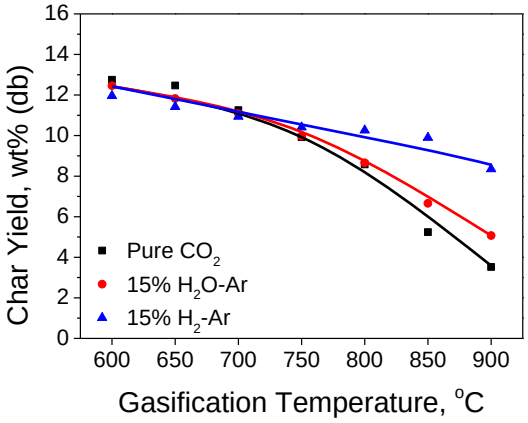

Figure 4-2. Char yields as a function of gasification temperatures for mallee wood in pure CO_2, 15% H_2O balanced with Ar and 15% H_2 balanced with Ar.

4.4.2 Formation of carbonates during the gasification in CO_2 at 900 ˚C

According to our previous studies [11,28], the extensive volatilisation of Ca and Mg from char matrix during gasification in CO_2 at 900 ˚C in a fluidised-bed reactor took place because of the formation and aggregation of carbonates on char surface. Some Ca and Mg species in biomass were present as the carboxyl-bound cations and would retain their high dispersion during fast pyrolysis even at high temperature (up to 950 ˚C) [6,28]. Once the char was exposed to CO_2 at 900 ˚C, the well-dispersed alkali earth metallic species could be carbonated to form $CaCO_3$ and $MgCO_3$ on char surface [28,29,30].

This result was confirmed by the XPS analysis in this work. Figure 4-3 shows the XPS spectra of a char from the gasification of mallee wood at 900 ˚C in pure CO_2. The high-resolution O 1s spectrum showed a very clear peak located at around 535.0 eV which was just the position of carbonate structures [31]. In order to clarify the nature of this band, the char was acid-washed with 0.2 M hydrochloric acid to remove the carbonates as well as the AAEM species on char surface. It can be seen from the survey scan that almost all Ca and Mg species were removed from char, and the band in the range of 534.0-536.0 eV in the O 1s high-resolution spectrum disappeared after the acid-washing, indicating the formation of $CaCO_3$ and $MgCO_3$ during gasification in CO_2 at 900 ˚C.

The alkali earth metallic carbonate on char could serve as excellent catalysts for the char gasification [31,32], partially explaining the high reactivity of chars from gasification in CO_2 at 900 ˚C.

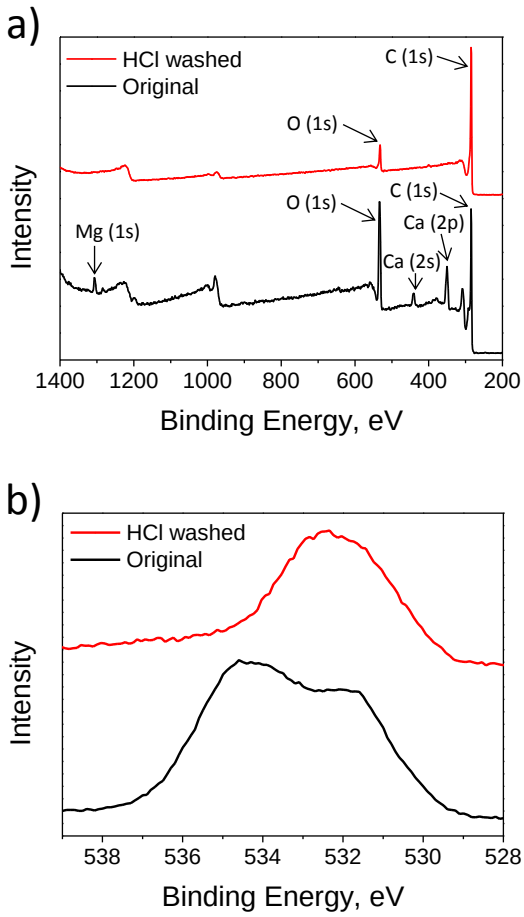

Figure 4-3. Effects of acid washing on the XPS spectra of (a) survey scan and (b) high-resolution of O 1s peak of the char from the gasification of mallee wood at 900 ˚C in pure CO_2.

4.4.3 Similarity in O/C ratio between surface and bulk analyses

In order to identify whether there were some difference in the contents of carbon and oxygen between char surface and char matrix, the results from elemental analysis were compared with those from XPS analysis. The contents of carbon and oxygen in char from XPS analysis were obtained by the calculation of total peak intensity and the relative sensitivity factors of each element. The content of inorganic oxygen was deducted from the total oxygen by calculating the amount of all metal oxide in the XPS spectra. Due to the inability to detect the H element through the XPS analysis, the O/C ratio of char during gasification was used to compare the difference between surface and bulk analyses.

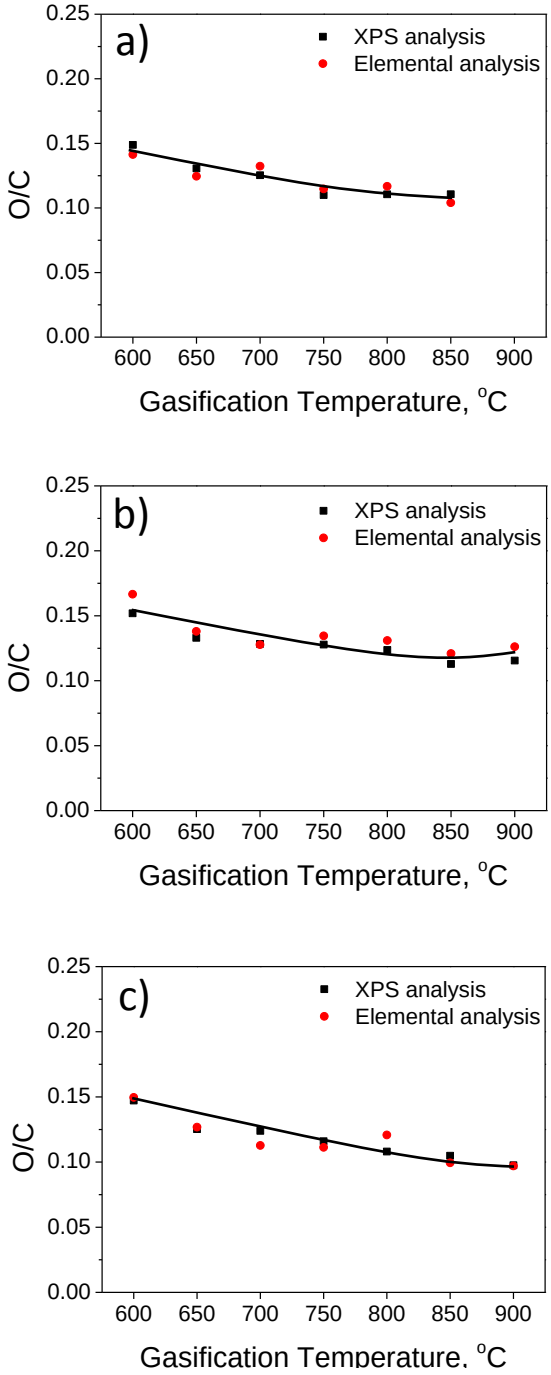

Figure 4-4. The O/C ratios of chars as a function of gasification temperatures for mallee wood in (a) pure CO_2, (b) 15% H_2O balanced with Ar and (c) 15% H_2 balanced with Ar.

As is shown in Figure 4-4, for a given temperature, the O/C ratios of char from XPS and elemental analysis were almost the same and the relative difference between

these two analysis results was less than 6%, which means the whole char particle was chemically uniformed so there was not much difference between the surface and char matrix. Although the XPS analysis can not detect the H element in char, based on the elemental analysis results, the content of H species in char was very little (less than 2%). Therefore, the XPS analysis can still be used as a characterisation method to indicate the concentration of carbon and oxygen species of the whole char particles during gasification.

4.4.4 Relative contents of chemical components in O 1s spectra

A clearer trend for the changes in O-containing functional groups can be found through the deconvolution of O 1s spectra of chars. Figure 4-5 illustrates the relative contents of O-containing structures in O 1s high-resolution spectra. The decreasing relative contents of aromatic C-O structures in O 1s spectra with increasing temperature confirmed the loss of C-O structures in char during gasification. The increases in aromatic C=O structures with increasing temperature might be attributed to its low reactivity compared with aromatic C-O structures in the reactive atmosphere so it was hard to be broken down during gasification. The other possibility was that some aromatic C-O structures may transform to aromatic C=O structures during gasification. The deconvolution result of O 1s spectra can only show the relative content of each O species, in order to identify the exact amount of O-containing structures left on char during gasification, the absolute quantity of each chemical component should be calculated, which will be discussed in the following section.

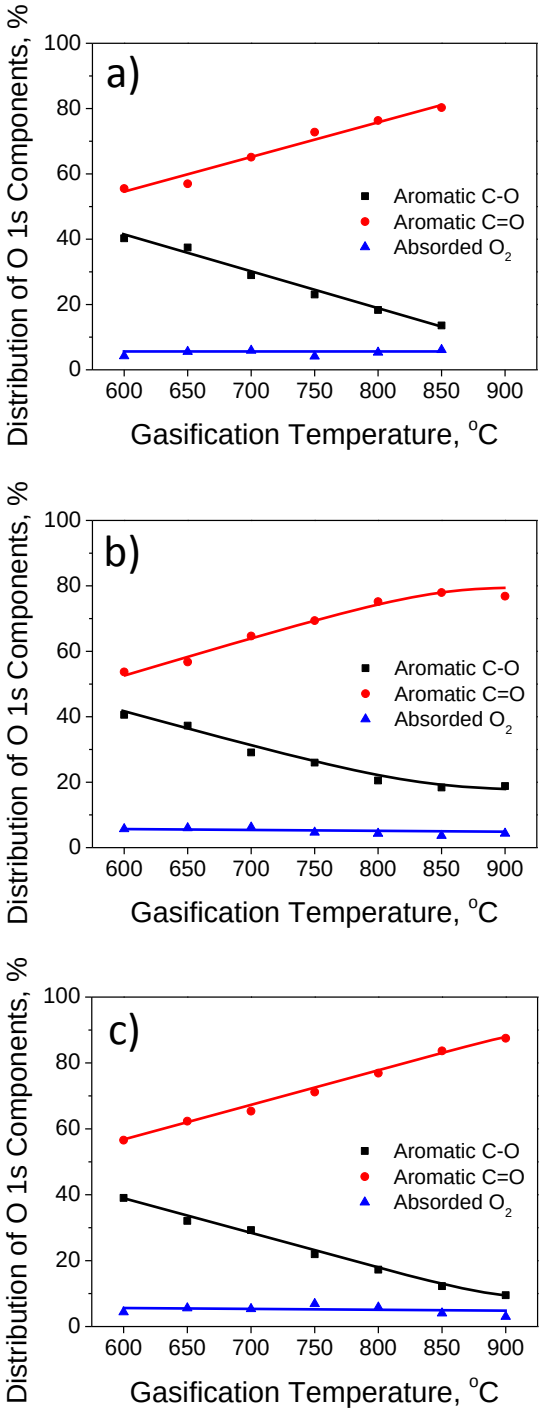

Figure 4-5. Relative contents of functional groups in O 1s spectra obtained by XPS analysis as a function of gasification temperatures for mallee wood in (a) pure CO_2, (b) 15% H_2O balanced with Ar and (c) 15% H_2 balanced with Ar.

4.4.5 Absolute amount of carbon and oxygen species in char during gasification

The absolute amount refers to the amount of residual species in char based on per initial gram of biomass char (before gasification). The absolute amounts of C and O species in char obtained by the XPS calculation results and the char yield of mallee wood during gasification are illustrated in Figure 4-6. As expected, the residual C and O species in char decreased with increasing temperature due to the enhanced thermal cracking and gasification reactions. Compared with the gasification in steam and in CO_2, much C and O species were left on char during the gasification in H_2 due to the slow consumption of C and O species in H_2 atmosphere.

Detailed information about the changes in O-containing structures can be obtained through further analysing the deconvolution results of the O 1s spectra of chars. As is shown in Figure 4-6 (c), there was a drastic decrease in the aromatic C-O structures in char with increasing temperature for all three gasification atmospheres, again indicating the high reactivity of aromatic C-O structures during gasification. In addition, a clear difference appeared for the residual C=O structures in char between gasification in H_2 atmosphere and the oxidising atmosphere (CO_2, H_2O). It can be seen from Figure 4-6 (d) that the amounts of C=O structures of char from the gasification in steam and in CO_2 continuously decreased with increasing temperature, especially at high temperature. However, such structure in chars from gasification in H_2 was almost constant until 850 ˚C. The char gasification in H_2 was quite slow and the loss of O-containing functional groups was mainly because of the enhanced thermal cracking, not the gasification reaction. Therefore, the chemical stability of the aromatic C=O structures made it more likely to survive during the thermal cracking and some aromatic C-O structures may transform to the more stable aromatic C=O structures, resulting in a steady amounts of aromatic C=O structures in char until 900 ˚C where the gasification become intensified. In contrast, for the bio-char gasification in steam atmosphere and CO_2 atmosphere, the aromatic C=O structures would be continuously consumed by the oxidising gasifying agent, especially with increasing temperature and thus intensified gasification.

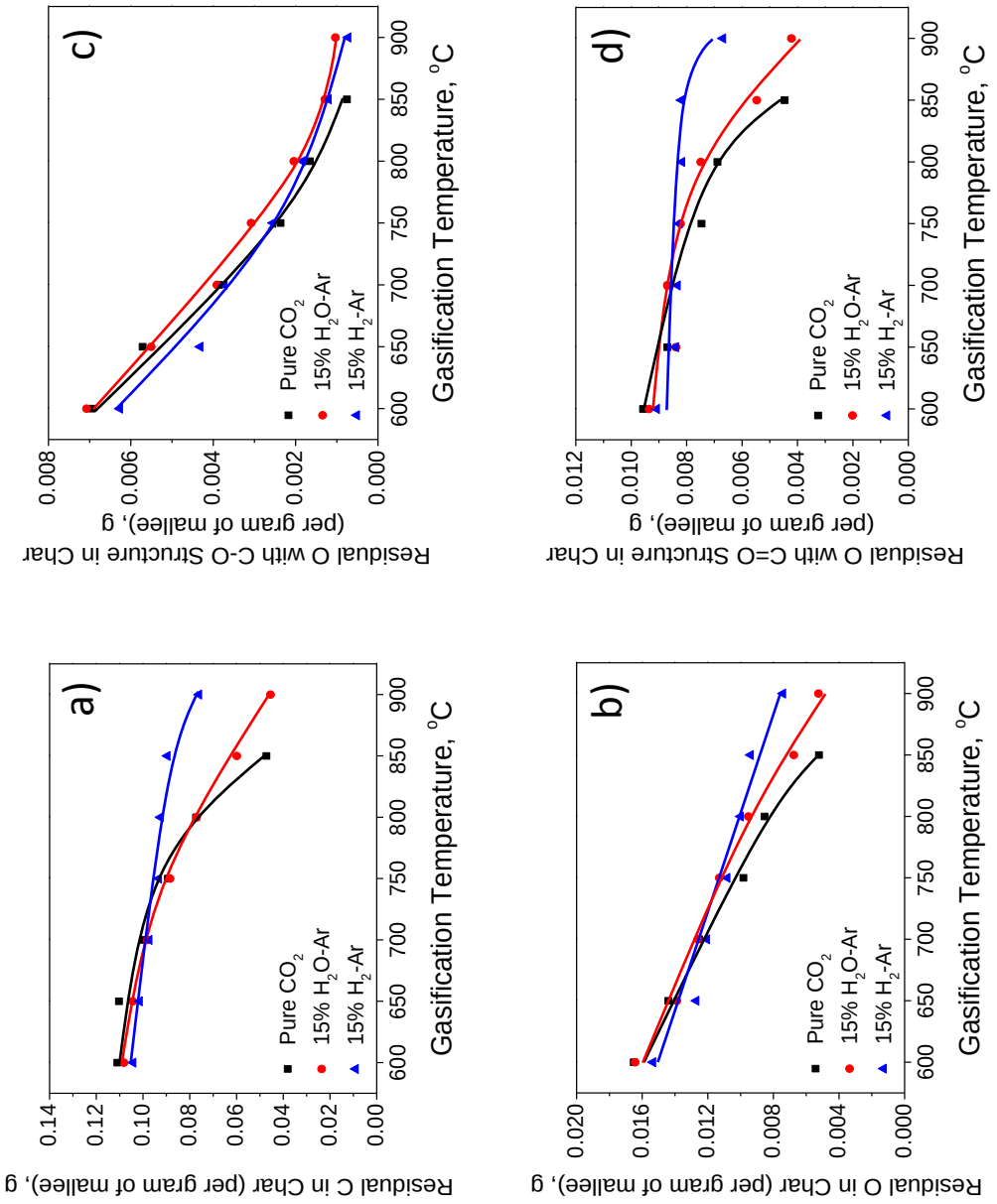

Figure 4-6. Amounts of (a) C species, (b) O species, (c) O with C-O structure and (d) O with C=O structure in char based on per gram of mallee wood obtained by XPS analysis as a function of gasification temperatures.

Figure 4-7 shows the absolute amounts of aromatic C-O structures and aromatic C=O structures in char as a function of char yield. It can be seen from Figure 4-7 (a) that, with the progress of gasification, the amounts of aromatic C-O structures of char from gasification in H_2 was significantly lower than that from gasification in the

oxidising atmospheres, indicating that the C-O structures was much easy to be consumed in the reducing atmospheres. However, at high char yields, the residual O with C-O structure for gasification in H_2 atmosphere seems higher than that in steam and CO_2 atmosphere. This is mainly due to the experimental errors. Because the highest char yield for the three gasification atmospheres in Figure 4-7 refer to the gasification at 600 ˚C, pyrolysis was the dominant reaction and the char yield should be almost the same among different atmospheres. However, the char yield of gasification at 600 ˚C under H_2 atmosphere (11.96%) is a little lower than that under steam atmosphere (12.46%) and CO_2 atmosphere (12.75%). Therefore, the residual O with C-O structure for gasification in H_2 seems higher than that in steam and CO_2 at high char yield. In addition, as is shown in Figure 4-7 (b), the amounts of aromatic C=O structures decreased with decreasing char yield and no much difference can be seen among the three atmospheres, which meant that the consumption of aromatic C=O structures was more likely related to the progress of gasification both in the reducing atmospheres and oxidising atmosphere. Therefore, the steady amounts of aromatic C=O structures in char with the increasing temperature during the gasification in H_2 atmosphere was due to weak gasification reaction at that stage.

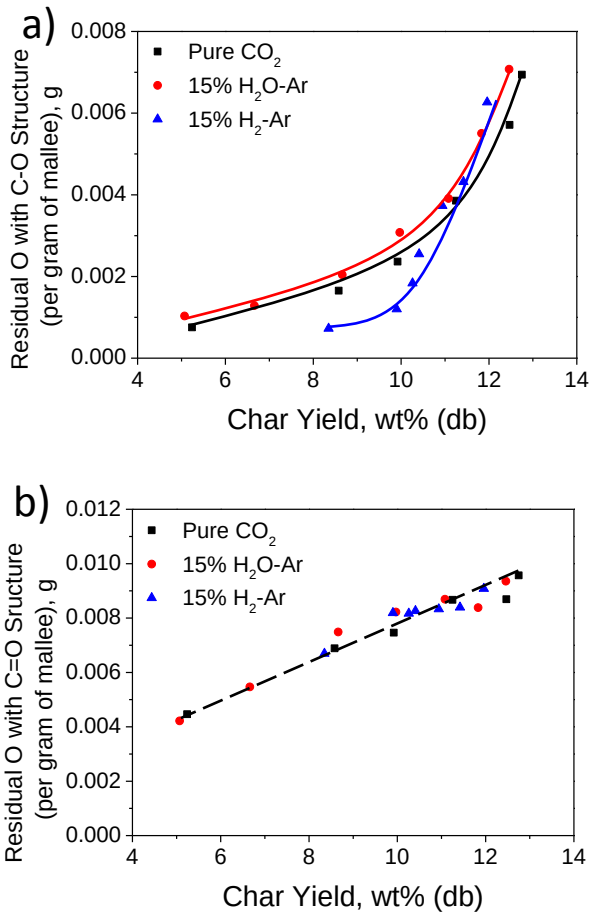

Figure 4-7. Amounts of (a) O with C-O structure and (b) O with C=O structure in char based on per gram of mallee wood obtained by XPS analysis as a function of char yield.

4.4.6 Oxygenation and de-oxygenation during char gasification

The gasification of low-rank fuels in oxidising atmospheres (e.g. H_2O, CO_2) is an oxygenation process based on our study of the total Raman intensity [4,7]. As mentioned above, the XPS analysis can also give a direct indication of the amount of O species in char during gasification, and it will involve all O species not just the O which have the resonance effect with the aromatic ring to which it is connected.

Figure 4-8 illustrates the relative contents of each chemical component in char. The relative contents refer to the contents of each chemical component in char based on per actual gram of biomass char (remaining after gasification). It can be seen from

Figure 4-8 (a) and (b) that the relative contents of C species in char continued to increase while relative contents of O species decreased with increasing gasification temperature, indicating that the O species were easier to be consumed or released from char matrix than the C species during gasification. In other words, high char yield should imply high O contents of char. Because the char yield from gasification in the oxidising atmospheres was much lower than that from the reducing atmosphere when the temperature was higher than 800 ˚C, it was reasonable to speculate that the relative contents of O species of char from gasification in CO_2 and in steam should be lower than that from gasification in H_2. However, when the temperature was higher than 800 ˚C where the gasification reaction became fierce, the relative contents of O species of char from gasification in the oxidising atmospheres were slightly higher than that in reducing atmosphere. Therefore, it was believed that some O derived from the oxidising gasifying agent would lead to the oxygenation of the aromatic ring system in term of forming some intermediates such as C(CO), C(OH) and C(O) structures in char matrix during gasification [7,33-35], contributing to the high contents of O species of char. Further information can be obtained from the deconvolution result of the O 1s spectra. As is shown in Figure 4-8 (c) and (d), the contents of aromatic C-O structures of chars from the gasification in the oxidising atmospheres were higher than that in the reducing atmosphere when the temperature was higher than 800 ˚C. In addition, for the contents of aromatic C=O structures in char among these three atmospheres, no much difference can be observed. All this indicated that the captured O species from the oxidising gasifying agent were much likely bonded to the char matrix with C-O structure.

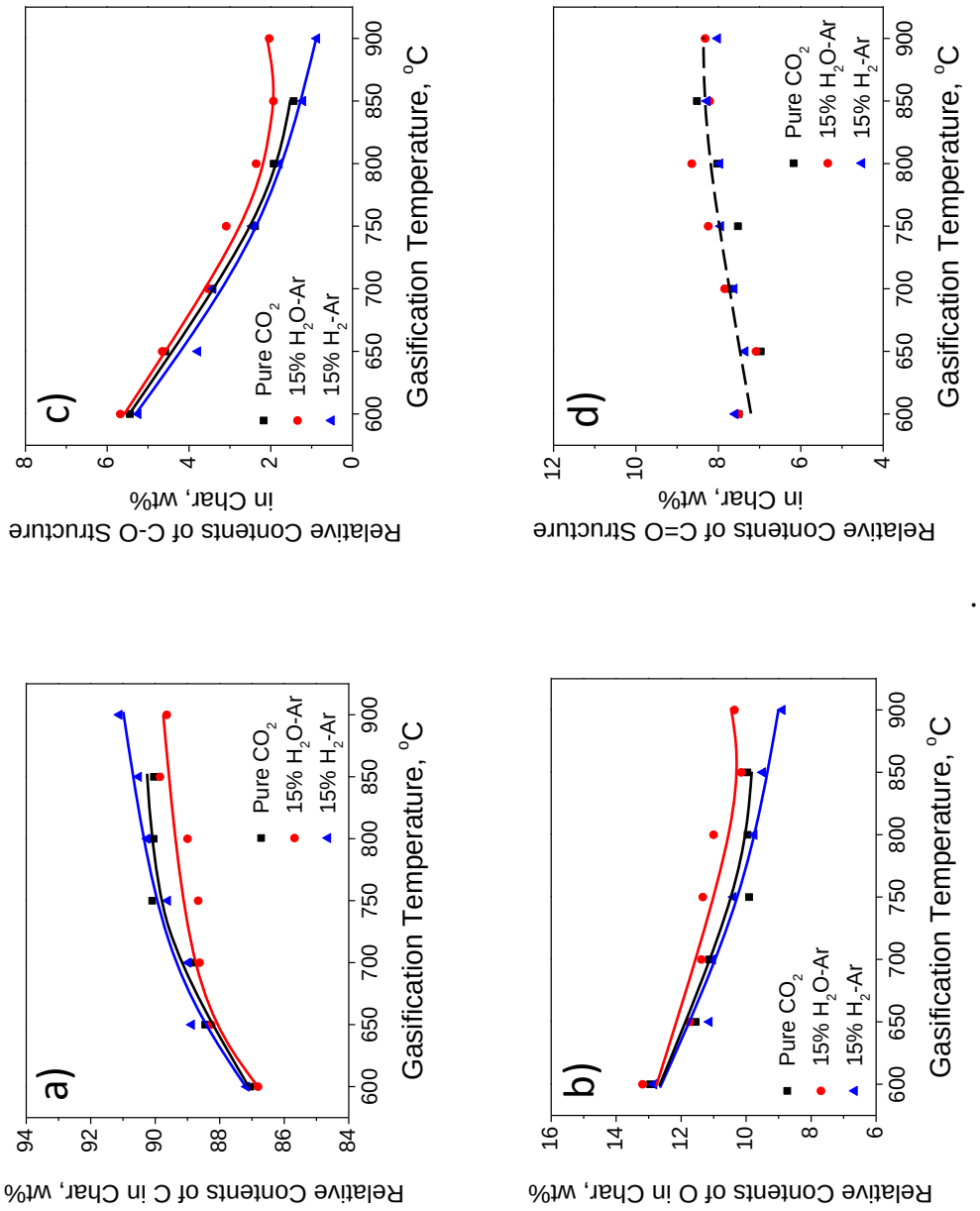

Figure 4-8. Relative contents of (a) C species, (b) O species, (c) O with C-O structure and (d) O with C=O structure in char obtained by XPS analysis as a function of gasification temperatures

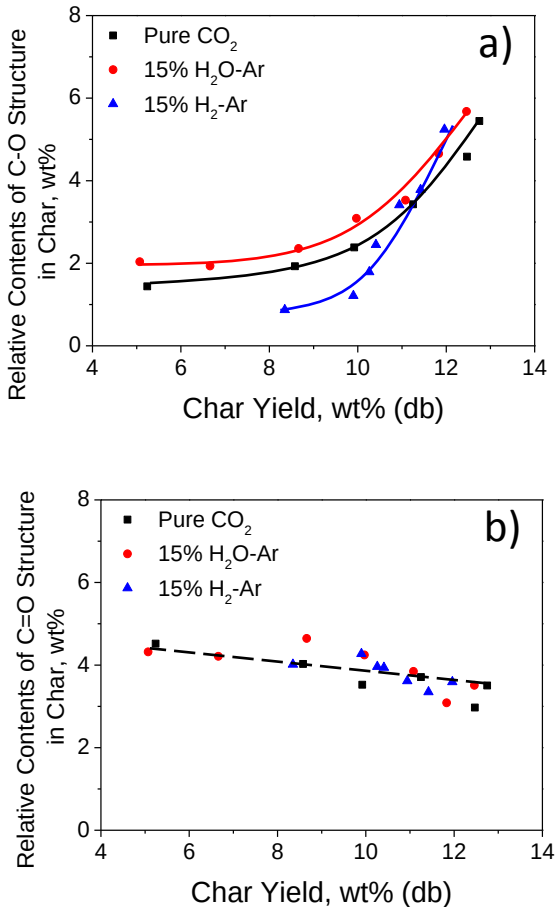

Figure 4-9. Relative contents of (a) O with C-O structure and (b) O with C=O structure in char obtained by XPS analysis as a function of char yield.

More evident can be found in Figure 4-9. It can be seen that the contents of aromatic C-O structure of char gasified in the oxidising atmosphere was much higher than that in the reducing atmosphere with the process of gasification, while no much difference can be observed for the contents of aromatic C=O structure among the three atmospheres. Furthermore, considering the high gasification rate of char from gasification in steam and in CO_2, the continuously generated C-O structures were most likely to be responsible for promoting the char gasification reactivity.

4.5 Conclusions

Australia mallee wood was gasified in a fluidised-bed reactor at 600-900 ˚C in oxidising and reducing atmospheres (pure CO_2, 15% H_2O-Ar and 15% H_2-Ar). Our

results revealed that the gasification of char in steam atmosphere and CO_2 atmosphere was much faster than that in H_2 atmosphere. For the gasification in CO_2 at 900 ˚C, some $CaCO_3$ and $MgCO_3$ formed in char and might serve as excellent catalysts for the char gasification, partially explaining the high gasification reactivity of char from such gasification condition. The similar O/C ratio of char from XPS and elemental analysis indicated the chemical similarity between char surface and char matrix. In addition, the aromatic C-O structure in char was highly reactive so that it can be easily removed or broken down while the low reactivity of the aromatic C=O structure made it more likely to survive during gasification. The amount of aromatic C-O structure left in char during gasification under reducing atmosphere was lower than that under oxidising atmosphere, while the consumption of aromatic C=O structure was related to the progress of gasification regardless of the atmosphere. Moreover, the high contents of O species of chars from gasification in steam and in CO_2 at high temperature confirmed the oxygenation of char gasified in the oxidising atmospheres. The formation of C-O structure in char during the oxygenation process was much likely to be responsible for the high gasification reactivity of char in the oxidising gasification atmospheres.

4.6 References

[1] C.-Z. Li, Special issue-gasification: A route to clean energy, Process Safety and Environmental Protection, 84 (2006) 407-408.

[2] C.-Z. Li, Importance of volatile-char interactions during the pyrolysis and gasification of low-rank fuels – A review, Fuel, 112 (2013) 609-623.

[3] C.-Z. Li, Some recent advances in the understanding of the pyrolysis and gasification behaviour of Victorian brown coal, Fuel, 86 (2007) 1664-1683.

[4] H.-L. Tay, S. Kajitani, S. Wang, C.-Z. Li, A preliminary Raman spectroscopic perspective for the roles of catalysts during char gasification, Fuel, 121 (2014) 165-172.

[5] C.-Z. Li, C. Sathe, J.R. Kershaw, Y Pang, Fates and roles of alkali and alkaline earth metals during the pyrolysis of a Victorian brown coal, Fuel, 79 (2000) 427-438.

[6] D.M. Quyn, H. Wu, SP Bhattacharya, C.-Z. Li, Volatilisation and catalytic effects of alkali and alkaline earth metallic species during the pyrolysis and gasification of Victorian brown coal. Part II. Effects of chemical form and valence, Fuel, 81 (2002) 151-158.

[7] T. Li, L. Zhang, L. Dong, C.-Z. Li, Effects of gasification atmosphere and temperature on char structural evolution during the gasification of Collie sub-bituminous coal, Fuel, 117 (2014) 1990-1995.

[8] H.-L. Tay, S. Kajitani, S. Zhang, C.-Z. Li, Effects of gasifying agent on the evolution of char structure during the gasification of Victorian brown coal, Fuel, 103 (2013) 22-28.

[9] Y. Zhao, D. Feng, Y. Zhang, Y. Huang, S. Sun, Effect of pyrolysis temperature on char structure and chemical speciation of alkali and alkaline earth metallic species in biochar, Fuel Processing Technology, 141 (2016) 54-60.

[10] X. Li, J.-i. Hayashi, C.-Z. Li, FT-Raman spectroscopic study of the evolution of char structure during the pyrolysis of a Victorian brown coal, Fuel, 85 (2006) 1700-1707.

[11] H.-L. Tay, C.-Z. Li, Changes in char reactivity and structure during the gasification of a Victorian brown coal: Comparison between gasification in O_2 and CO_2, Fuel Processing Technology, 91 (2010) 800-804.

[12] H.-L. Tay, S. Kajitani, S. Zhang, C.-Z. Li, Inhibiting and other effects of hydrogen during gasification: Further insights from FT-Raman spectroscopy, Fuel, 116 (2014) 1-6.

[13] X. Liu, Y. Zheng, Z. Liu, H. Ding, X. Huang, C. Zheng, Study on the evolution of the char structure during hydrogasification process using Raman spectroscopy, Fuel, 157 (2015) 97-106.

[14] S. Wang, T. Li, L. Wu, L. Zhang, L. Dong, X. Hu, C.-Z. Li, Second-order Raman spectroscopy of char during gasification, Fuel Processing Technology, 135 (2015) 105-111.

[15] D.L. Perry, A. Grint, Application of XPS to coal characterization, Fuel, 62 (1983) 1024-1033.

[16] S.G. Chen, R.T. Yang, F. Kapteijn, J.A. Moulijn, A new surface oxygen complex on carbon: toward a unified mechanism for carbon gasification reactions, Industrial & Engineering Chemistry Research, 32 (1993) 2835-2840.

[17] S.D. Gardner, C.S.K. Singamsetty, G.L. Booth, G.-R. He, C.U. Pittman, Surface characterization of carbon fibers using angle-resolved XPS and ISS, Carbon, 33 (1995) 587-595.

[18] F. Marquez-Montesinos, T. Cordero, J. Rodriguez-Mirasol, J.J. Rodriguez, CO_2 and steam gasification of a grapefruit skin char, Fuel, 81 (2002) 423-429.

[19] A.R. Gonzalez-Elipe, A. Martinez-Alonso, J.M.D. Tascon, XPS characterization of coal surfaces: study of aerial oxidation of brown coals, Surface and Interface Analysis, 12 (1988) 565-571.

[20] Y. Qiao, S. Chen, Y. Liu, H. Sun, S. Jia, J. Shi, C.M. Pedersen, Y. Wang, X. Hou, Pyrolysis of chitin biomass: TG-MS analysis and solid char residue characterization, Carbohydrate Polymers, 133 (2015) 163-170.

[21] G. Levi, O. Senneca, M. Causa, P. Salatino, P. Lacovig, S. Lizzit, Probing the chemical nature of surface oxides during coal char oxidation by high-resolution XPS, Carbon, 90 (2015) 181-196.

[22] A.M. Puziy, O.I. Poddubnaya, R.P. Socha, J. Gurgul, M. Wisniewski, XPS and NMR studies of phosphoric acid activated carbons, Carbon, 46 (2008) 2113-2123.

[23] M. Asadullah, S. Zhang, Z. Min, P. Yimsiri, C.-Z. Li, Effects of biomass char structure on its gasification reactivity, Bioresource Technology, 101 (2010) 7935-7943.

[24] W. Xia, J. Yang, C. Liang, Investigation of changes in surface properties of bituminous coal during natural weathering processes by XPS and SEM, Applied Surface Science, 293 (2014) 293-298.

[25] D. Briggs, G. Beamson, XPS studies of the oxygen 1s and 2s levels in a wide range of functional polymers, Analytical Chemistry, 65 (1993) 1517-1523.

[26] E. Desimoni, G.I. Casella, A. Morone, A.M. Salvi, XPS determination of oxygen-containing functional groups on carbon-fibre surfaces and the cleaning of these surfaces, Surface and Interface Analysis, 15 (1990) 627-634.

[27] S. Glenis, M. Benz, E. LeGoff, J.L. Schindler, C.R. Kannewurf, M.G. Kanatzidis, Polyfuran: a new synthetic approach and electronic properties, Journal of the American Chemical Society, 115 (1993) 12519-12525.

[28] D.M. Quyn, J.-i. Hayashi, C.-Z. Li, Volatilisation of alkali and alkaline earth metallic species during the gasification of a Victorian brown coal in CO_2, Fuel Processing Technology, 86 (2005) 1241-1251.

[29] C.S.M. Lecea, M. Almela-Alarcon, A. Linares-Solano, Calcium-catalysed carbon gasification in CO_2 and steam, Fuel, 69 (1990) 21-27.

[30] M.B. Cerfontain, J.A. Moulijn, The interaction of CO_2 and CO with an alkali carbonate carbon system studied by in-situ Fourier Transform infrared spectroscopy, Fuel, 65 (1986) 1349-1355.

[31] M. Ni, B.D. Ratner, Differentiating calcium carbonate polymorphs by surface analysis techniques – an XPS and TOF-SIMS study, Surface and Interface Analysis, 40 (2008) 1356-1361.

[32] M. Jiang, J. Hu, J. Wang, Calcium-promoted catalytic activity of potassium carbonate for steam gasification of coal char: effect of hydrothermal pretreatment, Fuel, 109 (2013) 14-20.

[33] T.-W. Kwon, S.D. Kim, D.P.C. Fung, Reaction kinetics of char-CO_2 gasification, Fuel, 67 (1988) 530-535.

[34] K.J. Huttinger, Mechanism of water vapor gasification at high hydrogen levels, Carbon, 26 (1988) 79-87.

[35] G. Hermann, K.J. Huttinger, Mechanism of water vapour gasification of carbon – A new model, Carbon, 24 (1986) 705-713.

Chapter 5

Changes in char structure during the low-temperature gasification of mallee bio-char in air

5.1 Introduction

Gasification is an effective technology to convert solid fuels into a combustible gas that can be further used to generate electricity and to synthesise liquid fuels as well as chemicals [1-2]. Gasification will invariably be an endothermic process if the main product is the gas with high heating value such as H_2. For a practical gasifier, the energy required for the endothermic process is afforded by the energy produced from the combustion of biomass itself without any external supply of thermal energy into the gasifier [3-6]. Therefore, apart from some commonly referred gasification reaction such as char-CO_2, char-H_2O and char-H_2 reaction, the char-O_2 and volatiles-O_2 reaction can also be inevitable in a practical and efficient gasifier. Theoretically, the thermal energy produced from char-O_2 reaction should be ideally released to maintain the required gasification temperature [7]. Therefore, a good understanding of the char-O_2 reaction mechanisms is important and necessary for the design and operation of a commercial gasifier.

Structural feature of char greatly influences its gasification reactivity [8-10]. FT-Raman spectroscopy has been proved to be one of the most powerful analytical methods to characterize the evolution of aromatic ring systems of char due to its outstanding ability in probing the non-polar bond vibration [11-18]. In addition, based on our previous studies [11,12,18], the total Raman intensity can also be used to indicate the presence of O species that have a resonance effect with aromatic ring to which it is connected. FT-IR spectroscopy is another analytical technique that has been widely used in the characterisation of char structure, especially the O-containing functional groups due to its high sensitivity in detecting the polar bond vibration [19-22]. The use of these two complementary analytical techniques together would provide a more comprehensive characterisation of the char structure.

Some studies have been performed to investigate the low temperature gasification of low-rank fuels in air by employing the Raman spectroscopy [7,23]. However, they mainly focused on the gasification behaviours of char prepared from the devolatilisation process. Gasifying agent such as CO_2, H_2O and H_2 will be

continuously released in a practical gasifier, and the devolatilised chars could have the chance to be partially gasified by such agents before it reacts with O_2, especially for the up-draft gasifier. Therefore, investigation on the structural changes of the partially gasified char during gasification in air would have some profound meaning and practical value for operating a commercial gasification plant.

The purpose of this study is to investigate the evolution of char structure during low-temperature gasification of the partially gasified chars in air. Four kinds of partially gasified chars were prepared, which were char gasified in steam at 600 ˚C representing the low temperature gasification and char gasified in CO_2, steam and H_2 at 900 ˚C representing the high temperature gasification. The partially gasified char was reacted with air in TGA at 375 ˚C to ensure that the conversion of char was rate-limited by the chemical reaction in order to better investigating the char-O_2 reaction mechanism. The collected char samples at different conversion levels during gasification in air were characterised by the FT-IR/Raman spectroscopies.

5.2 Experimental

5.2.1 Gasification of biomass in CO_2, steam and H_2

The four kinds of partially gasified chars used in this study were obtained from the experiments in Chapter 4. Briefly, Australia mallee wood with particle size between 4.75 and 5.60 mm was used. The biomass sample had an ash yield of 0.9 wt% and a volatile yield of 81.6 wt% with an elemental composition of 48.2 wt% C, 6.1 wt% H, 0.2 wt% N and 45.5 wt% O (dry and ash-free basis) [9]. A fluidised bed quartz reactor was used to carry out the gasification experiments. The details of this reactor can be found elsewhere [9]. About 2 g biomass (accurately weighted) was continuously fed into the reactor with the flow of Ar inside the reactor when the desired temperature (600, 900 ˚C) was reached, followed by holding for 20 minutes to ensure that all volatiles have been released. The gasification reaction was commenced by switching the gas from Ar to the gasifying agent (pure CO_2, 15% H_2O-Ar, 15% H_2-Ar). After 4 minutes holding in the gasification atmosphere, the

reactor was lifted out the furnace immediately and cooled down naturally with Ar flowing through the reactor instead of the gasifying agents.

5.2.2 Char gasification in air

Chars produced from different gasification conditions were reacted with air in a Perkin-Elmer Pyris 1 TGA. Char samples were first heated to 375 ˚C in N_2 atmosphere and then switched to air to commence the gasification in air. When acquired char conversion level was reached, the reaction was stopped by lowering down the furnace to let the char residue cooling down naturally to the room temperature. Figure 5-1 shows the specific reactivity (R) of char calculated by the following equation:

$$R = -\frac{1}{W}\frac{dW}{dt} \quad (1)$$

where W is the mass (dry and ash-free basis) of the char at any given time t during gasification.

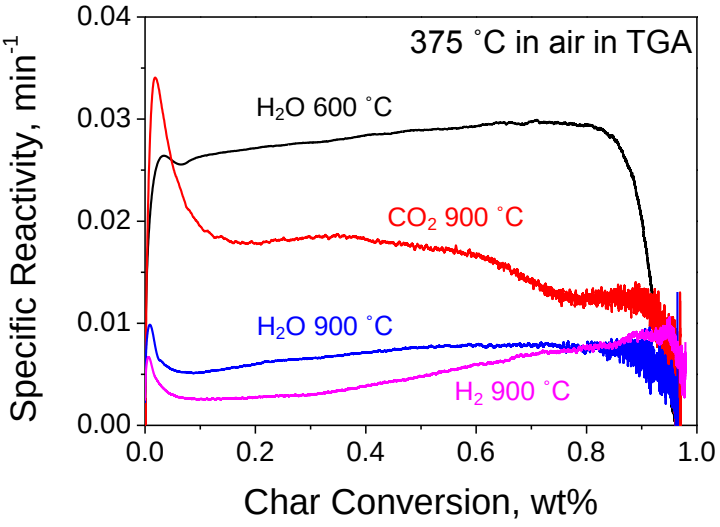

Figure 5-1. Specific char-O_2 reactivity analysed at 375 ˚C in air in TGA.

5.2.3 Char characterisation

A Perkin-Elmer Spectrum GX FT-IR/Raman spectrometer was used to characterise the char structure. Raman spectra of chars were recorded by an InGaAs detector using a back scattering configuration with a Nd:YAG excitation laser of 1064 nm. The char sample was diluted with spectroscopic grade KBr and then ground into powder making the char concentration of 0.5 wt% in the char-KBr mixture, which achieved a plateau value for the total Raman intensity. Each Raman spectrum represents the average of 200 scans and the spectral resolution was 4 cm^{-1}. IR spectra of chars were acquired by a DTGS detector equipped with a HeNe laser beam. The char concentration of 1.0 wt% in char-KBr pellets was chosen. Each IR spectrum represents the average of 32 scans and the spectral resolution was 4 cm^{-1}. All Raman and IR spectra were baseline corrected by using the software provided by Perkin-Elmer with the spectrometer.

The Raman spectra were deconvolution into 10 Gaussian bands in the first-order region (800-1800 cm^{-1}) and 8 Gaussian bands in the second-order region (2000-3300 cm^{-1}) to obtain the detailed structural features of char. The position and assignment of these bands has been described in our previous studies [11,12]. One modification has been made on the deconvolution method of the second-order Raman spectra because of the presence of an additional peak at around 2950 cm^{-1} for the chars from low temperature gasification (600 ˚C) and gasification in air in TGA. This band was originated from the overtone of V_L band in the first-order [11,24], thus named as $2V_L$, representing amorphous carbon structures. A typical example of the spectral deconvolution of the first and second-order Raman spectra of chars is shown in Figure 5-2.

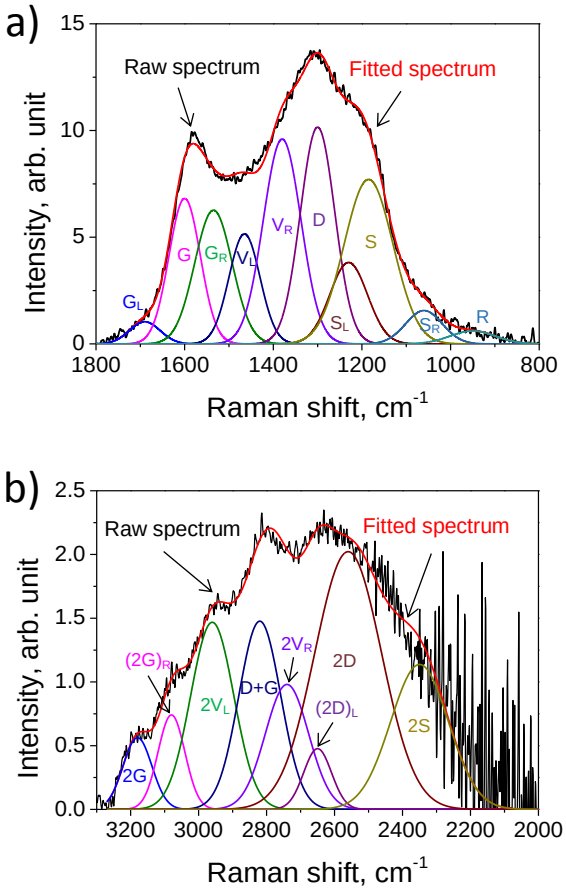

Figure 5-2. Spectral deconvolution of a Raman spectrum in (a) first-order region and (b) second-order region of the chars from gasification in 15% H_2O-Ar at 600 ˚C.

The IR spectra in the wavenumber of 700-1900 cm^{-1} was shown to indicate the typical chemical structures of char. Figure 5-3 illustrates the IR spectra of chars at different conversion levels during gasification in air at 375 ˚C in TGA. Five major bands can be found in the IR spectra. The assignments of these five bands are summarised in Table 5-1. Briefly, one band located at around 1700 cm^{-1} was assigned to carbonyl or carboxyl C=O stretch [20-22,24,25]. One band appearing at about 1580 cm^{-1} was attributed to the aromatic ring quadrant stretch [24], and another band at around 1450 cm^{-1} was attributed to the aromatic ring semi-circle stretch [24]. One band at around 1330 cm^{-1} was assigned to the aryl-CH_3 bending vibration [20-22,24] and another band at around 1150 cm^{-1} was assigned to the aromatic C-O stretching vibration [20-22,24,25].

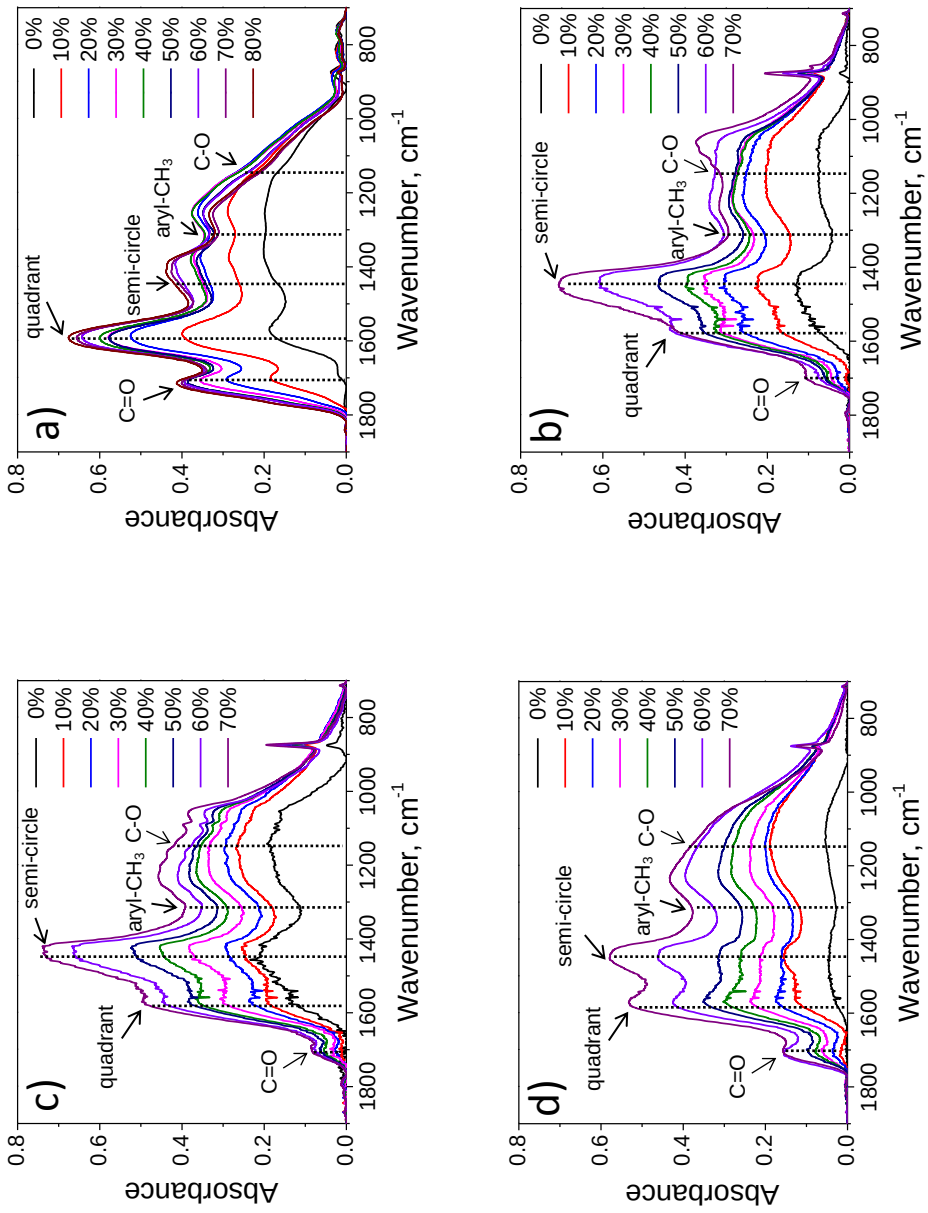

Figure 5-3. FT-IR spectra of chars from (a) gasification in 15% H_2O-Ar at 600 ˚C, (b) gasification in pure CO_2 at 900 ˚C, (c) gasification in 15% H_2O-Ar at 900 ˚C and (d) gasification in 15% H_2-Ar at 900 ˚C during the gasification in air at 375 ˚C in TGA.

Table 5-1. Summary of band assignment of IR peaks/bands.

Band position, cm^{-1}	Description	References
1700	carbonyl or carboxyl C=O stretching vibration	20-22,24,25
1580	aromatic ring quadrant stretching vibration	24
1450	aromatic ring semi-circle stretching vibration	24
1330	aryl-CH_3 bending vibration	20-22,24
1150	aromatic C-O stretching vibration	20-22,24,25

5.3 Results and discussion

5.3.1 Oxygenation of the char

Based on our previous studies [7,9,11,12,18,23], the presence of O-containing structures in char can be indicated by the total Raman band area (measured hereafter as the total peak area in the range of 800-1800 cm^{-1} for the first-order Raman and 2000-3300 cm^{-1} for the second-order Raman). The electron-rich O species would have resonance effects with the aromatic ring structure to which it is connected, which would greatly enhance the Raman scattering ability and subsequently increase the total Raman intensity of char [17]. Figure 5-4 exhibits the changes in the total intensity of the first-order Raman during the gasification of chars at 375 °C in air for the chars prepared under different gasification conditions. 0% conversion means that the char was just after gasification in the quartz reactor and before gasification in air in TGA.

At 0% char conversion, the observed total Raman band area of chars from gasification at 600 ˚C was much higher than that from gasification at 900 ˚C. The decreased total Raman band area with increasing temperature indicated the loss of the O species from the aromatic ring structure to which it is connected during gasification [7,9,11,23]. In addition, for the gasification in three different atmospheres at 900 ˚C, the Raman intensity of chars from gasification in steam and CO_2 was higher than that from gasification in H_2, which meant that some O derived

from the oxidising atmosphere would possibly form some oxygen complexes on char matrix [12,18]. The highest Raman intensity of the char from gasification in steam indicated its highest of the aromatic-connected O species among three gasification atmospheres. Once the char was exposed to air at 375 ˚C, the observed Raman intensity continuously increased with increasing conversion level for all four kinds of chars, indicating the oxygenation process during gasification in air (for the char produce at 600 ˚C, the decrease in the total Raman intensity for the char conversion from 80% to 90% was mainly due to the low carbonaceous content as well as the high ash yield in the char samples at that stage). Compared with the chars prepared at 900 ˚C, such increases for the char prepared at 600 ˚C was much significant. It can be seen from Figure 5-1 that the reactivity of char prepared at 600 ˚C was much higher than that of char prepared at 900 ˚C. Therefore, the oxygenation was much easy to take place on the active chars, resulting in the drastic increase of the total Rama intensity.

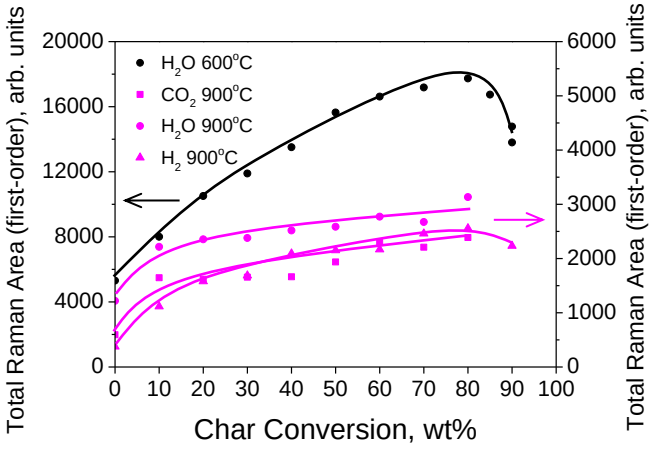

Figure 5-4. The changes in total Raman areas (first-order) during the gasification of chars in air at 375 ˚C in TGA. (the Y-axis scale is different for the char produced from 600 and 900 ˚C)

Evidence of the formation of additional O species in char during gasification in air can also be obtained from the IR spectra. As is illustrated in Figure 5-3, the total IR intensity of char at 0% conversion was quite low and would increase with increasing char conversion level. The IR intensity was also related to the O-containing functional groups in char because the electron-rich O species would effectively increase the electron cloud density of the aromatic system, and thus enhance the IR intensity [24]. More importantly, for the chars from gasification in steam at 600 ˚C, once the char reacted with O_2, a clear band can be seen from the spectra at the position of 1700 cm^{-1}, which represented the carbonyl or carboxyl structures in char. The newly formed carbonyl or carboxyl structure clearly demonstrated the creation of additional O species in char during gasification in air. Such carbonyl or carboxyl structure would directly connect to the aromatic ring system particularly as aromatic ketone or ester [23], directly explaining the drastic increase in the total Raman intensity of char during gasification in air. However, for the chars prepared from gasification at 900 ˚C, the presence of carbonyl or carboxyl structure was not obvious during the char gasification in air, only a small peak can be observed at the position of 1700 cm^{-1}. All of these indicated that the chars prepared at 600 ˚C and 900 ˚C followed different reaction pathways during gasification in air.

5.3.2 Changes in the aromatic systems of char during gasification in air

The deconvolution of Raman spectra allows further insight into the evolution of aromatic ring system of char during gasification in air. Based on the bands assignment of first-order Raman spectra [11], the D band mainly represented the large aromatic ring systems with no less than 6 fused rings, while the Gr, Vl and Vr bands were usually combined together to represent the small aromatic ring systems with 3-5 fused rings in char. Therefore, the band area ratios $I_D/I_{(Gr+Vl+Vr)}$ can be used as an indirect indication of the changes in aromatic ring systems in char during gasification.

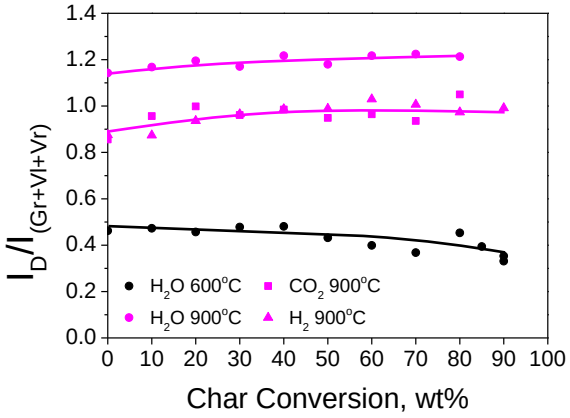

Figure 5-5. The changes in Raman band area ratios $D/(G_R+V_L+V_R)$ during the gasification of chars in air at 375 ˚C in TGA.

It can be seen from Figure 5-5 that, as expected, at 0% char conversion, the band area ratios $I_D/I_{(Gr+Vl+Vr)}$ of char from gasification at 900 ˚C was much higher than that from gasification at 600 ˚C, confirming the high concentration of large aromatic ring systems for the char produced from high temperature gasification [7,9,11,23]. In addition, the highest $I_D/I_{(Gr+Vl+Vr)}$ ratios of char from gasification in steam at 900 ˚C was mainly due to the fierce aromatic ring condensation induced by the steam-generated H radicals [18].

Once the gasification of chars in air commenced in TGA, two different trends were found in the ratios $I_D/I_{(Gr+Vl+Vr)}$ with increasing char conversion level. Chars prepared at 600 ˚C showed a slight decrease in this ratio while a small increasing trend could be observed for the chars prepared at 900 ˚C. The high concentration of O-containing structures and small aromatic ring systems of chars prepared at 600 ˚C indicated its high reactivity. Therefore, during gasification in air, the large aromatic rings could be easily consumed as small aromatic rings, and some small aromatic rings might be produced by the breakdown of large aromatic rings, resulting in a decreasing ratio of large to small aromatic ring systems of chars. However, the structures of chars prepared at 900 ˚C have become much stable during gasification. When the chars were gasified with air, the small aromatic ring systems were the preferential sites for O_2 to react with, and the breakdown of further-fused large aromatic ring systems did

not necessarily produce small ones, leading to an increase in the ratio of large to small aromatic ring systems.

5.3.3 Changes in the relative intensity of other major bands in the Raman spectra

5.3.3.1 Changes of the cross-linking structures in char during gasification in air

The cross-linking density of chars can be described by the intensity of S band in the first-order Raman spectra. Based on the band assignment [11], the S band mainly represents some sp^3-rich structures such as alkyl-aryl C-C structures, and these substitutional groups would interweave with each other to make a close aromatic ring systems of char.

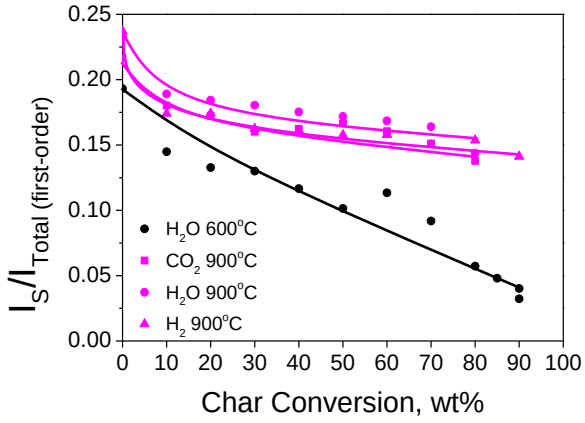

Figure 5-6. The changes in Raman band area ratios S/Total (first-order) during the gasification of chars in air at 375 ˚C in TGA.

Figure 5-6 illustrates the changes in the ratio of I_S to I_{Total} (first-order Raman) as a function of char conversion level. At 0% char conversion, it can be seen that the relative intensity of S band of chars prepared at 900 ˚C was higher that at 600 ˚C, indicating the formation of new cross-linking structures during high temperature gasification. Once the chars react with O_2 in TGA, a clearly decreasing trend in the ratios I_S/I_{Total} can be observed with increasing char conversion, which indicated such sp^3-rich structures were continuously consumed by O_2, and subsequently the char matrix was loosened with the progress of gasification in air [23]. Such decrease is especially evident for the chars prepared from gasification at 600 ˚C, which means that the loss of cross-linking structures was much easy to take place on the char with less structural stability.

5.3.3.2 Formation of the dangling structures in char during gasification in air

Based on our previous studies [11,26], the R band in the first-order Raman spectra was mainly attributed to the C-C on alkanes/cyclic alkanes as well as aliphatic/cyclic aliphatic structures. Figure 5-7 illustrates the changes in the ratio of I_R to $I_{Total\ (first\text{-}order\ Raman)}$ as a function of char conversion level.

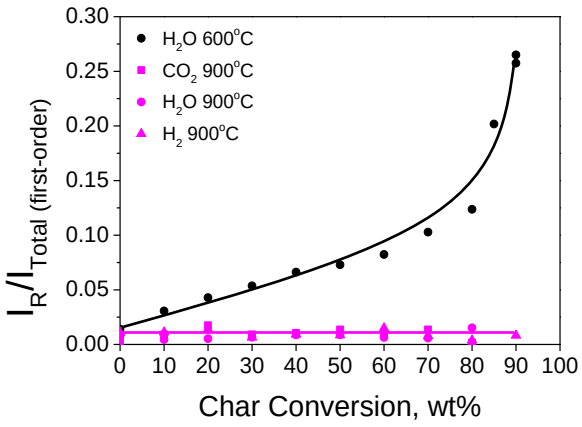

Figure 5-7. The changes in Raman band area ratios R/Total (first-order) during the gasification of chars in air at 375 ˚C in TGA.

At 0% char conversion, the less contribution (<2%) of R band in the first-order Raman spectra for all four kinds of chars indicated that these structures were very active and easy to be broken off during gasification. However, with the start of char-O_2 reaction in TGA, the relative intensity of R band exhibited a monotonic increasing trend with the progress of gasification for the char prepared at 600 ˚C. This observation consists with what Lei Zhang and co-workers have found during the gasification of nascent chars in air in our group. As discussed above, for the char prepared from 600 ˚C, the large and small aromatic rings were broken up and lots of carbonyl or carboxyl structures (at 1700 cm^{-1} in IR spectra) were formed in char during gasification in air. Such newly formed broken structures with sp^3 nature were more likely to "hang" on the aromatic rings, creating some dangling structures in char [26]. When the char conversion was higher than 80%, the R band accounted for 25% of the total Raman area in the first-order region, indicating the char has become less aromatic at that stage. However, for the chars prepared from the gasification at 900 ˚C, not much change can be observed. The high stability of char structures make the breakdown of aromatic system and the oxygenation of char hard to happen, and thus cause the absence of the dangling structures in char during gasification in air. In other words, the dominance of very large aromatics in the chars produced at high temperature make them hard to be detected as dangling structures (such as C=O structures) at the partially broken status.

5.3.3.3 Changes of structural compactness of char during gasification in air

Additional information can be obtained through the deconvolution of Raman spectra in the second-order region. One major band in the range of 2350-2500 cm^{-1} can be found in the second-order Raman spectra of some carbonaceous materials [12,27-30]. The relative intensity of this band, named as 2S [12], was supposed to indicate the structural compactness of char.

As is illustrated in Figure 5-8, at 0% conversion, the $I_{2S}/I_{Total\ (second\text{-}order\ Raman)}$ ratios of chars from gasification in H_2O at 600 ˚C was higher than that from gasification in CO_2 and H_2O at 900 ˚C (such ratios of char from gasification in H_2 at 900 ˚C but not

experiencing the gasification in air was not displayed here due to the much low intensity of the second-order Raman spectra), again demonstrating the enhancing structural compactness of char with increasing gasification temperature both in the aspect of the aromatic ring size and the cross-linking as well as dangling structures. With the progress of gasification in air in TGA, a clearly increasing trend of the relative intensity of 2S band can be observed for the char prepared from gasification at 600 ˚C, indicating that the char structure become less and less compact with the increasing char conversion. Little changes can be observed for the chars prepared from gasification at 900 ˚C, again demonstrating the different reaction pathway during oxygenation process for the chars prepared at 600 ˚C and 900 ˚C.

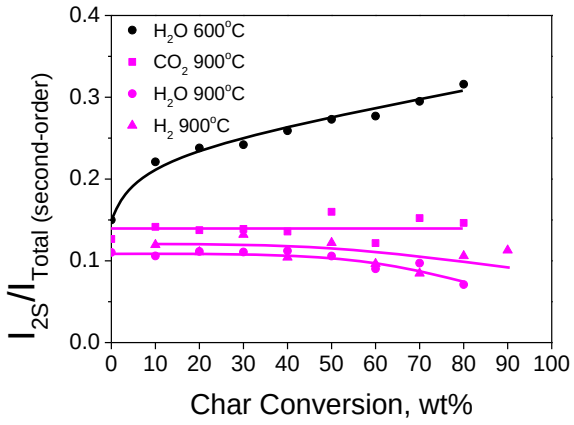

Figure 5-8. The changes in Raman band area ratios 2S/Total (second-order) during the gasification of chars in air at 375 ˚C in TGA.

5.3.4 Influences of char structures on the char-O_2 reactivity

As is shown in Figure 1-1, the overall reactivity of char prepared from gasification at 600 ˚C was much higher than that from gasification at 900 ˚C. Chars prepared at 600 ˚C exhibited the highest total Raman intensity and lowest $I_D/I_{(Gr+Vl+Vr)}$ ratios, indicating the enrichment of O-containing structures and small aromatic ring systems in the char. The presence of these structures would make the char become less ordered, and thus lead to its high reactivity in air [7].

Differences can also be observed for the chars prepared from gasification at 900 ˚C in different atmospheres. Chars prepared from gasification in CO_2 exhibited the highest reactivity in air. However, the char from gasification in steam showed the highest content of O-aromatic species. Therefore, the oxygenation of the char reflected by the total Raman intensity was not the decisive factor determining the reactivity of char in air. This observation consists with what Tingting Li and co-workers have found during the gasification of Collie coal in our group. For the gasification in steam, the presence of H radical would greatly activate the aromatic rings [18], and the consequence was the drastic growth of large aromatic ring systems reflected by the $I_D/I_{(Gr+Vl+Vr)}$ ratios of char. For the gasification in H_2, based on our previous study [18], the release of AAEM species from the char matrix could be enhanced during the gasification in reducing atmospheres. Whether the aromatic rings condensation or the volatilisation of AAEM species would result in low reactivity in air.

5.4 Conclusions

The purpose of this study was to investigate the structural changes of the partially gasified char during low-temperature gasification in air. Four kinds of chars prepared from the gasification of mallee wood in 15% H_2O-Ar or pure CO_2 or 15% H_2-Ar at 600 ˚C or 900 ˚C were gasified in air at 375 ˚C in a TGA respectively. The oxidisation of char prepared at 600 ˚C was more significant than that prepared at 900 ˚C during the gasification in air. In addition, for the chars produced at 600 ˚C, the

breakage of large aromatic ring system, consumption of cross-linking structures and formation of dangling structures indicated the decreasing structural compactness of char with the progress of gasification in air. However, such destruction of the aromatic ring system was difficult to take place for the chars produced at 900 ˚C. Furthermore, chars produced from gasification at 600 ˚C exhibited the highest reactivity in air mainly due to the presence of more O-containing structures as well as small aromatic ring systems in char. While for the chars produced at 900 ˚C in three different atmospheres, the aromatic ring size were mainly responsible for their reactivity in air rather than the O-containing structures of char.

5.5 References

[1] C.-Z. Li, Special issue-gasification: A route to clean energy, Process Safety and Environmental Protection, 84 (2006) 407-408.

[2] C.-Z. Li, Some recent advances in the understanding of the pyrolysis and gasification behaviour of Victorian brown coal, Fuel, 86 (2007) 1664-1683.

[3] L. Dong, M. Asadullah, S. Zhang, X.-S. Wang, H. Wu, C.-Z. Li, An advanced biomass gasification technology with integrated catalytic hot gas cleaning: Part I. Technology and initial experimental results in a lab-scale facility, Fuel, 108 (2013) 409-416.

[4] Y. Sakurai, S. Yamamoto, S. Kudo, K. Norinaga, J.-I. Hayashi, Conversion characteristics of aromatic hydrocarbons in simulated gaseous atmospheres in reducing section of two-stage entrained-flow coal gasifier in air-and O_2/CO_2-blown modes, Energy & Fuels, 27 (2013) 1974-1981.

[5] L. Wang, C.L. Weller, D.D. Jones, M.A. Hanna, Contemporary issues in thermal gasification of biomass and its application to electricity and fuel production, Biomass and Bioenergy, 32 (2008) 573-581.

[6] P.M. Lv, Z.H. Xiong, J. Chang, C.Z. Wu, Y. Chen, J.X. Zhu, An experimental study on biomass air–steam gasification in a fluidized bed, Bioresource Technology, 95 (2004) 95-101.

[7] D.M. Keown, X. Li, J.-I. Hayashi, C.-Z. Li, Evolution of biomass char structure during oxidation in O_2 as revealed with FT-Raman spectroscopy, Fuel Processing Technology, 89 (2008) 1429-1435.

[8] Y. Sekine, K. Ishikawa, E. Kikuchi, M. Matsukata, A. Akimoto, Reactivity and structural change of coal char during steam gasification, Fuel, 85 (2006) 122-126.

[9] M. Asadullah, S. Zhang, Z. Min, P. Yimsiri, C.-Z. Li, Effects of biomass char structure on its gasification reactivity, Bioresource Technology, 101 (2010) 7935-7943.

[10] C. Sheng, Char structure characterised by Raman spectroscopy and its correlations with combustion reactivity, Fuel, 86 (2007) 2316-2324.

[11] X. Li, J.-I. Hayashi, C.-Z. Li, FT-Raman spectroscopic study of the evolution of char structure during the pyrolysis of a Victorian brown coal, Fuel, 85 (2006) 1700-1707.

[12] S. Wang, T. Li, L. Wu, L. Zhang, L. Dong, X. Hu, C.-Z. Li, Second-order Raman spectroscopy of char during gasification, Fuel Processing Technology, 135 (2015) 105-111.

[13] A. Guedes, B. Valentim, A.C. Prieto, F. Noronha, Raman spectroscopy of coal macerals and fluidized bed char morphotypes, Fuel, 97 (2012) 443-449.

[14] V.P. Chabalala, N. Wagner, S. Potgieter-Vermaak, Investigation into the evolution of char structure using Raman spectroscopy in conjunction with coal petrography; Part 1, Fuel Processing Technology, 92 (2011) 750-756.

[15] C.A. Johnson, J.W. Patrick, K.M. Thomas, Characterization of coal chars by Raman spectroscopy, X-ray diffraction and reflectance measurements, Fuel, 65 (1986) 1284-1290.

[16] S. Dong, P. Alvarez, N. Paterson, D.R. Dugwell, R. Kandiyoti, Study on the effect of heat treatment and gasification on the carbon structure of coal chars and metallurgical cokes using Fourier Transform Raman Spectroscopy, Energy & Fuels, 23 (2009) 1651-1661.

[17] L.A. Leites, S.S. Bukalov, Raman intensity and conjugation with participation of ordinary σ-bonds, Journal of Raman Spectroscopy, 32 (2001) 413-424.

[18] H.-L. Tay, S. Kajitani, S. Wang, C.-Z. Li, A preliminary Raman spectroscopic perspective for the roles of catalysts during char gasification, Fuel, 121 (2014) 165-172.

[19] J.V. Ibarra, R. Moliner, A.J. Bonet, FT-IR investigation on char formation during the early stages of coal pyrolysis, Fuel, 73 (1994) 918-924.

[20] I. Pastorova, R.E. Botto, P. W. Arisz, J.J. Boon, Cellulose char structure: a combined analytical Py-GC-MS, FTIR, and NMR study, Carbohydrate Research, 262 (1994) 27-47.

[21] J.V. Ibarra, E. Munoz, R. Moliner, FTIR study of the evolution of coal structure during the coalification process, Organic Geochemistry, 24 (1996) 725-735.

[22] V. Gomez-Serrano, J. Pastor-Villegas, A. Perez-Florindo, C. Duran-Valle, C. Valenzuela-Calahorro, FT-IR study of rockrose and of char and activated carbon, Journal of Analytical and Applied Pyrolysis, 36 (1996) 71-80.

[23] X. Li, J.-I. Hayashi, C.-Z. Li, Volatilisation and catalytic effects of alkali and alkaline earth metallic species during the pyrolysis and gasification of Victoria brown coal. Part VII. Raman spectroscopic study on the changes in char structure during the catalytic gasification in air, Fuel, 85 (2004) 1509-1517.

[24] D. Lin-Vien, N.B. Colthup, W.G. Fateley, J.G. Grasselli, The handbook of infrared and Raman characteristic frequencies of organic molecules, Academic Press, San Diego, 1991.

[25] Y. Zhao, D. Feng, Y. Zhang, Y. Huang, S. Sun, Effect of pyrolysis temperature on char structure and chemical speciation of alkali and alkaline earth metallic species in biochar, Fuel Processing Technology, 141 (2016) 54-60.

[26] L. Zhang, T. Li, D. Quyn, L. Dong, P. Qiu, C.-Z. Li, Formation of nascent char structure during the fast pyrolysis of mallee wood and low-rank coals, Fuel, 150 (2015) 486-492.

[27] S. Vollebregt, R. Ishihara, F.D. Tichelaar, Y. Hou, C.I.M. Beenakker, Influence of the growth temperature on the first and second-order Raman band ratios and widths of carbon nanotubes and fibers, Carbon, 50 (2012) 3542-3554.

[28] A. Sadezky, H. Muckenhuber, H. Grothe, R. Niessner, U. Poschl, Raman microspectroscopy of soot and related carbonaceous materials: Spectral analysis and structural information, Carbon, 43 (2005) 1731-1742.

[29] T. Shimada, T. Sugai, C. Fantini, M. Souza, L.G. Cancado, A. Jorio, et al, Origin of the 2450 cm^{-1} Raman bands in HOPG, single-wall and double-wall carbon nanotubes, Carbon, 43 (2005) 1049-1054.

[30] A. Zaida, E. Bar-Ziv, L.R. Radovic, Y.-J. Lee, Further development of Raman microprobe spectroscopy for characterization of char reactivity, Proceeding of the Combustion Institute, 31 (2007) 1881-1887.

Chapter 6

Evolution of O-containing structures during char gasification as revealed with FT-IR/Raman and X-ray photoelectron spectroscopies

6.1 Introduction

Char structure is a major factor influencing its gasification reactivity [1-3]. Many studies [4-6] have carried out to investigate the changes in char structure in term of aromatic ring size as well as the dispersion of AAEM species during gasification. The O-containing structures also play an important role in affecting the gasification behaviour of char [4]. However, insufficient attention has been paid in this area. Many factors can influence the evolution of O-containing structures. For example, increasing gasification temperature tends to reduce the oxygen content of char due to the enhanced thermal cracking [7-9]. Moreover, additional O-containing functional groups would form on char with the progress of gasification in oxidising atmosphere [10,11]. Therefore, investigation on the evolution of O-containing structures of char can provide another aspect in understanding the gasification mechanism.

Many analytical techniques can be used to characterise the O-containing structures in char. Some studies [7-11] used the FT-Raman spectroscopy to investigate the changes in oxygen species in char during gasification. However, it can only indicate the relative content of oxygen that have a resonance effect with the aromatic ring to which it is connected [4,12,13]. FT-IR spectroscopy has also been widely used in the characterisation of O-containing functional groups of char due to its high sensitivity in detecting the polar bond vibration [14-17]. X-ray photoelectron spectroscopy is another powerful analytical method to characterise the oxygen species in char. As is discussed in Chapter 4, detailed quantitative information about the O-containing structures can be obtained by deconvoluting the high-resolution O 1s spectra [18-21]. Biomass is rich in oxygen and various O-containing structures can be left in char during gasification. However, detailed structural feature of these O-containing structures is still not clear. As is discussed above, different analytical techniques have different foci on the characterisation of the oxygen species. Therefore, the use of these three analytical techniques together would provide a more comprehensive understanding of the evolution of O-containing structures in char during gasification.

The purpose of this study was to investigate the gasification mechanism in term of the evolution of oxygen species of char during gasification. Biomass gasification in steam was carried out at different temperatures ranging from 600 to 900 ˚C, and the bio-chars produced at 600 and 900 ˚C were gasified with air in TGA at 375 ˚C to ensure that the conversion of char was rate-limited by the chemical reaction in order to better investigate the char-O_2 reaction mechanism. Char samples produced from the gasification in steam and low-temperature gasification in air were collected and characterised by the FT-IR/Raman and X-ray photoelectron spectroscopies.

6.2 Experimental

6.2.1 Biomass gasification

The char samples produced from biomass gasification in steam used in this study were obtained from the experiments in Chapter 4. Briefly, the gasification of Australia mallee wood particles between 4.75-5.60 mm was carried in a fluidised bed quartz reactor [9] in steam atmosphere at 600-900 ˚C. The preparation of the wood sample and the procedure of the gasification experiment can be found in Chapter 4 and elsewhere [9]. The data on char yield were reported previously in Chapter 4.

The char samples produced from low-temperature gasification of char in air used in this study were obtained from the experiments in Chapter 5. Briefly, chars produced from the gasification in steam at 600 and 900 ˚C were gasified with air in a TGA at 375 ˚C respectively. The procedure of the low-temperature gasification of char in air can be found in Chapter 5 and elsewhere [10,11].

6.2.2 Char characterisation

The collected char samples after each experiment were characterised by the FT-IR/Raman and X-ray photoelectron spectroscopies. Detailed procedures about the XPS and FT-IR/Raman analysis as well as the data processing can be found in Chapters 4 and 5 respectively. Briefly, the XPS high-resolution O 1s spectra were

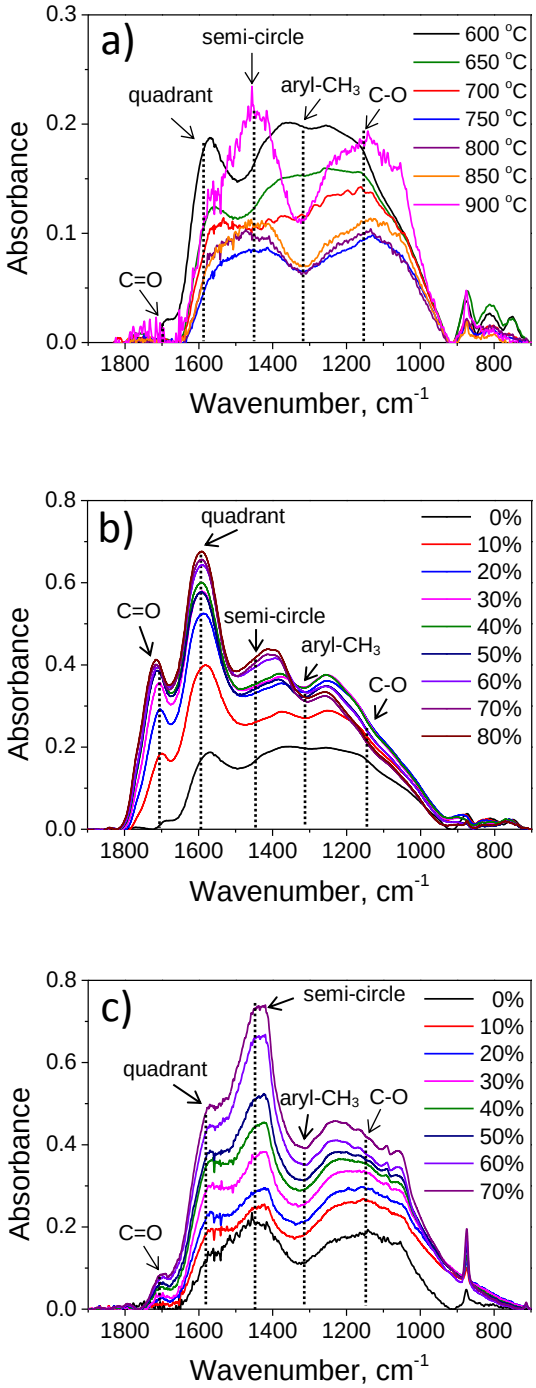

Figure 6-1. FT-IR spectra of chars from (a) biomass gasification in 15% H_2O-Ar, (b) char produced at 600 ˚C but having experienced gasification in air in TGA at 375 ˚C (c) char produced at 900 ˚C but having experienced gasification in air in TGA at 375 ˚C. Figure 6-1 (b) and (c) were reprinted from Chapter 5.

deconvoluted into 3 bands and the Raman spectra (in the first-order region) were deconvoluted into 10 bands to obtain detail structural information of char [12]. The data on the XPS analysis of chars produced from biomass gasification in steam were reported previously on Chapter 4 and the data on the FT-Raman analysis of chars produced from low-temperature gasification of char in air were re-calculated from Chapter 5. Figure 6-1 illustrates the IR spectra of chars during gasification in steam and the low-temperature gasification in air. The IR spectra shown in Figure 6-1(b) and (c) were reprinted from Chapter 5.

6.3 Results and discussion

6.3.1 XPS analysis

The relative contents of carbon and oxygen species in char were calculated through their total peak area in the XPS spectra and the corresponding relative sensitivity factors. The high-resolution O 1s spectra were further deconvoluted in order to get detailed quantitative information about the O-containing structure of char. The absolute amounts (per g of biomass/char) of carbon and oxygen species left in the char residual after gasification in steam and low-temperature gasification in air were also calculated using char conversion and contents of carbon and oxygen of the chars.

6.3.1.1 Evolution of O-containing structures of char during gasification in steam

Figure 6-2 illustrates the XPS analysis results of chars during the gasification in steam from 600 to 900 ˚C. The data on the XPS analysis of chars and the char yields used in this section were reported previously in Chapter 4. It can be seen from Figure 6-2 (a) that the O/C ratios of chars decreased with increasing gasification temperature, which indicated that the oxygen species were easier to be released or consumed than the carbon species with the intensified gasification reaction. Figure 6-2 (b) illustrates the absolute amounts of O-containing structures left in char residual based on one gram biomass experiencing the gasification in steam at different temperatures. The deconvolution results of the O 1s spectra showed that the

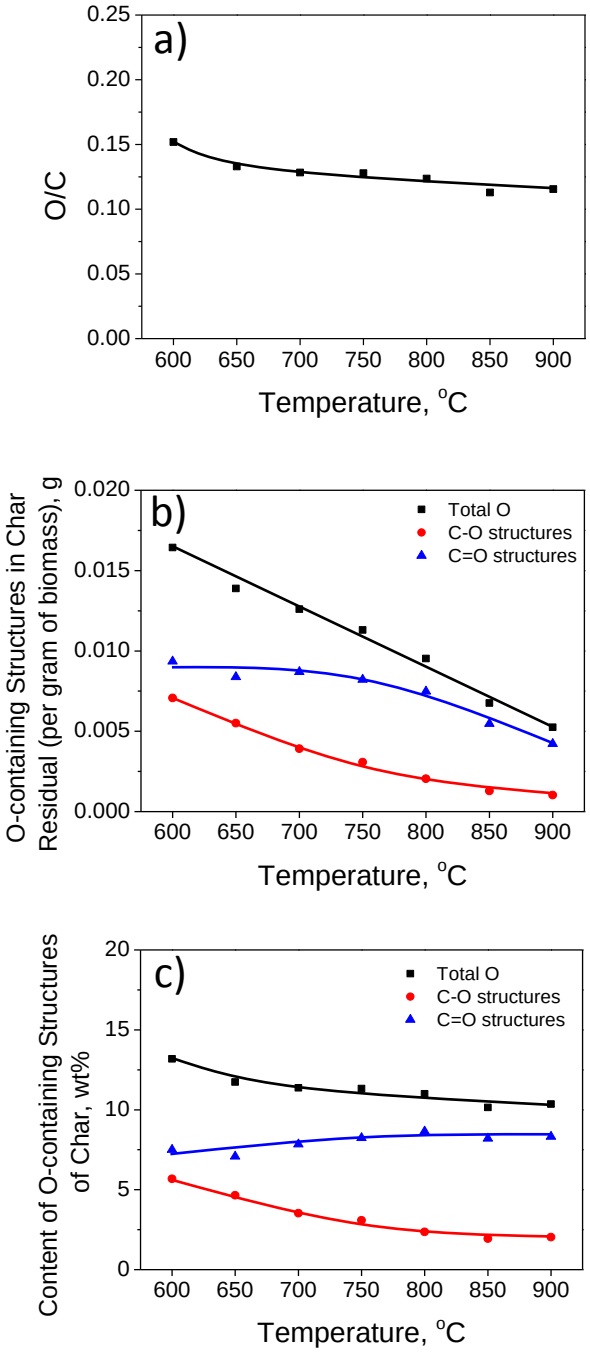

Figure 6-2. The (a) O/C ratios, (b) absolute amounts of O-containing structures and (c) relative contents of O-containing structures of chars obtained by XPS analysis as a function of temperature during gasification in 15% H_2O-Ar. The data were reported previously in Chapter 4.

absolute amounts of aromatic C-O structures left in char residual decreased continuously with increasing temperature. However, for the aromatic C=O structures,

no significant changes could be observed when the temperature was lower than 700 ˚C. It is obvious that the gasification reaction was very slow at temperatures lower than 700 ˚C, and the almost constant amount indicated the high thermal stability of the inherent aromatic C=O structures during the thermal cracking. However, the absolute amounts of aromatic C=O structures left in char residual started to decrease when the gasification reaction became increasingly fierce (> 700 ˚C). Figure 6-2 (c) illustrates the relative concentration of O-containing structures in char during gasification in steam. It can be seen that the relative contents of aromatic C=O structures increased while that of the aromatic C-O structures decreased with increasing temperature, also demonstrating the higher thermal stability of the inherent aromatic C=O structures than that of the aromatic C-O structures.

6.3.1.2 Evolution of O-containing structures of char during gasification in air

Figure 6-3 shows the XPS results of chars produced from gasification in steam at 900 ˚C but having experienced gasification in air in TGA at 375 ˚C. The data on the XPS analysis of chars at 0% conversion level were reported previously in Chapter 4. It can be seen from Figure 6-3 (a) that, as expected, there were increases in the O/C ratios with increasing char conversion, which indicated that more carbon spices was consumed from char matrix than oxygen or some new oxygen complexes were formed in char during the gasification in air.

Figure 6-3 (b) shows the absolute amounts of O-containing structures left in char residual based on one gram char experiencing the gasification in air to reach different conversion level. It can be seen that the absolute amounts of O-containing structures left in char residual increased at the initial stage of gasification in air (char conversion < 10%), indicating that the oxidation of char was much fierce and additional O-containing structures were formed during this period even the total amounts of char decreased. Detailed information about the evolution of O-containing structures can be obtained through further analysing the deconvolution results of the O 1s spectra. It can be seen that the amounts of aromatic C-O structures left in char

residual also showed a significant increase at the initial stage of gasification. However, the amounts of aromatic C=O structures left in char residual continuously decreased with increasing char conversion level even at the initial stage where the oxidation of char was intensified and lots of newly formed O-containing structures connected to the aromatic ring system. Therefore, the increasing amounts of oxygen species left in char residual were mainly due to the additional formation of aromatic C-O structures at the initial stage of gasification. With the progress of gasification in air, the total oxygen species left in char residual significantly decreased. Some oxygen species may also form on char with the progress of gasification, while the amounts of such newly formed O-containing structures were much less than the consumed inherent oxygen species of char, resulting in a continuous decrease in the amounts with increasing char conversion both for the aromatic C-O structures and aromatic C=O structures.

The data in Figure 6-3 (c) show that the relative contents of aromatic C-O structures in char continuously increased with the progress of gasification, especially at the initially stage, while the relative contents of aromatic C=O structures showed a possible slight decrease firstly and then became almost constant with increasing conversion of char. For the char produced at 900 ˚C but not experiencing the low-temperature gasification in air, as is shown in Figure 6-3 (c) at 0% conversion, the main component of the oxygen species was the aromatic C=O structures that account for about 80% of the total oxygen. In addition, based on the FT-IR spectra shown in Figure 6-1 (a), for the char produced at 900 ˚C, no clear peak can be observed at the position of 1700 cm^{-1}, which represents the carbonyl and carboxyl structures. Therefore, the most likely structures for these aromatic C=O functional group were the benzoquinone-type structures rather than the aromatic ketone or ester. Because the chars produced at 900 ˚C were highly aromatic, these benzoquinone-type C=O structures might be the preferred sites for the O_2 to react with at the initial stage, and some kinds of aromatic C-O structures such as aromatic ether could be formed, or even some benzoquinone-liked C=O structures might be transformed to the such aromatic C-O structures, resulting in a significant increase in the contents of aromatic C-O structures with the progress of gasification.

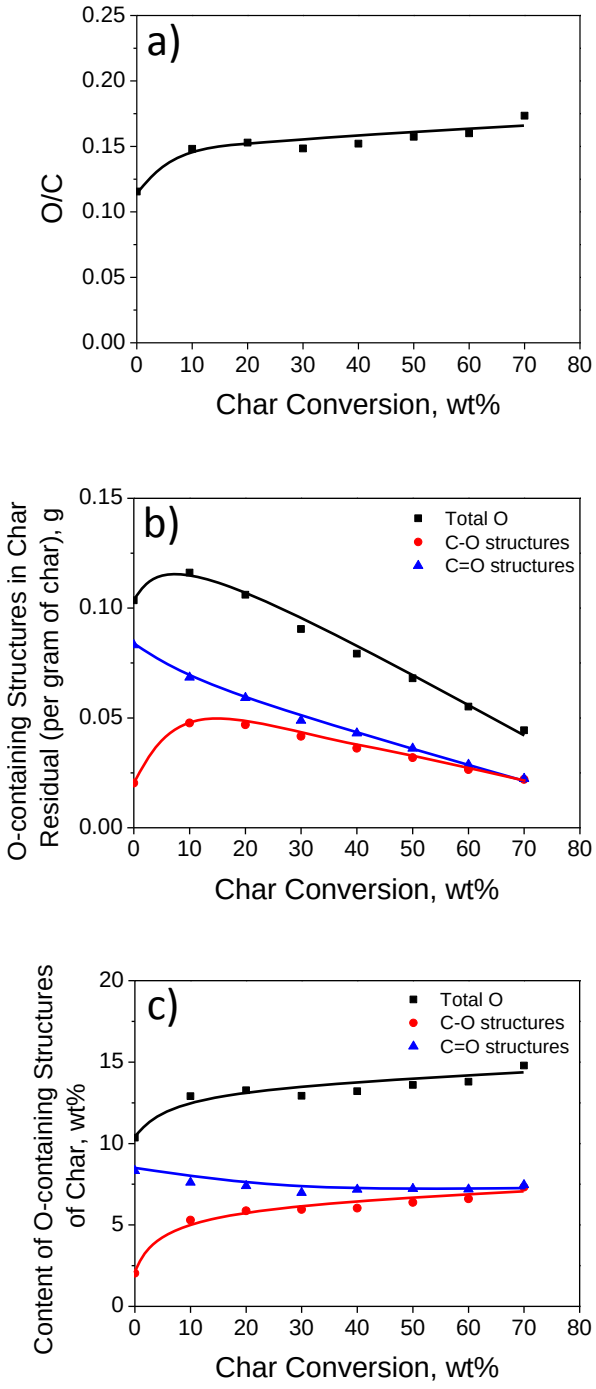

Figure 6-3. The (a) O/C ratios, (b) absolute amounts of O-containing structures and (c) relative contents of O-containing structures of chars obtained by XPS analysis from gasification at 900 ˚C as a function of char conversion level during gasification in air. The data of the chars at 0% conversion level were reported previously in Chapter 4.

Figure 6-4 shows the XPS results of chars produced from 600 ˚C but having experienced gasification in air in TGA at 375 ˚C. The data on the XPS analysis of chars at 0% conversion level were reported previously in Chapter 4. The increases in the O/C ratios of chars with increasing char conversion, as are shown in Figure 6-4 (a), again demonstrated the oxidation of char during gasification in air.

As is shown in Figure 6-4 (b), an increasing trend, although weak, for the total amounts of oxygen could also be observed at the initial stage of gasification in air (char conversion < 10%), again indicating that additional O-containing structures could be formed during this period. It can be seen that the amounts of aromatic C-O structures left in char residual also showed an slight increase at the initial stage of gasification, while the amounts of the aromatic C=O structures were almost same. Therefore, the newly formed aromatic C-O structures could be also most responsible for the increasing total amounts of oxygen. Again with the process of gasification in air, the total oxygen species left in char residual showed a significant decrease, demonstrating that the amounts of such newly formed O-containing structures was much less than the consumed inherent oxygen species of char during gasification.

Figure 6-4 (c) illustrates the relative contents of O-containing structures in char during the gasification in air. As was discussed above, the increases in the relative contents of O-containing structures both for the aromatic C-O structures and aromatic C=O structures were mainly due to the additional formation of some O-containing structures during the gasification in air. Further information about the evolution of oxygen species can also be found from the FT-IR spectra of char. The FT-IR spectra shown in Figure 6-1(b) were reprinted from Chapter 5. As is shown in Figure 6-1 (b), there was a significant increase in the intensity of the band at the position of 1700 cm^{-1} which represent the carbonyl and carboxyl structures. Therefore, for the aromatic C=O structures, the new formed O-containing functional group were, mostly likely, some aromatic ketone and aromatic ester with the progress of gasification

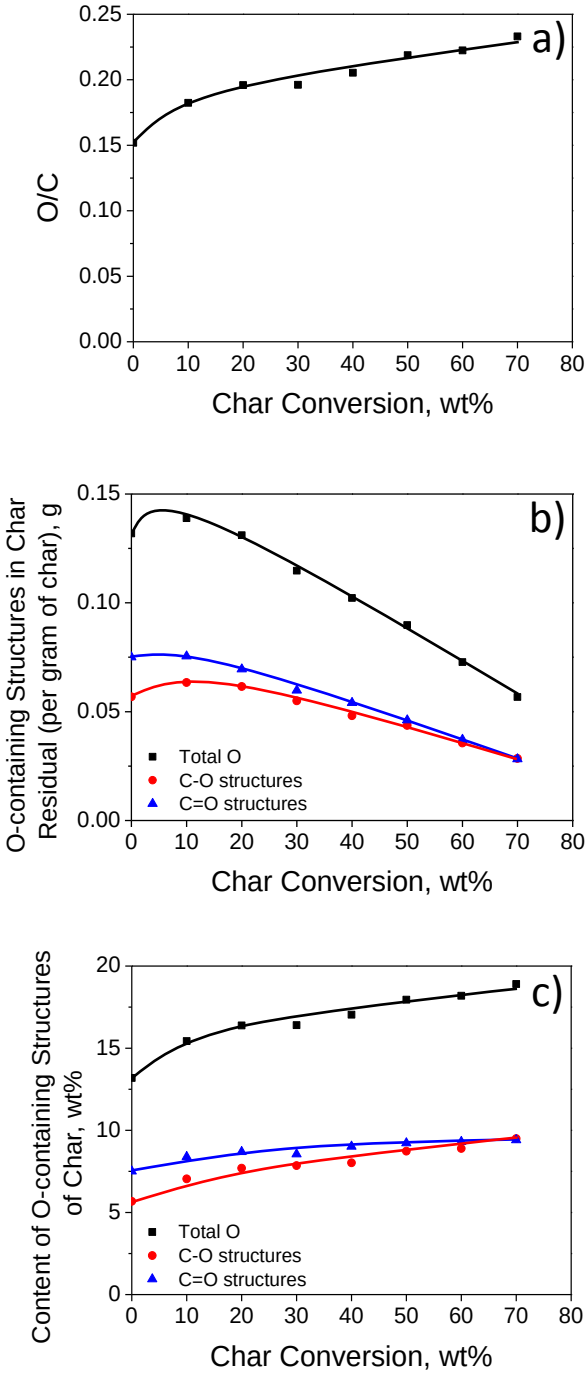

Figure 6-4. The (a) O/C ratios, (b) absolute amounts of O-containing structures and (c) relative contents of O-containing structures of chars obtained by XPS analysis from gasification at 600 ˚C as a function of char conversion level during gasification in air. The data of the chars at 0% conversion level were reported previously in Chapter 4.

6.3.1.3 Evolution of the O-containing structures during gasification as revealed by XPS

The XPS results of char during the gasification in steam and low-temperature gasification in air were plotted together (Figure 6-5) in order to understand the changes in the O-containing structures of char. The data on the XPS analysis of chars during the gasification in steam used in this section were reported previously in Chapter 4.

The data in Figure 6-5 (a) and (b) show that the changes in the contents of total O-containing structure were most related to the changes in the contents of aromatic C-O structure in char. As was discussed above, the thermal stability of inherent aromatic C-O structures in char was lower than that of aromatic C=O structures, thus the aromatic C-O structures could be easily removed from the char matrix with increasing gasification temperature. While during the low-temperature gasification in air, the newly formed aromatic C-O structures might have higher chemical stability than the aromatic C=O structures in the oxidising atmosphere, thus much newly formed aromatic C-O structures could survive with the progress of gasification. Therefore, as is illustrated in Figure 6-5 (c), high oxygen contents were usually accompanied by high C-O/C=O ratios of char during gasification.

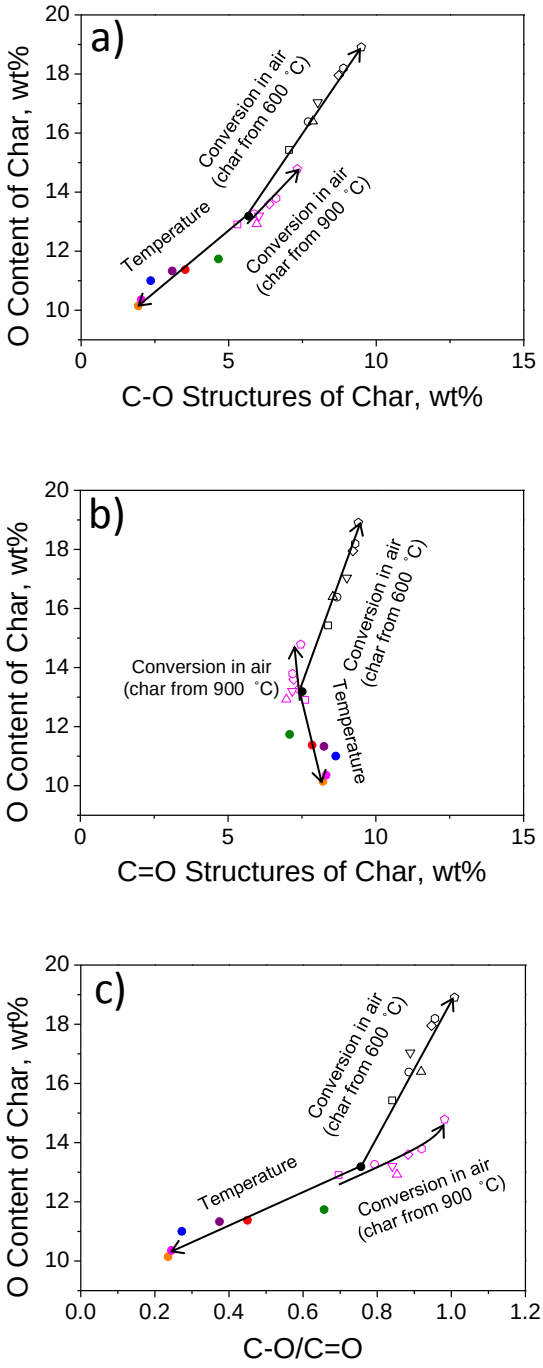

Figure 6-5. The total oxygen contents of chars as a function of (a) C-O structure in char, (b) C=O structure in char and (c) C-O/C=O ratio of char obtained by XPS analysis. The data of the chars during the gasification in steam were reported previously in Chapter 4.

6.3.2 FT-IR/Raman analysis

6.3.2.1 Evolution of aromatic ring systems of char during gasification in steam

The absolute Raman band area was calculated using the relative band intensity (I_{Band}/I_{Total}) and char conversion based on one gram biomass experiencing the gasification in steam at different temperatures. The absolute Raman band area can be used as an indirect indication of the amounts of large/small aromatic systems left in char residual. Figure 6-6 (a) shows the changes in the absolute Raman band area during gasification in steam. The data on char yield used in this section were reported previously in Chapter 4 and the data on the Raman analysis of chars produced from the gasification in steam at 600 and 900 ˚C used in this section were re-calculated from Chapter 5. It can be seen that the band area of $G_R+V_L+V_R$ decreased with increasing gasification temperature, indicating the continuous removal of small aromatic rings during gasification [4,13]. In addition, the band area of D remained almost unchanged when the temperature was less than 700 ˚C, indicating the high chemical stability of large aromatics during thermal cracking [12]. The large aromatics started to be consumed when the gasification reaction became intensified (> 700 ˚C). The relative band area during gasification in steam is shown in Figure 6-6 (b). It can be seen that relative contents of large aromatics increased monotonically while the small aromatics decreased with increasing gasification temperature [4,13].

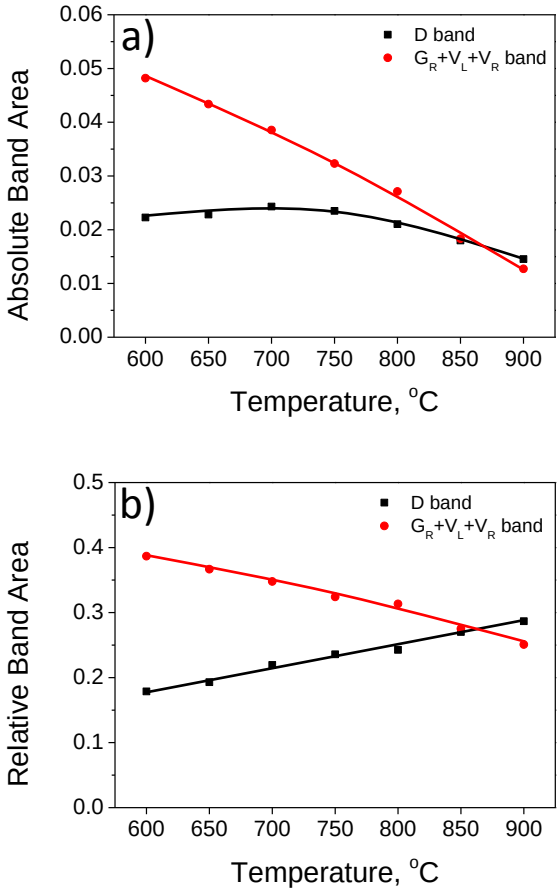

Figure 6-6. The (a) absolute Raman band intensity and (b) relative Raman band intensity of chars as a function of temperature during gasification in 15% H_2O-Ar. The data on char yield were reported previously in Chapter 4 and the data on the Raman analysis of chars produced from the gasification in steam at 600 and 900 ˚C were re-calculated from Chapter 5.

6.3.2.2 Evolution of aromatic ring systems of char during gasification in air

The absolute Raman band area was calculated using the relative band intensity (I_{Band}/I_{Total}) and char conversion based on one gram char experiencing the gasification in air. The changes in the absolute Raman band area of char prepared from 600 ˚C during gasification in air in TGA at 375 ˚C is shown in Figure 6-7 (a). The data on the Raman analysis used in this section were re-calculated from Chapter 5. As expected, the large aromatics as well as the small aromatics were continuously consumed with the progress of gasification in air. It can be seen from Figure 6-7 (b)

that the relative band area of D slight decreased while a slight increase of $G_R+V_L+V_R$ can be observed with increasing char conversion. Considering that the char produced from 600 ˚C was not highly aromatic [10,12], some small aromatic rings would be produced by the breakdown of large aromatic rings during gasification, resulting in a decreasing ratio of large to small aromatic ring systems of chars.

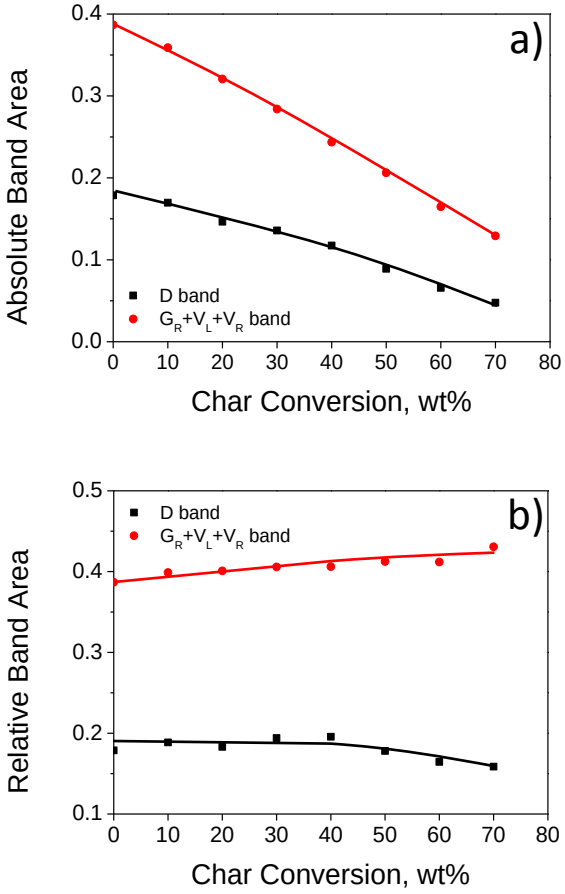

Figure 6-7. The (a) absolute Raman band intensity and (b) relative Raman band intensity of chars produced at 600 ˚C as a function of char conversion level during gasification in air. The data on the Raman analysis used in this section were re-calculated from Chapter 5.

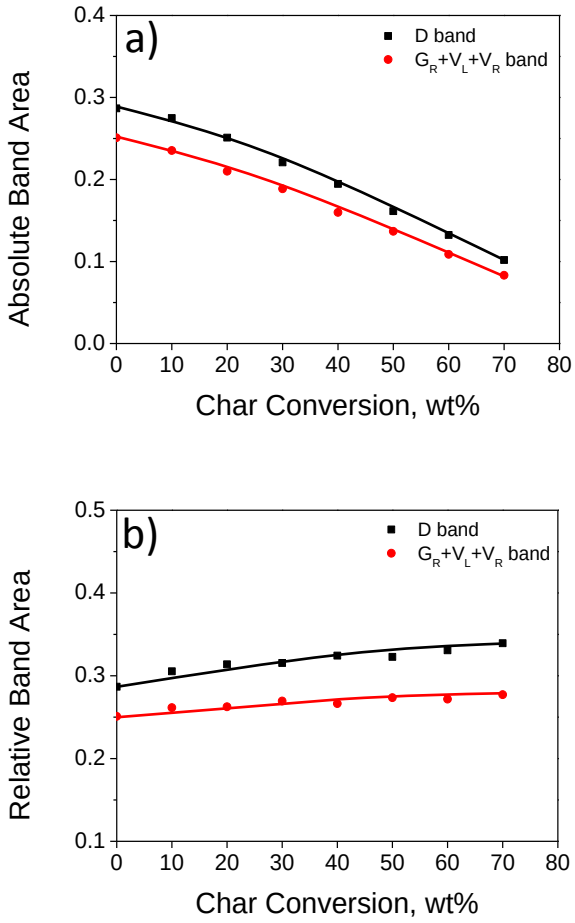

Figure 6-8. The (a) absolute Raman band intensity and (b) relative Raman band intensity of chars produced at 900 ˚C as a function of char conversion level during gasification in air. The data on the Raman analysis used in this section were re-calculated from Chapter 5

As is shown in Figure 6-8 (a), the continuous consumption of large aromatics and small aromatics with the progress of gasification in air can also be seen for the char produce from 900 ˚C. The data on the Raman analysis used in this section were re-calculated from Chapter 5. In addition, it can be seen from Figure 6-8 (b) that the relative band area of D and $G_R+V_L+V_R$ increased with increasing char conversion. The trend of D band for the char produced at 900 ˚C was different from that produced at 600 ˚C with the progress of gasification in air. This is mainly because the structures of char have become much stable and aromatic during gasification in steam at 900 ˚C [10], some carbon sp^3 structures such as dangling structure and cross-linking structures of char were easier to be removed than the aromatic rings

during gasification, resulting in an increasing trend of the relative intensity both for D band and $G_R+V_L+V_R$ band.

6.3.2.3 Evolution of aromatic ring systems of char during gasification as revealed by Raman spectroscopy

Based on our previous studies [4,12], the total Raman area of char can be used as an indication of the amounts of oxygen species that have a resonance effect with the aromatic ring systems to which it is connected. Therefore, it can be speculated that there should be an increase in the relative intensity of D band (or $G_R+V_L+V_R$ band) if more oxygen species is formed that connect to the large aromatic rings (or small aromatic rings). Instead, a decrease should be observed in the relative intensity of D band (or $G_R+V_L+V_R$ band) if more oxygen species is consumed that was connected with the large aromatic rings (or small aromatic rings).

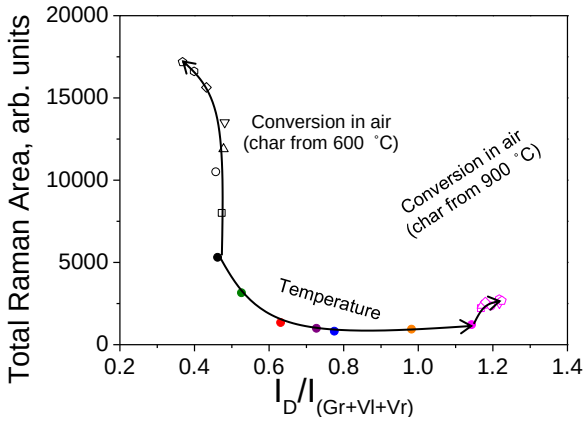

Figure 6-9. Total Raman areas (first-order) of chars as a function of $I_D/I_{Gr+Vl+Vr}$ ratio of chars. The data on the Raman analysis of chars during the low-temperature gasification in air were reported previously in Chapter 5.

Figure 6-9 illustrates the total Raman area as a function of the area ratio of D band to $G_R+V_L+V_R$ band during gasification in steam and low-temperature gasification in air. The data on the Raman analysis of chars during the low-temperature gasification in air used in this section were reported previously in Chapter 5. For the gasification in steam, the total Raman area decreased with increasing $I_D/I_{Gr+Vl+Vr}$, indicating that the small aromatics as well as the oxygen species to which it is connected were easier to be removed from char than large aromatics, thus more large-aromatic-connected oxygen species survived with enhanced thermal cracking and gasification reactions. For the low-temperature gasification in air, the increasing total Raman area was accompanied with a decreasing $I_D/I_{Gr+Vl+Vr}$ for char from 600 ˚C and an increasing $I_D/I_{Gr+Vl+Vr}$ for the char from 900 ˚C. As discussed above, the char produced at 600 ˚C was not highly aromatic [10,12]. Therefore, some small aromatic rings would be produced by the breakdown of large aromatic rings, resulting in more newly formed oxygen species connecting to the small aromatics than large aromatics. However, for the char from 900 ˚C, the breakdown of the further condensed large aromatics was harder than that of small aromatics during gasification in air, and the breakdown of large aromatics to form small ones was not easy to happen [10]. Therefore, oxygen species connected to the large aromatics have more chances to survive, resulting in the increases in $I_D/I_{Gr+Vl+Vr}$ with increasing total Raman area.

6.3.3 Types of O-containing structures in term of total IR and total Raman intensity

Besides the total Raman area, the total IR area of char can also be used as an indication of the relative contents of oxygen species in char because the presences of electron-rich oxygen species will increase the IR absorption of char by increasing the electron cloud density of the aromatic systems to which it is connected.

Figure 6-10 illustrates the total Raman areas as a function of the total IR areas for chars during the gasification in steam and low-temperature gasification in air. The data on the total Raman areas of chars during the low-temperature gasification in air used in this section were reported previously in Chapter 5. It can be seen that, with increasing gasification temperature (up to 850 ˚C), there were decreases both for the

Raman intensity and IR intensity. While for the char produced from gasification in steam at 900 ˚C, a high IR intensity can be observed. As discussed above, the gasification reaction is much fierce at 900 ˚C and some oxygen derived from steam would connect to the aromatic rings [4,13]. This kind of newly formed oxygen species seem to be very IR-sensitive. In addition, for the chars produced from gasification in steam at 600 ˚C but having experienced gasification in air in TGA at 375 ˚C, the Raman intensity continuously increased with increasing char conversion while the IR intensity achieved a plateau value when the char conversion was higher than 30%. However, for the chars produced from 900 ˚C, there was a clear increase for the IR intensity with the progress of gasification in air while the increase for the Raman intensity was not obvious. All of these indicated that different types of O-containing structures were formed during char oxygenation. Some O-containing functional groups could enhance the Raman scattering ability of char while some could promote the IR absorption [22].

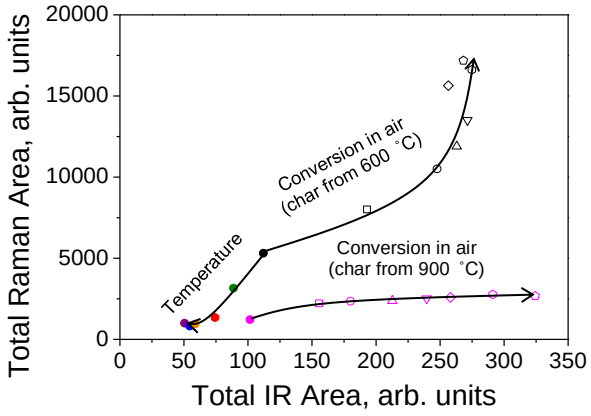

Figure 6-10. Total Raman area (first-order) of chars as a function of Total IR area of chars. The data on the total Raman areas of chars during the low-temperature gasification in air were reported previously in Chapter 5.

6.4 Conclusions

Australia mallee wood was gasified in a fluidised-bed reactor at 600-900 ˚C in steam atmosphere, and the bio-chars from the gasification in steam at 600 and 900 ˚C were gasified with air in TGA at 375 ˚C. The experimental results showed that the decreases in the oxygen contents of char with increasing gasification temperature were mainly related to the loss of aromatic C-O structures. In addition, oxygen species that were connected to the small aromatic ring systems (3-5 fused rings) would be selectively removed with increasing gasification temperature. There were significant increases in the amount of oxygen species in char at the initial stage of low-temperature gasification in air, which was mainly due to the newly formed C-O structures. The additional formation of aromatic C-O structures was also mainly responsible for the continuously increased oxygen content of char with the progress of gasification in air, indicating that the chemical stability of the newly formed C-O structures could be higher than aromatic C=O structures with the progress of gasification in the oxidising atmosphere. Different types of O-containing structures would be formed during char oxygenation according to their different behaviour in the total Raman and IR intensity.

6.5 References

[1] C.-Z. Li, Special issue-gasification: A route to clean energy, Process Safety and Environmental Protection, 84 (2006) 407-408.

[2] C.-Z. Li, Importance of volatile-char interactions during the pyrolysis and gasification of low-rank fuels – A review, Fuel, 112 (2013) 609-623.

[3] C.-Z. Li, Some recent advances in the understanding of the pyrolysis and gasification behaviour of Victorian brown coal, Fuel, 86 (2007) 1664-1683.

[4] H.-L. Tay, S. Kajitani, S. Wang, C.-Z. Li, A preliminary Raman spectroscopic perspective for the roles of catalysts during char gasification, Fuel, 121 (2014) 165-172.

[5] C.-Z. Li, C. Sathe, J.R. Kershaw, Y. Pang, Fates and roles of alkali and alkaline earth metals during the pyrolysis of a Victorian brown coal, Fuel, 79 (2000) 427-438.

[6] D.M. Quyn, H. Wu, S.P. Bhattacharya, C.-Z. Li, Volatilisation and catalytic effects of alkali and alkaline earth metallic species during the pyrolysis and gasification of Victorian brown coal. Part II. Effects of chemical form and valence, Fuel, 81 (2002) 151-158.

[7] T. Li, L. Zhang, L. Dong, C.-Z. Li, Effects of gasification atmosphere and temperature on char structural evolution during the gasification of Collie sub-bituminous coal, Fuel, 117 (2014) 1190-1195.

[8] S. Zhang, Z. Min, H.-L. Tay, Y. Wang, L. Dong, C.-Z. Li, Changes in char structure during the gasification of mallee wood: effects of particle size and steam supply, Energy & Fuels, 26 (2011) 193-198.

[9] M. Asadullah, S. Zhang, Z. Min, P. Yimsiri, C.-Z. Li, Importance of biomass particle size in structural evolution and reactivity of char in steam gasification, Industrial & Engineering Chemistry Research, 48 (2009) 9858-9863.

[10] D.M. Keown, X. Li, J.-I. Hayashi, C.-Z. Li, Evolution of biomass char structure during oxidation in O_2 as revealed with FT-Raman spectroscopy, Fuel, Processing Technology 89 (2008) 1429-1435.

[11] X. Li, J.-i. Hayashi, C.-Z. Li, Volatilisation and catalytic effects of alkali and alkaline earth metallic species during the pyrolysis and gasification of Victorian brown coal. Part VII. Raman spectroscopic study on the changes in char structure during the catalytic gasification in air, Fuel, 85 (2006) 1509-1517.

[12] X. Li, J.-i. Hayashi, C.-Z. Li, FT-Raman spectroscopic study of the evolution of char structure during the pyrolysis of a Victorian brown coal, Fuel, 85 (2006) 1700-1707.

[13] S. Wang, T. Li, L. Wu, L. Zhang, L. Dong, X. Hu, C.-Z. Li, Second-order Raman spectroscopy of char during gasification, Fuel Processing Technology, 135 (2015) 105-111.

[14] J.V. Ibarra, R. Moliner, A.J. Bonet, FT-IR investigation on char formation during the early stages of coal pyrolysis, Fuel, 73 (1994) 918-924.

[15] I. Pastorova, R.E. Botto, P. W. Arisz, J.J. Boon, Cellulose char structure: a combined analytical Py-GC-MS, FTIR, and NMR study, Carbohydrate Research, 262 (1994) 27-47.

[16] J.V. Ibarra, E. Munoz, R. Moliner, FTIR study of the evolution of coal structure during the coalification process, Organic Geochemistry, 24 (1996) 725-735.

[17] Y. Zhao, D. Feng, Y. Zhang, Y. Huang, S. Sun, Effect of pyrolysis temperature on char structure and chemical speciation of alkali and alkaline earth metallic species in biochar, Fuel Processing Technology, 141 (2016) 54-60.

[18] D.L. Perry, A. Grint, Application of XPS to coal characterization, Fuel, 62 (1983) 1024-1033.

[19] S.G. Chen, R.T. Yang, F. Kapteijn, J.A. Moulijn, A new surface oxygen complex on carbon: toward a unified mechanism for carbon gasification reactions, Industrial & Engineering Chemistry Research, 32 (1993) 2835-2840.

[20] F. Marquez-Montesinos, T. Cordero, J. Rodriguez-Mirasol, J.J. Rodriguez, CO_2 and steam gasification of a grapefruit skin char, Fuel, 81 (2002) 423-429.

[21] A.R. Gonzalez-Elipe, A. Martinez-Alonso, J.M.D. Tascon, XPS characterization of coal surfaces: study of aerial oxidation of brown coals, Surface and Interface Analysis, 12 (1988) 565-571.

[22] L. Zhang, S. Kajitani, S. Umemoto, S. Wang, D. Quyn, Y. Song, T. Li, S. Zhang, L. Dong, C.-Z. Li, Changes in nascent char structure during the gasification of low-rank coals in CO_2, Fuel, 158 (2015) 711-718.

Chapter 7

Conclusions and Recommendations

7.1 Aims of this study

The purpose of this study was to gain fundamental understanding on the effect of char structure on its gasification behaviour. A fluidised-bed quartz reactor was used to carry out the gasification experiment and mallee wood from Western Australia was chosen as the feedstock. The FT-IR/Raman and X-ray photoelectron spectroscopies were applied to characterise the chemical structural feature of char, especially the evolution of aromatic ring systems and O-containing structures under different gasification conditions including different temperatures and atmospheres. The main conclusions from the present study are listed below.

7.2 Conclusions

7.2.1 Effect of gasification condition on char yield

- The increasing gasification temperature would greatly reduce the char yield due to the enhanced gasification reaction between the char and gasifying agent.

- Gasification of chars in the steam and CO_2 atmospheres proceeded much faster than that in H_2 atmosphere. The additional formation of some O-containing structures in char during the gasification in the oxidising atmosphere was most likely to be responsible for enhancing the gasification rate.

- High char yield was observed during gasification for the biomass with large particle size, which was mainly due to the differences in the intra-particle heat and mass transfer between small and large particle sizes during pyrolysis. While for the consequent gasification of char, the intra-particle diffusion of the gasifying agent was not a rate-limited step under the present experimental conditions.

7.2.2 Evolution of the aromatic ring systems of char during gasification

- Second-order Raman can also be used to characterise the structural feature of char. The deconvolution results of the second-order Raman of char in terms of the evolution of aromatic ring systems were consistent with the findings in the first-order Raman analysis.

- The increasing gasification temperature would greatly increase the content of large aromatic rings systems in char during gasification in the steam, CO_2, and H_2 atmosphere because the enhanced thermal cracking and gasification reaction would selectively remove the small aromatic ring systems.

- The chars produced from gasification in steam atmosphere exhibited the highest content of large aromatic rings systems. This was mainly due to the presence of H radical which would induce the ring condensation during gasification in steam.

- Biomass particle size had minimal effect on char structure during the gasification of char in steam atmosphere and CO_2 atmosphere under the present experimental conditions.

- The breakage of large aromatic ring system, consumption of cross-linking structures and formation of dangling structures can be observed for the char produced from gasification at 600 ˚C during the low-temperature gasification in air. While the destruction of aromatic ring system was not obvious for the char produced from gasification at 900 ˚C.

7.2.3 Evolution of the O-containing structures of char during gasification

- The increasing gasification temperature would greatly reduce the content of oxygen in char. The loss of aromatic C-O structure in char was mainly responsible for this decrease.

- ❖ The amount of aromatic C-O structure left in char during the gasification under reducing atmosphere was lower than that under oxidising atmosphere, while the consumption of aromatic C=O structure was related to the progress of gasification regardless of the atmosphere.

- ❖ The continuously increased total Raman and total IR intensity with the increasing char conversion level demonstrated that the low-temperature gasification in air was a significant oxygenation process, and the additional formation of aromatic C-O structure was mainly responsible for this increase.

- ❖ Char oxygenation can lead to the formation of various O-containing structures in char. Some could enhance the Raman scattering ability while some could promote the IR absorption.

7.3 Recommendations

1. This study is mainly focused on the evolution of char structure during the gasification of mallee wood. Bark and leaves constitute important parts of any woody biomass, and they can also be used to produce biofuels and chemicals. It is ideal that all parts of woody biomass can be used as the feedstock without the need of being separated into wood, bark and leave for a practical gasifier. Therefore, the study on the gasification behaviour of bark and leaves is also important.

2. Various kinds of O-containing structures would form in char matrix during the gasification in oxidising atmospheres. It is clear that the additional oxygen species formed in char during the gasification in steam and CO_2 atmosphere were different based on the total Raman intensity of char. Real-time monitoring the release of oxygen species (e.g. CO) of char after gasification could provide very helpful information in understanding the

formation of different O-containing structures during the gasification in different oxidising atmospheres.

3. This study mainly investigated the evolution of char structure during the gasification of biomass in single gasification atmosphere. It is well-known that variously gasifying agent such CO_2, H_2O H_2 and O_2 will be continuously released in a practical gaisifier. Therefore, understanding the gasification behaviour of biomass in a mixture of gasifier agents would have profound meaning and application value for designing and operating a commercial gasification plant.

Appendix I

Permission of Reproduction from the Copyright Owner

Title:	Importance of volatile–char interactions during the pyrolysis and gasification of low-rank fuels – A review	Logged in as: shuai wang Account #: 3001040406 LOGOUT
Author:	Chun-Zhu Li	
Publication:	Fuel	
Publisher:	Elsevier	
Date:	October 2013	

Order Completed

Thank you for your order.

This Agreement between shuai wang ("You") and Elsevier ("Elsevier") consists of your license details and the terms and conditions provided by Elsevier and Copyright Clearance Center.

Your confirmation email will contain your order number for future reference.

Get the printable license.

License Number	3898530239769
License date	Jun 29, 2016
Licensed Content Publisher	Elsevier
Licensed Content Publication	Fuel
Licensed Content Title	Importance of volatile–char interactions during the pyrolysis and gasification of low-rank fuels – A review
Licensed Content Author	Chun-Zhu Li
Licensed Content Date	October 2013
Licensed Content Volume	112
Licensed Content Issue	n/a
Licensed Content Pages	15
Type of Use	reuse in a thesis/dissertation
Portion	figures/tables/illustrations
Number of figures/tables/illustrations	1
Format	both print and electronic
Are you the author of this Elsevier article?	No
Will you be translating?	No
Order reference number	
Original figure numbers	
Title of your thesis/dissertation	Evolution of Char Structure and Reactivity during Gasification
Expected completion date	Jul 2016
Estimated size (number of pages)	150
Elsevier VAT number	GB 494 6272 12
Requestor Location	shuai wang 1 turner avenue, bentley perth, WA 6102 Australia Attn: shuai wang
Total	0.00 USD

ORDER MORE CLOSE WINDOW

Title:	FT-Raman spectroscopic study of the evolution of char structure during the pyrolysis of a Victorian brown coal	Logged in as: shuai wang Account #: 3001040406
Author:	Xiaojiang Li,Jun-ichiro Hayashi,Chun-Zhu Li	LOGOUT
Publication:	Fuel	
Publisher:	Elsevier	
Date:	September 2006	

Order Completed

Thank you for your order.

This Agreement between shuai wang ("You") and Elsevier ("Elsevier") consists of your license details and the terms and conditions provided by Elsevier and Copyright Clearance Center.

Your confirmation email will contain your order number for future reference.

Get the printable license.

License Number	3898521445852
License date	Jun 29, 2016
Licensed Content Publisher	Elsevier
Licensed Content Publication	Fuel
Licensed Content Title	FT-Raman spectroscopic study of the evolution of char structure during the pyrolysis of a Victorian brown coal
Licensed Content Author	Xiaojiang Li,Jun-ichiro Hayashi,Chun-Zhu Li
Licensed Content Date	September 2006
Licensed Content Volume	85
Licensed Content Issue	12-13
Licensed Content Pages	8
Type of Use	reuse in a thesis/dissertation
Portion	figures/tables/illustrations
Number of figures/tables/illustrations	1
Format	both print and electronic
Are you the author of this Elsevier article?	No
Will you be translating?	No
Order reference number	
Original figure numbers	
Title of your thesis/dissertation	Evolution of Char Structure and Reactivity during Gasification
Expected completion date	Jul 2016
Estimated size (number of pages)	150
Elsevier VAT number	GB 494 6272 12
Requestor Location	shuai wang 1 turner avenue, bentley perth, WA 6102 Australia Attn: shuai wang
Total	0.00 USD

ORDER MORE CLOSE WINDOW

Copyright Clearance Center RightsLink®

Home | Account Info | Help | Live Chat

Title: Second-order Raman spectroscopy of char during gasification

Author: Shuai Wang,Tingting Li,Liping Wu,Lei Zhang,Li Dong,Xun Hu,Chun-Zhu Li

Publication: Fuel Processing Technology

Publisher: Elsevier

Date: July 2015

Logged in as:
shuai wang
Account #:
3001040406
LOGOUT

Order Completed

Thank you for your order.

This Agreement between shuai wang ("You") and Elsevier ("Elsevier") consists of your license details and the terms and conditions provided by Elsevier and Copyright Clearance Center.

Your confirmation email will contain your order number for future reference.

Get the printable license.

License Number	3898551318466
License date	Jun 29, 2016
Licensed Content Publisher	Elsevier
Licensed Content Publication	Fuel Processing Technology
Licensed Content Title	Second-order Raman spectroscopy of char during gasification
Licensed Content Author	Shuai Wang,Tingting Li,Liping Wu,Lei Zhang,Li Dong,Xun Hu,Chun-Zhu Li
Licensed Content Date	July 2015
Licensed Content Volume	135
Licensed Content Issue	n/a
Licensed Content Pages	7
Type of Use	reuse in a thesis/dissertation
Portion	full article
Format	both print and electronic
Are you the author of this Elsevier article?	Yes
Will you be translating?	No
Order reference number	
Title of your thesis/dissertation	Evolution of Char Structure and Reactivity during Gasification
Expected completion date	Jul 2016
Estimated size (number of pages)	150
Elsevier VAT number	GB 494 6272 12
Requestor Location	shuai wang 1 turner avenue, bentley perth, WA 6102 Australia Attn: shuai wang
Total	0.00 USD

ORDER MORE CLOSE WINDOW